THE EFFECT OF FREEZE-DRYING ON THE PHYSICAL PROPERTIES OF CELLULOSE FIBRES AND PAPER

THE CAPILLARY FLOW OF LIQUIDS WITH ENTRAPPED AIR BUBBLES

by

Robert H. Marchessault, B.Sc.

A thesis submitted to the Faculty of Graduate
Studies and Research at McGill University, in
partial fulfilment of the requirements for the
degree of Doctor of Philosophy

McGill University,
Montreal,
Canada.

April 1954

ACKNOWLEDGEMENTS

The writer wishes to thank Dr. S.G. Mason whose direction and assistance were never lacking throughout this investigation.

Grateful acknowledgement is made:- to Canadian Industries Limited for a Fellowship during the 1951-52 session,

to the National Research Council for a Studentship during the session 1952-53, and for a Summer Award during 1953,

to the Province of Quebec for a Bursary during the session 1953-54,

to the Canadian Pulp and Paper Association for financial assistance during the summers of 1950 and 1951,

to the Pulp and Paper Research Institute of Canada for financial assistance during the summer of 1952,

to Mr. W.C. Lodge of the Pulp and Paper Research Institute of Canada for valuable advice and assistance in connection with the preparation and testing of paper sheets.

TABLE OF CONTENTS

PART I

The Effect of Freeze-Drying on the Physical Properties of Cellulose Fibres and Paper

Page

INTRODUCTION

EXPERIMENTAL AND RESULTS

PART II

Capillary Flow of Liquids with Entrapped Air Bubbles

INTRODUCTION

EXPERIMENTAL AND RESULTS

ENERAL DISCUSSION

LIST OF TABLES

PART I

PART II

LIST OF FIGURES

PART I

PART II

LIST OF PLATES

PART I

PART II

PART I

EFFECT OF FREEZE-DRYING ON THE PHYSICAL PROPERTIES OF CELLULOSE FIBRES AND PAPER

INTRODUCTION

The recorded history of papermaking extends almost 2000 years back to the early Chinese who clubbed vegetable fibres to a pulp which they formed into a mat and dried in the sun. Although methods have vastly improved, the basic principle has not changed - the evaporation of liquid water from a mat of wet cellulose fibres.

At some stage of the drying procedure the loose wet web is transformed into the solid dense sheet known as paper. The transformation occurs over a relatively short period of time and is generally termed "bonding". Although it has been the object of much speculation it is nevertheless true that the nature of the fibre-to-fibre bond in paper remains to be established.

In the present investigation it was attempted to gain a further knowledge of the factors which promote interfibre bonding. This was done by changing the conventional method of drying. Because drying is the critical step in the formation of paper, it was of interest, although probably only theoretical, to evaluate the effect of drying by sublimation (freeze-drying) on the physical properties of paper. The moreso, because such an experiment affords a test of the hypothesis, proposed by Campbell (22), that during drying of the wet paper web, internal liquid tension draws fibre elements into intimate contact which appears to be a necessary condition for bonding to occur. At the same time parallel experiments on cellulose fibres were conducted to show the effect of freeze-drying on their physico-chemical properties. In this manner, useful information was obtained concerning the cellulose-water relationship, the mechanism of bonding in paper and the effect of freeze-drying on the fine structure of cellulose fibres.

The following discussion will fall under three headings:

1. The process of freeze-drying.

2. The structure and constitution of cellulose with particular reference to the make-up of softwood fibres.

3. Theories of fibre-to-fibre bonding and the principal factors which influence it.

4. Special Methods of Drying Cellulose.

This discussion will prepare the way for presentation of experimental results on:

1. The effect of freeze-drying on the physical properties of paper and of paper made from alkali-extracted pulp.

2. The effect of repeated wetting and drying cycles on the paper-making properties of beaten cellulose fibres.

3. The effect of freeze-drying on some physico-chemical properties of cellulose fibres.

I. Freeze-Drying

In freeze-drying, the process of drying by sublimation, the starting material which may be either a solution or a moist solid, is initially frozen and then sublimed under high vacuum. Thus the ice or frozen solvent evaporates without drying leaving the starting material as a highly porous framework, often with the same overall volume as the original frozen material.

Although it is only within the last ten years that the method has achieved commercial importance, it has been a common laboratory technique for several decades particularly among bacteriologists and biologists.

The major advantages of the method appear to be: (a) its ability to attain a very low moisture content, which is important for the preservation of many labile substances during storage, (b) its ability to eliminate case-hardening or shrinkage. Thus, the solubility of products dried in this way is remarkably fast and complete.

Mechanism of Freeze-Drying

There are two stages in drying by sublimation: in the first, ice is evaporated from a frozen mass; in the second, moisture is removed from the final dry solid to lower the residual content to a minimal level. The relative amounts of vapour removed in each stage depend on the nature of the product and its concentration prior to freezing.

The actual temperature of the frozen product during drying depends on several factors, the main ones being: the method and rate of vapour removal and the rate of heat exchange of the frozen product to the surrounding atmosphere. Generally, temperature will be lower during the first stage of drying because of the faster rate of sublimation and the consequently higher cooling effect. In present practice (23), controlled heating of the frozen product is used to supply the latent heat of sublimation to the evaporating solid and thus maintain a reasonable drying rate. The faster heat can be supplied, the faster drying can be carried out, but the temperature of the product must not be allowed to rise above its melting point.

Three general methods may be used for the removal of water vapour from the vacuum system: (a) condensation at low temperature, (b) combination with desiccating substances, and (c) direct pumping. In this investigation, methods (a) and (b) were used for the removal of water vapour while non-condensable gases were removed by method (c).

The high degree of dispersion of freeze-dried material suggests many new applications in the field of colloid chemistry, where case-hardening of hydrophilic substances on drying often seriously affects their subsequent rate of reaction. Cellulose is a prime example of this. Wyckoff (23) has reported the use of quick-freezing and desiccation from the frozen state for the preparation of mono-dispersed colloidal particles for electron microscopy.

II. Constitution and Structure of Cellulose

A. General Properties

Extensive chemical analysis has shown that the basis molecular unit is the β-anhydro-glucoside group (60). The molecular units are condensed through 1:4 acetal linkages to form linear macromolecules having varying degrees of polymerization which are reported to exceed 3500 in the original plant form (24). In the fibre these molecules tend to crystallize through strong intermolecular binding forces to form a solid structure (25).

Perfect crystallization is not achieved due to the restricted freedom of movement of the chains imposed by their great length. The resultant structure is regarded as having regions of varying order or perfection of chain alignment. For convenience these regions may be divided into two classes: amorphous, in which the degree of order is low; and crystalline in which the degree of order approaches that of pure crystalline solids. The terms low density and high density are equally descriptive.

Estimates of the relative proportions of crystalline and amorphous material may be had from X-ray data (26) or from the various methods of determining the amorphous or "accessible" portion such as water sorption

27), density (28) and the reaction rate methods involving hydrolysis (29), oxidation (30), deuterium exchange (31) or ethylation (13). Considerable care must be given to the interpretation of the results from the various methods, for as Howsmon (27) has pointed out, the actual proportion of crystalline material is of limited significance; the size, distribution and orientation of these regions also plays a decisive role in determining the properties of the fibre.

In naturally-occurring fibres there is a preferred orientation of the chains in the direction of the fibre, which gives rise to anisotropy. f, however, the cellulose is brought into solution and reprecipitated in the form of a continuous filament, the resulting structure may be prepared in a completely isotropic form (26). Stretching of these isotropic filaments tends to align the molecules by plastic rearrangement and anisotropy again appears. Anisotropy in fibres is most readily detected by the difference in axial and radial swelling and by their birefringence.

When perfectly dry, cellulose is hard and inflexible. It is, however, readily plasticized by water and other liquids of a polar nature with accompanying swelling, characteristic of gel systems. The chemical and physical properties of the fibre are highly dependent on the amount and nature of plasticizing liquid.

Because each glucose unit possesses three alcoholic hydroxyls, cellulose undergoes all the reactions typical of this group, such as nitration, esterification and etherification. By means of these reactions, products of greatly varying physical properties have been prepared (32).

It is noteworthy that the cohesiveness of the cellulose fibre as measured by solubility or degree of swelling increases initially with degree of substitution in the hydroxyl groups, then passes through a maximum (32). This is evidence of the important contribution of Van der

Waal's forces in holding the chains together. Lateral intermolecular forces increase with increasing uniformity of substitution.

B. Softwood Cellulose

Since the investigation was concerned with softwood cellulose fibres, a review of their structure and composition is in order. In a later section, these factors will be related to the papermaking properties of the fibre. Giertz (19) and other Swedish workers (33, 34) have recently made very significant advances in this field.

Figure 8 is a cross-section of a wood fibre with adjoining areas. In wood, the cells or fibres are held together by a cementing intercellular substance called the middle lamella (area iso in Figure 8). Together with the adjacent primary walls (p) it forms the compound middle lamella which has been shown to be 70% lignin (35). In the pulping process, the middle lamella is attacked and dissolved.

The primary wall (p) forms a very thin (0.5 micron) elastic membrane around the fibre. Because it surrounds the fibre, it greatly influences its surface characteristics. The chemical constitution of the primary wall is not well known. It contains a high percentage of lignin as well as highly oriented cellulose and some hemicellulosic material.

The term hemicellulose is applied in a general way to short chain non-cellulosic components of wood. They are distinguished from pure cellulose by their greater solubility in 17.5% caustic soda (under standard conditions) (36). Thus the fraction which is insoluble in 17.5% NaOH is called alpha-cellulose. Of the soluble fraction, that part which is precipitated on acidification is beta-cellulose and the remainder is gamma-cellulose. Present custom loosely refers to the beta and gamma

FIGURE 8

Cross-Section of Wood Fibre with Adjoining Areas

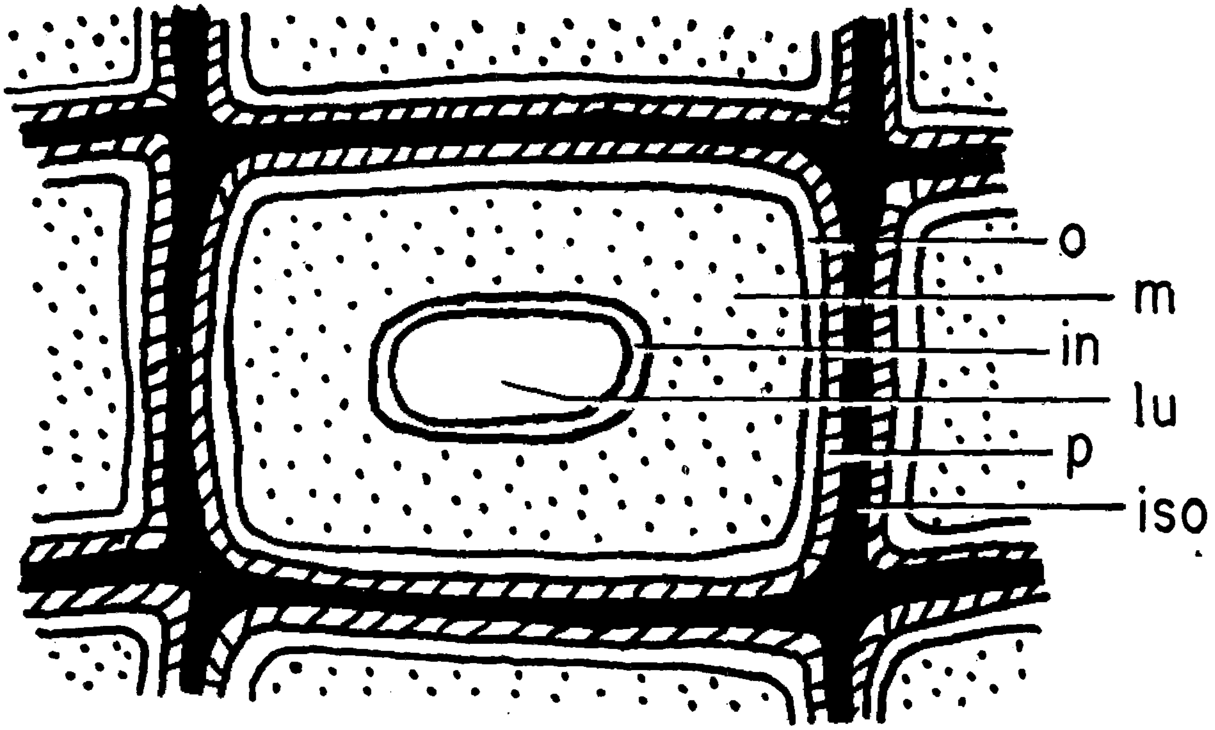
o
m
in
lu
p
iso

fractions as hemicellulose.

The main part of the fibre consists of the secondary wall which can be divided into three layers - outer layer, middle layer and inner layer (o, m, in, respectively in Figure 8). The outer layer, the most highly lignified of the three, is closely related to the primary wall in structure and in function of elastic sheath around the thick middle layer.

The middle layer of the secondary wall is considerably thicker than the outer one and is laminated into zones which differ in composition and arrangement of fibrils. Fibrils are long thin threads, which seem to be parallel units in the cell wall, encircling the fibre axis in the form of spirals of varying pitch. In the inner and outer layers, fibrils are oriented at right angles to the fibre axis while in the middle layer the pitch is from 10 to 30 degrees. The spiral angle becomes steeper with increasing fibre length and the steepness of this angle influences fibre strength. The middle layer consists chiefly of cellulose and hemicellulose with a small amount of lignin.

The boundary between the lumen and the fibre is formed by the inner layer.

Mechanical or chemical action causes the secondary wall to disintegrate into long thin fibrils which spiral loosely around the fibre axis. Widerkehr (37) has compared it to the untwisting of staple textile yarn. Papermakers have long been familiar with these fibrils which are easily detected in the ordinary microscope. Within the last few years, more drastic mechanical action in the form of ultrasonic irradiation has been applied to the fibre. As a result of this treatment, fibrils are divided into still thinner strings or microfibrils (38).

Fibrils observable in the optical microscope are not of uniform thickness and appear to be dependent on the method of disintegration (19). By contrast, electron micrographs show the microfibrils to be truly individual and of uniform thickness; hence they must be considered as fundamental elements in the framework of wood fibres.

Rånby (33) has studied the rod-like particles which result when ultrasonic treatment is carried out after acid hydrolysis. They show the same X-ray diffraction pattern as pure native cellulose, are of the same width as the fine strings and vary in length from 200 to 1000 Å. These findings indicate that the cellulose strings consist of highly crystalline material. Chemical analysis shows them to be chiefly glucosan (19).

Rånby's particles form aqueous colloidal solutions which are coagulated by small amounts of neutral electrolyte and are therefore to be classed as hydrophobic. The sols may be stabilized by means of water-soluble cellulose derivatives such as carboxymethylcellulose. These observations imply that the cellulose particles are non-swelling or only slightly so. By contrast, cellulose fibres show comparatively high water regain.

Interestingly enough the primary wall contains the same cellulose strings (19) as the secondary wall but they are arranged into a tightly cross-woven textile pattern. This accounts for the elastic membrane effect.

In the secondary wall the cellulose strings run parallel and the hollows and capillaries between them are filled with non-cellulosic components: true hemicellulose and lignin. The former is composed of short chain polysaccharides, mannans, xylans and galactans (39). They form a continuous interpenetrating system in the cell wall but without the well-ordered arrangement of the cellulose strings. This explains why hemicellulose content so often correlates with accessibility and swelling.

Purves (61) believes that the hemicellulose fraction contains a certain amount of branched polyoses, which accounts for the high degree of disorder.

Giertz (19) and Rånby (34) have offered strong evidence that the readily-accessible component of cellulose, as determined by acid hydrolysis, and the gamma fraction of cellulose, as determined by the alkali solubility method, are one and the same, and correspond to the interfibrillar material which we have described above as true hemicellulose. From their experiments it would appear that beta-cellulose is simple, degraded cellulose. In support of this hypothesis they point out that holocellulose, which is undegraded delignified wood, has no beta-cellulose.

III. Interfibre Bonding

The investigation reported in this thesis was undertaken with the idea that observations of the effect of freeze-drying on paper properties would allow certain fundamental deductions to be made concerning the mechanism of fibre-to-fibre bonding in paper. Although it is the basis of papermaking, very little is known about interfibre bonding except that it appears to be influenced by almost all the important variables which enter into the manufacture of pulp and paper. For this reason, the following discussion will fall under three general headings which will cover the major steps in the manufacture of pulp and paper:

A. Effect of Pulping on Paper Properties

B. Fibre Preparation

C. Theories of Interfibre Bonding.

A. Effect of Pulping on Paper Properties

Pulp manufacture is the first step in papermaking from wood cellulose. It involves the reduction of the raw material to the fibrous state by chemical treatment, (except for groundwood pulp) which attacks and dissolves the lignin. In the initial stages of the cooking cycle, reaction is mostly confined to the middle lamella, which cements the fibres together, thereby loosening the individual fibres. In the second stage of cooking, delignification of the fibre wall occurs.

The second stage of cooking is extremely critical. Because of the complex association of cellulose, hemicellulose and lignin within the fibre wall, all three components are exposed to the cooking liquors. Of these substances cellulose is most resistant to chemical attack. The hemicelluloses and lignin, however, are both removed to greater or lesser extent. Depending on the relative amounts of each remaining, the papermaking properties of the fibre may be varied over wide limits.

High hemicellulose content is associated with rapid strength development on beating and greater fibre flexibility (40). The amount of residual lignin affects bleaching properties and beating characteristics.

There are other factors affecting papermaking properties which depend on the pulping operation. Thus, the discolouration of paper on ageing is linked both with quantity and quality of hemicellulose (41). Lately, the importance of fibre strength has come to be appreciated (42). Although it is not easy to measure, one would expect it to be influenced by any degradation of the cellulose which occurs during pulping and bleaching. In terms of fibre structure, degradation consists in a weakening or rupture of the cellulose strings which provide longitudinal strength to the fibre.

B. Fibre Preparation

A very important phase of papermaking lies in the preparation of the pulp for the paper machine. This preparation, which is called refining, or more traditionally beating, significantly affects every physical property of the finished product. Essentially the fibres are subject to a combination pounding, squeezing, rubbing and tearing. As a result of such treatment the finished product becomes more dense and the burst and tensile strengths increase to a maximum.

The changes which beating produces in the fibres have been the subject of a number of investigations (8,9,43,44,45). Increase in external specific surface (46) and in swollen specific volume (47) have been correlated with increase in strength properties with beating. Fibrillation and cutting as well as degradation of the cellulose fibres have been shown to occur as a result of beating (14, 48). However, present evidence (19,47,49) indicates that beating contributes towards paper strength mainly through the promotion of fibre-water interaction of which swelling is the principal result. Thus the fibre is altered from a relatively stiff elastic structure to a flexible plastic character.

In terms of fibre structure the following mechanism has been proposed (19) to explain the effect of beating on the fibre. Mechanical action loosens the internal fibre structure:

a) by rupturing the retaining primary wall if it is still present

b) by loosening the lateral cohesion of the fibre, probably by breaking secondary valency forces between the longitudinal elements, so that the hemicellulose is free to swell to a greater extent. Swelling leads to a dispersion of the structure into fibrils and ultimately into the individual units or cellulose strings. The formed fibrils are very probably covered by a thin layer of swollen hemicellulose.

If swelling constitutes an unravelling of the cellulose structure, through the cleaving of secondary valences, then it must be accompanied by an increase in both external and internal surface (13). It should be understood that in the initial stages, fibrillation will not necessarily be visible in the light microscope. Campbell (22) used the term "internal fibrillation" to express the fact that a loosening of the surface fibrils precedes their actual appearance as broken out from the fibre. Thus, increase in swelling and specific surface are complimentary effects both of which provide an appreciably greater opportunity for bonding between fibres.

The importance of fibre plasticity, per se, is illustrated by the fact that a highly fibrillated pulp, as shown by electron micrographs, but very low in hemicellulose, will not form a strong paper (19).

C. Theories of Interfibre Bonding

The subject of interfibre bonding is so intimately related to the subject of fibre preparation that it is impossible to discuss one without the other. In the preceding comments, mention was made of the observed effects of beating on the fibre and on the finished product. In this section, some of the mechanisms, which have been proposed, for the transformation of beating effects into bonding phenomena will be discussed.

Unfortunately, it is not possible to give a clear-cut definition of bonding as it occurs in paper. In a general sense the term refers to the cohesive forces between fibrous elements. For a given pulp, paper density probably provides a good measure of the relative degree of interfibre bonding after various amounts of beating. Paper strength as measured by standard tests is only an indirect measure of bonding since the tests are complex functions of fibre length, fibre size, fibre orientation, fibre stiffness, etc.

The fact that paper can, under special conditions, be made with a density which approaches that of pure cellulose indicates that the association between fibres approaches the limits of molecular dimensions. Furthermore, the bonds between fibres can be broken by the same liquids which swell cellulose. It would seem, therefore, that the same bonds which link cellulose chains within the fibre are also operative between fibres. These are forces of secondary valence.

Widerkher (37) believes that paper strength is due almost entirely to the effect of interlocked surfaces, i.e. frictional forces. Increased density with beating, he attributes to the improved felting properties of the fibres. Most papermakers admit that interfibre friction may be a factor in the strength of dry paper but only a minor one.

It is now believed that the surface tension theory as proposed by Campbell (22) correctly explains the mechanism of bonding. The theory is based on the idea that the affinity of cellulose for water produces what may be termed: a state of two-dimensional solution on the surface of the cellulose crystallites. When two such surfaces are brought together and the water evaporated, the solvated molecules form a randomly crystallized transition layer between the two cellulosic elements.

Campbell further postulates that as drying proceeds in paper, water is held in small layers or drops between two or more fibres. With further drying, the films of water between contiguous fibre elements diminish in thickness and, in consequence, the tension stress in the water increases, thus causing the elements to be brought together with increasing force. As the final layers of water evaporate, intercrystallization occurs which further compacts the fibre structure.

Campbell (22) has shown that the surface tension forces, which are equivalent to an externally applied pressure on the drying sheets, can be very considerable. Furthermore, they increase with decreasing fibre size (fibrillation) and with increasing fibre plasticity (swelling) both of which are promoted by beating.

Present-day knowledge of fibre structure suggests that surface solution of cellulose would be due mainly to the hemicellulosic components of the wood fibre since the cellulose strings are composed predominantly of crystalline material (33) which swells to a very limited degree. Thus, Giertz (19) believes that it is the shrinking of a veritable hemicellulose gel which pulls fibre elements together to form a dense sheet. Dixson's work (50) also supports this view. He added hydrophilic gels to pulp and noted that strength increase was in the order of the water binding capacity of the gel.

IV. Special Methods of Drying Cellulose

The drying of cellulose from the water-swollen state is the final step in most pulping and purification processes. When the cellulose is destined for chemical modification, "drying out" generally has a very undesirable effect on its reactivity (51). The presence of water increases the penetration of reagents into cellulose because systems of cavities within fibres are produced by swelling but do not exist in the dry material (52). The decrease in reactivity has been explained as a "collapse" of the swollen structure with formation of secondary valence bonds between chain molecules within the fibre. "Collapse" on drying is attributed to internal liquid tension in capillary spaces (22, 53). On reimmersion in water some of the new junction points are so arranged that they are not solvated, hence the fibre is not capable of swelling to the same degree (54). The effect of air-drying on the reactivity and swelling capacity of native and regenerated cellulose has been the object of several investigations (51,54,55,56).

The advantage of being able to dry cellulose without "collapse" has been sought by several investigators. Thus Kistler (57) succeeded in preserving the open structure of water-swollen cellophane by solvent-exchanging the water through an intermediary solvent to liquid propane. The latter was removed above its critical temperature with practically no "collapse". However, this aerogel, which was opaque, on being wetted then dried became transparent again and underwent "collapse" to its original dimensions but with less shrinkage than when dried from water. Kistler attributed this latter phenomenon to an increase in rigidity of the cellulose framework due to excessive dehydration.

Assaff, Haas and Purves (13) succeeded in drying cellulosic fibres, with relatively little "collapse", by solvent-exchanging the alkali-swollen mass through methanol to benzene. The accessibility of cellulose dried in this manner was from fifty to one hundred times greater than that of a normal air-dried sample. A determination of total specific surface by N_2 adsorption (58) at -195°C on both air-dried and solvent exchange dried cellulose confirmed the accessibility results. Furthermore, it has been shown that the non-freezing water capacity, which has been defined as the amount of moisture in a saturated fibre which does not freeze when the fibre is cooled below 0°C., is almost twice as great for solvent exchange dried cotton as for air-dried cotton (59).

It is of particular interest to this investigation that freeze-drying has also been used as a method to dry beaten pulp fractions (14). It was observed that subsequent nitration of the pulp proceeded more rapidly than when the fractions were air-dried. Unfortunately, no comparison was made of the actual degree of nitration of freeze-dried and air-dried pulp. It is not impossible that freeze-drying does leave the inner fibre structure in an expanded state. This is one of the questions which this investigation attempts to answer.

V. The Work of Van den Akker

Before presenting the results of this investigation, the work of Van den Akker (2) in this same field should be considered. He presented evidence supporting Campbell's theory of the action of internal tension in water on the formation of fibre-fibre bonds during the drying of paper. His conclusions were based on the observed effect of drying by sublimation, which eliminates surface tension, on the physical properties of paper. Starting with a well-beaten pulp, he found the resulting freeze-dried handsheet to be soft, bulky and to possess low strength and high opacity relative to air-dried paper.

Despite his fragmentary results, Van den Akker's work represents a significant advance in our understanding of interfibre bonding. In the present investigation, an improved method of freeze-drying allowed the attainment of lower moisture content and the significance of such factors as swelling, surface solution and fibrillation were evaluated by carrying out experiments at different degrees of beating.

EXPERIMENTAL PART AND RESULTS

I. Scope of the Investigation

The experimental work which follows is divided into two sections. The first section deals with experiments which were carried out to evaluate in some detail the effect of freeze-drying on the physical properties of paper. The second section describes experiments made on unbonded cellulose fibres to determine the effect of freeze-drying and of other methods of drying on their physico-chemical properties. Each section includes several related but separate experiments which are outlined below.

Effect of Freeze-Drying on Paper

The work of Van den Akker (1) and its significance with respect to the "surface tension theory" was discussed in the Introduction. The present investigation on paper was similar but more extensive in nature. It may be outlined as follows:

1. Development of a rapid and convenient method of freeze-drying large quantities of laboratory handsheets.

2. The effect of freeze-drying on the physical properties of paper was evaluated, first of all qualitatively from visual and microscopic observations on air-dried and freeze-dried paper. Quantitative evaluation was made by comparing the results of physical measurements on both papers. The observations were made at various degrees of beating.

3. Measurements similar to 2. were made on hemicellulose-free pulp.

4. The result of repeated wetting and drying cycles on the paper-making properties of beaten cellulose fibres was determined and the relative

effect of air-drying and freeze-drying on these properties was determined.

An unbleached kraft pulp was used in all the above experiments. A high strength pulp was desirable since it appeared likely that such a pulp would produce the largest differences in the strength properties of air-dried and freeze-dried sheets.

Effect of Freeze-Drying on Cellulose Fibres

As mentioned in the Introduction, there is evidence that the Campbell theory applies to the capillary-held water in cellulose fibres as well as interfibre water (1). The possibility that freeze-drying might leave the fibre with an open structure appears attractive since it would enhance its reactivity. The following experiments were designed to measure some of the physico-chemical changes in fibres which might result from freeze-drying:

1) The sorption isotherms of freeze-dried and air-dried fibres were determined.

2) Helium and Mercury displacement densities were determined.

3) Pore-size distribution curves were determined using a mercury porosimeter.

4) Microscopic examination of the fibres which had been dried in different ways.

Since the above experiments involved sensitive physico-chemical measurements, a relatively pure material was desirable in order to avoid any complicating factors due to the presence of non-cellulosic material. For this reason, the above experiments were carried out on the same sample of bleached sulphite pulp.

II. Effect of Freeze-Drying on Paper

A. Freeze-Drying Technique

The freeze drying of material with a large surface-to-volume ratio, such as laboratory handsheets, required a special "batch" technique. Laboratory handsheets were prepared according to Tappi Standard No. T 205 m-50; after wet-pressing they were peeled off the ferroplates and laid flat on the bottom of a crystallization dish placed in a large vessel containing a dry ice-acetone freezing mixture at -78°C. The sheets froze immediately and were then placed in a large flat-bottomed desiccator inside the "frozen food" compartment of a Philco refrigerator. The bottom of the desiccator was covered with a half-inch layer of powdered calcium chloride to take up the moisture which tended to trap out there because the desiccator rested on the cooling coils of the refrigerator. The sheets were placed horizontally inside the desiccator, supported one on top of the other by small screen wire stands so as to leave a half-inch airgap between them. A length of pressure tubing through a hole drilled in the side of the refrigerator connected the desiccator through a cold trap to a Hyvac pump. The temperature within the compartment was maintained at -10°C to -15°C. Two desiccators each containing ten handsheets could be accommodated in the compartment at once and sublimation drying to a moisture content of 5 to 6% generally took sixty hours.

In the experiments dealing with the effect of freeze-drying on the physical properties of cellulose fibres, instead of handsheets, loose fibre-pads were formed in a Büchner funnel and these were subsequently frozen and put into the desiccator.

B. Effect of Freeze-Drying on the Physical Properties of Paper

1. Experimental

An unbleached kraft pulp was soaked overnight and was beaten in a Valley laboratory beater in duplicate runs to give six 55-gram samples which will henceforth be identified by their respective Canadian Standard freeness. Tappi Standards Nos. T 200 m-45 and T 227 m-50 respectively, were followed for all beater runs and freeness measurements which were made. From each portion, four sets of ten laboratory handsheets were prepared according to Tappi Standard No. T 205 m-50 up to and including the couching operation after which certain variations were introduced in the drying procedure as described below. In all subsequent references to handsheets, it is to be understood that they were formed as above up to the couching operation.

The sets were identified according to their method of drying e.g. ADS-k where k denotes the appropriate freeness and ADS an air-dried sheet dried according to the standard Tappi method, requiring the wet-pressed sheet to be dried with a ferroplate backing and clamped in a ring arrangement which prevents diametric shrinkage. The markings used and their significance were:

a) ADS-k air-dried according to Tappi standard procedure

b) AD-k air-dried on blotters

c) FAD-k frozen at -78°C and kept for one hour at -10°C after which they were allowed to thaw and air-dry.

d) FD-k freeze-dried as described above.

Set FAD was a control on the effect of freezing on sheet formation, this precaution being necessary because of the 8% increase in volume of water on freezing. It should be noted that sets AD and FAD were not pressed onto the blotters and so they were completely free of restraints.

The effect of freeze-drying on paper was evaluated by comparing the results of extensive physical tests for the various sets. The following Tappi Standard tests were carried out in the testing laboratory of the Pulp and Paper Research Institute of Canada after the handsheets had been conditioned at 73°F and 50% relative humidity.

The diameter shrinkage of all sheets which were allowed to dry without tension was measured by carefully marking each one with two pencil points 5.00 ± .06 inches apart immediately after wet pressing. The decrease in this distance was determined when the sheets were dry. Aside from its experimental significance, determination of the diameter shrinkage was necessary in order to calculate the true basis weight of the sheet which was then used to convert the results of the physical test to a standard basis weight.

TABLE I

Paper Tests which Were Carried Out on All Handsheets Throughout this Investigation

Test	Tappi Standard No.	Reported as
Bulk	T 411 m-44	cc./gm.
Bursting Strength	T 403 m-47	Burst Factor
Internal Tearing Resistance	T 414 m-39	Tear Factor
Tensile Breaking Strength	T 404 m-50	Breaking Length
Tensile Stretch	T 457 m-46	% Stretch
Opacity	T 425 m-44	

2. Results

As mentioned by Van den Akker (2), there a number of differences between freeze-dried and air-dried paper which are apparent on inspection. These differences will be discussed in the following paragraphs specifically for sets AD and FD which were both dried without tension.

a) AD

First of all these sheets possessed the usual dark brown colour characteristic of unbleached kraft paper. They presented a rough shrivelled surface with overall cockling and had a pronounced "rattle" when crumpled. All the above properties became more pronounced with degree of beating.

b) FD

In contrast with air-dried paper these sheets were light fawn in colour, evidently due to their greater unbonded area. Furthermore, they had a smooth velvety feel and were completely uncockled regardless of the degree of beating. The absence of rattle was also noted. Despite the apparently lower degree of bonding the FD sets were not difficult to handle. In fact they possessed a certain rigidity due to their extreme bulkiness.

There were no apparent differences between sets AD and FAD. All ADS sheets, of course, were smooth and uncockled but otherwise similar to AD.

Plates I and II are photomicrographs of sheets made with the same sample of unbleached kraft pulp beaten to 300 freeness. Plate I shows an air-dried sample and Plate II a freeze-dried sample. The rough cockled surface of the latter is evident from the variation in focus across the picture, while the bonding density is so great that it is impossible to

PLATES I, II, III

Photomicrographs of Handsheets Made of Unbleached Kraft Pulp Beaten to 300 Freeness

PLATE I

Air-Dried Handsheet (AD) Made of Unbleached Kraft at 300 Freeness. (X 30)

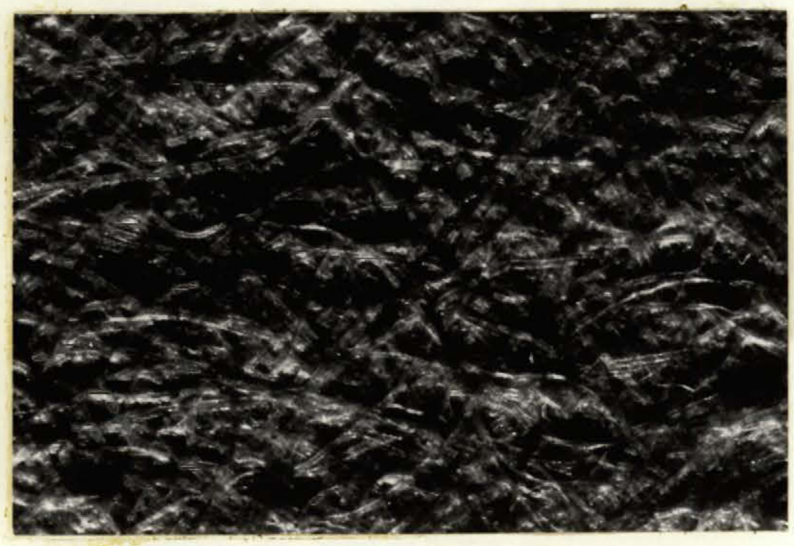

PLATE II

Freeze-Dried Handsheet (FD) Made of Unbleached Kraft at 300 Freeness. (X 30)

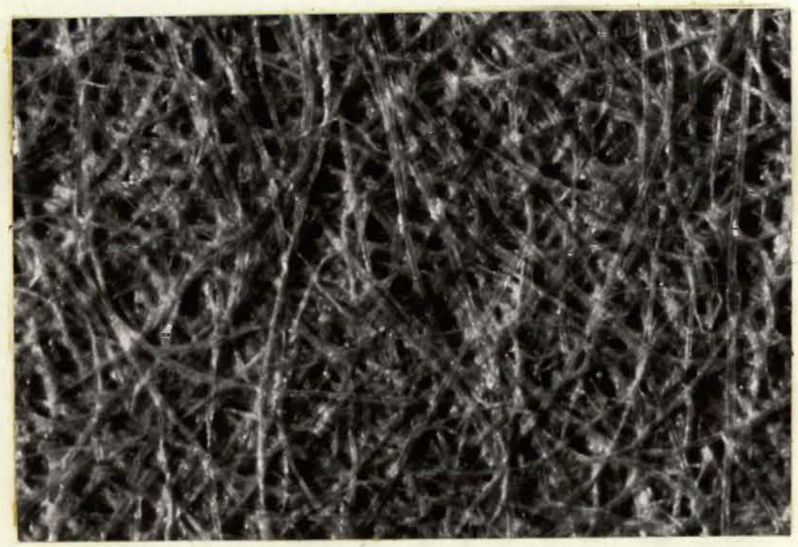

PLATE III

Freeze-Dried Handsheet Made of Unbleached Kraft at 300 Freeness. Not Wet-Pressed. (X 30) pick out individual fibres. By contrast the freeze-dried specimen presents a more even texture in which individual fibres have not lost their identity. The interweaving of fibres may be followed plainly so that the picture suggests a piece of textile material rather than paper.

The low-bonding density of freeze-dried paper is best illustrated by Plate III which pictures a handsheet completely identical with the one in Plate II except that it was not wet-pressed.

The results of the physical tests are recorded in Table II along with the standard deviation of the mean calculated as where is the standard deviation of single observations from the mean value of N observations. The data are plotted against freeness in Figure 1.

3. Significance of Results

Since results are to be evaluated on the basis of the difference between sets AD and FD it is important to note that the standard deviation of the mean is negligible relative to the large differences observed. The standard deviation of the mean for bulk and % shrinkage were of the order of 0.7% hence their differences are also significant.

Set FAD was a control on the effect of water expansion on freezing which would tend to move fibre elements apart. From Figure 1, it is apparent that this factor had a relatively small but real influence on the strength properties of the paper, the FAD curves being always distinct from the AD curves. The data presented therefore show that any loss in strength attributable to ice formation is relatively small as compared with the observed differences in strength between air-dried and freeze-dried paper.

Unfortunately, this control did not distinguish between the effect

TABLE II

Results of Physical Tests on Air-Dried and Freeze-Dried Paper

Treatment	Bulk cc./gm.	Burst Factor	Tear Factor	Breaking Length	Stretch %	% Diam. Shrinkage
ADS-700	2.03	13.9 ± .317	2.10 ± .0652	2680 ± 160	2.0	0
AD -700	1.95	16.0 ± .313	1.94 ± .0652	2270 ± 156	3.2	1.20
FAD-700	2.34	9.8 ± .291	1.58 ± .0424	1690 ± 31	2.2	1.70
FD -700	2.60	2.0 ± .08	0.51 ± .0212	880	.8	1.10
ADS-636	1.54	61.0 ± .959	1.38 ± .132	7410 ± 186	3.9	0
AD -636	1.63	61.8 ± .750	1.62 ± .0389	6060 ± 357	6.3	2.62
FAD-636	1.85	48.2 ± .877	2.14 ± .0415	4500 ± 214	5.3	2.54
FD -636	2.51	8.5 ± .535	1.27 ± .0500	1310 ± 33	1.7	1.06
ADS-544	1.43	68.8 ± 1.77	1.28 ± .0209	8550 ± 342	4.0	0
AD -544	1.56	77.6 ± .910	1.60 ± .0695	6700 ± 277	7.6	3.42
FAD-544	1.68	64.7 ± 1.19	1.69 ± .0360	6240 ± 292	6.0	2.42
FD -544	2.34	17.2 ± 1.16	1.88 ± .0565	2210 ± 160	3.2	1.05
ADS-517	1.39	73.0 ± 1.10	1.26 ± .0287	9500 ± 328	4.1	0
AD -517	1.48	80.0 ± 1.09	1.64 ± .0380	6820 ± 286	7.1	3.74
FAD-517	1.60	74.2 ± 1.57	1.58 ± .0261	7390 ± 224	6.8	2.76
FD -517	2.30	22.7 ± .97	2.07 ± .0645	2270 ± 34	3.2	0.94
ADS-361	1.30	84.2 ± 1.24	1.10 ± .0193	11360 ± 256	4.6	0
AD -361	1.47	91.6 ± 1.08	1.44 ± .0367	9420 ± 116	8.9	3.86
FAD-361	1.59	80.2 ± 1.15	1.51 ± .0470	7120 ± 270	7.8	3.86
FD -361	2.30	30.7 ± 5.92	2.22 ± .126	2770 ± 65	4.2	1.22
ADS-167	1.24	83.4 ± 1.13	.98 ± .0133	11000 ± 330	4.1	0
AD -167	1.46	98.6 ± .990	1.47 ± .0100	7980 ± 320	10.3	6.05
FAD-167	1.49	84.6 ± 1.74	1.44 ± .0173	7590 ± 397	8.6	4.82
FD -167	2.27	38.4 ± 1.47	2.36 ± .0670	3520 ± 110	4.5	1.3

FIGURE 1

Results of Physical Tests on Freeze-Dried and Air-Dried Paper. Test Values plotted vs. Freeness.

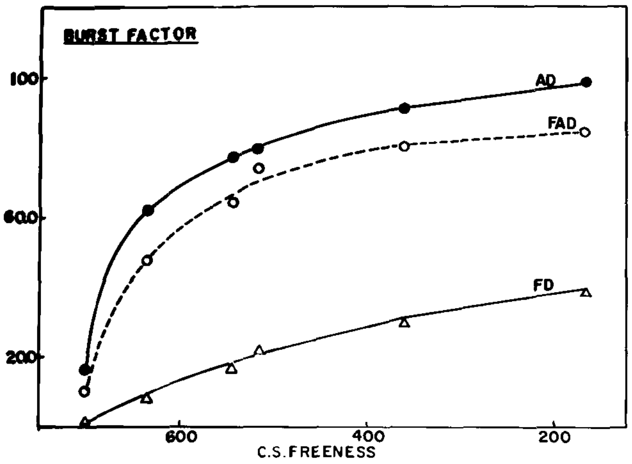
BURST FACTOR
100
60.0
20.0
AD
FAD
FD
600
400
200
C.S. FREENESS

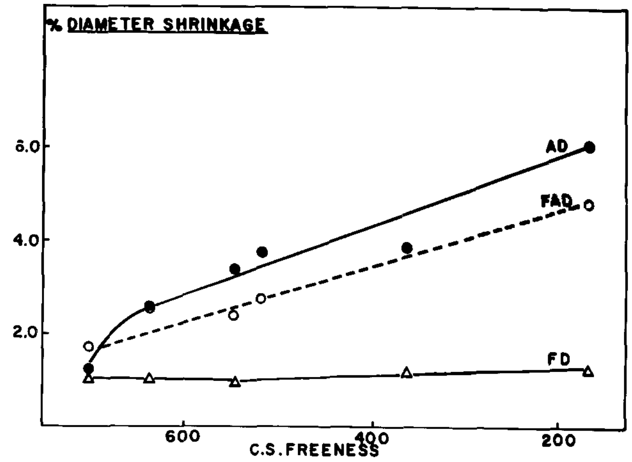
% DIAMETER SHRINKAGE
6.0
4.0
2.0
AD
FAD
FD
600
400
200
C.S. FREENESS

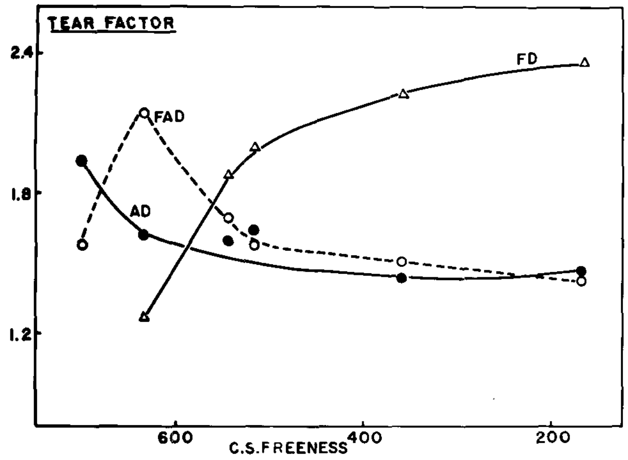
TEAR FACTOR
2.4
1.8
1.2
FD
FAD
AD
600
400
200
C.S. FREENESS

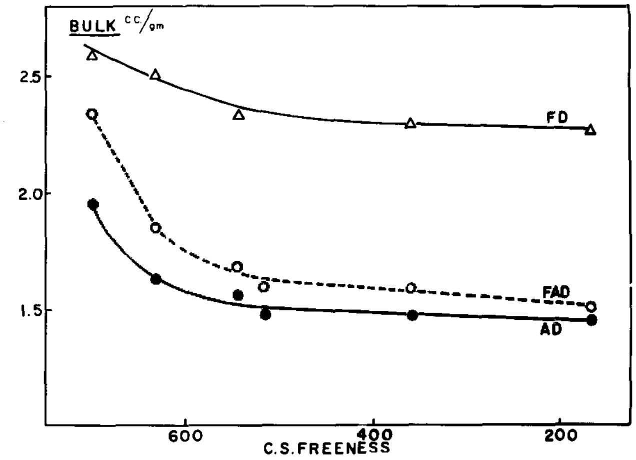
BULK cc/gm
2.5
2.0
1.5
FD
FAD
AD
600
400
200
C.S. FREENESS

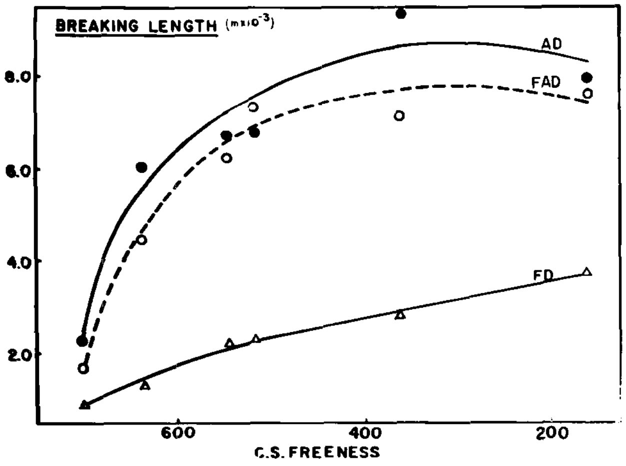
BREAKING LENGTH (m×10⁻³)
8.0
6.0
4.0
2.0
AD
FAD
FD
600
400
200
C.S. FREENESS

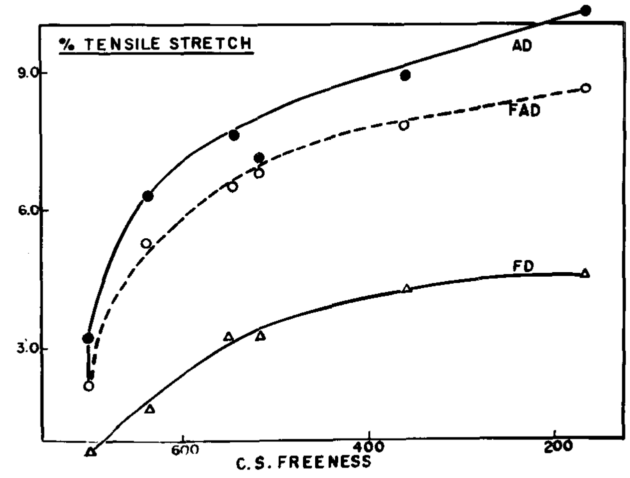
% TENSILE STRETCH
9.0
6.0
3.0
AD
FAD
FD
600
400
200
C.S. FREENESS

of freezing on the formation of paper and on the fibre itself. In order to evaluate the latter a sample of the same pulp at about 380 freeness was divided into two parts, one of which was immediately formed into handsheets with the marking ADS. The other was quick-frozen at -70°C., was maintained for one hour at -12°C., and then was placed in a beaker of water overnight. After five minutes in the British disintegrator, this second part was also made into handsheets marked FADS. The results of the paper tests are recorded in Table III.

TABLE III

Marking	ADS	FADS
Bulk	1.34 ± 0.00553	1.40 ± 0.00171
Burst Factor	89.6 ± 0.936	79.8 ± 0.630
Tear Factor	1.02 ± 0.0114	1.18 ± 0.0354
Breaking Length	11,400 ± 162	10,850 ± 108
% Tensile Stretch	3.9	3.9

While these results cannot be directly compared with sets AD and FAD because the sheets were dried under tension, nevertheless, it would appear that ice formation has an adverse effect on the papermaking properties of the fibre. This conclusion, which was arrived at by Van den Akker also, can only be tentative until confirmed by more sensitive chemical or physical tests.

The data of Table II show the strength properties, (excepting tear factor), of the sheets which were dried by sublimation, to be from 1/3 to 1/7 lower than those of the air-dried samples. The low strength and high bulk of the FD sets clearly are evidence of a low degree of bonding between fibres. It should be understood however that because the freeze-dried handsheets were wet-pressed, some of the benefits of beating were bound to show up, e.g. a slight increase in density with degree of beating. The noteworthy fact is that the difference between the properties of AD and FD increased with beating, particularly in the initial stages. Paper properties which depend on density of bonding such as bulk, burst and tensile, always show their steepest rise during this period of beating (3). It would seem therefore that sublimation-drying is lacking in some factor which promotes bonding.

In this regard the results of tear tests are particularly interesting. Tear factor varies inversely as bonding density, often after an initial increase (4). Stated differently, as the sheet increases in cohesion and stiffness as a result of beating, the tearing forces are concentrated on a smaller area with the result that lower tearing values are obtained. The increasing tear factor for freeze-dried sheets is evidence of slightly increasing bonding with beating but necessarily slight and intermittent throughout the sheet otherwise it would fall off rapidly.

Another interesting result is the nearly constant diameter shrinkage of the freeze-dried sets. It would seem that their shrinkage mechanism is almost independent of the development which occurs in the beater which, again, is evidence in favour of the surface tension forces being responsible for bonding in paper, since their effectiveness increases with beating. The observed shrinkage of the freeze-dried handsheets is probably due to the natural contraction of the fibres when their moisture content falls below the value which corresponds to saturation, or 100% relative humidity.

4. Optical Properties of Freeze-Dried and Air-Dried Paper

a) Introduction

The optical properties of paper are determined by the relative amount of light reaching the paper and the manner in which the incident light is absorbed, reflected and transmitted by the paper. Absorption of light refers to the capacity of paper for converting light energy into other forms of energy, usually thermal. The absorption coefficient which measures this capacity is influenced by the chemical nature of the constituents and to a lesser extent by the degree of bonding and the index of refraction of the sheet.

When light strikes a smooth, optically flat surface, a high percentage of the incident light is reflected at an angle equal to the angle of incidence. This is known as mirror reflection. In the case of a perfectly matte surface, the light penetrates beyond the surface into the body of the material where the light is scattered approximately equally in all directions so that it emerges as a semicircle of diffused light. Most of the light reflected from a paper surface is diffused light.

In this investigation a Steele opacimeter (5) was used to measure the diffuse reflectance of laboratory handsheets. The following quantities were determined:

(i) R_o, the reflectance when a single sheet is backed by a black cavity.

(ii) R_∞, the reflectance of a pad of test paper thick enough so that no change in reflectance occurs when the backing is doubled. This quantity is known as brightness.

(iii) Printing Opacity, which is defined as R_o/R_∞

(iv) Apparent scattering coefficient (S') which is derived from the theory of Kubelka and Munk (6). Parsons (7) has shown that S' is a linear function of the specific surface or unbonded area per unit of mass of the paper.

b) Calculation of Apparent Scattering Coefficient

The Kubelka-Munk theory is based on the definition of two fundamental optical constants: the specific scattering coefficient (S) and the specific absorption coefficient (K). The theory relates the reflectance of thin homogeneous layers of material to these fundamental quantities. As applied to paper, the K value is determined mostly by the chemical nature of the paper while S is a function of sheet structure. It is to be noted that in applying the theory in this particular case, it is assumed that K is independent of the degree of beating and of interfibre bonding.

If the scattering coefficient S is multiplied by X (the thickness of the paper), the product, SX, is the scattering coefficient of the paper. For convenience X is generally expressed in terms of weight instead of thickness. Thus, following Parsons (7), the value $\frac{SX}{W}$, where W is the basis weight in grams per square metre, will be used to characterize the reflectance of a particular set of sheets. The quantity is termed the apparent scattering coefficient (S').

Generally SX values are obtained by interpolation from graphs given by Steele (6) which show the interrelationship between brightness or reflectivity (R_∞), reflectance (R_0), printing opacity (R_0/R_∞) and scattering power SX. These graphs are based on the equation

$$R_o = \frac{R_\infty (\varepsilon^{\beta SX} - 1)}{\varepsilon^{\beta SX} - R_\infty^{2}} \qquad (1)$$

where $\beta = \left(\frac{1}{R_\infty} - R_\infty \right)$, $\varepsilon = 2.71828$

and R_0 and R_∞ are absolute values. Unfortunately, the data in question were not in the range of these graphs and SX values were obtained directly from equation (1) by rearranging it so that SX was an explicit function of R_0 and R_∞. On rearrangement, equation (1) becomes:

$$SX = \frac{1}{\beta} \log_\varepsilon \frac{(1 - R_0 R_\infty)}{(1 - R_0/R_\infty)} \qquad (2)$$

c) Results and Discussion

The measured and calculated quantities for each set are listed in Table IV. Of these data only the apparent scattering coefficients are not influenced by basis weight, hence only these quantities will be compared.

Figure 2 shows a plot of apparent scattering coefficient vs. freeness. The first fact to be noted in this plot is the almost identical values of S' for sets ADS and AD at the different freeness values, although the basis weights are quite different due to the shrinkage of the latter set. The second fact to be noted is the decline of the S' curve with beating for air-dried paper. Thus, in the first 30 minutes of beating, interfibre bonding more than absorbs the increase in total surface which is produced by beating.

The maximum in the FD curve is particularly significant and represents a balance between increasing total surface produced by beating and increasing bonded area. The latter is reflected in the slowly increasing strength values of freeze-dried sheets with beating. However, the important feature is that initially S' varies oppositely for freeze-dried and air-dried

TABLE IV

Optical* Properties of Freeze-Dried and Air-Dried Paper

Sample	Basis Weight gms/m^2	% Reflectance (R_0)	Brightness % (R_∞)	Opacity (R_0/R_∞)	App. Scatt. Coefficient per gram
ADS-700	60.9	46.0	47.1	97.7	.0338
AD -700	59.9	44.8	46.3	96.8	.0314
FAD-700	61.9	44.6	45.8	97.7	-
FD -700	60.4	49.4	50.6	97.5	.0373
ADS-636	60.0	50.2	42.0	95.7	.0245
AD -636	65.2	40.8	42.2	96.7	.0253
FAD-636	59.4	43.2	44.4	97.3	-
FD -636	59.4	52.5	53.5	98.2	.0442
ADS-544	64.4	37.4	39.7	94.3	.0188
AD -544	68.2	38.1	39.9	95.2	.0204
FAD-544	66.5	41.9	42.9	97.7	-
FD -544	65.1	53.6	54.0	99.4	.0512
ADS-361	65.6	36.2	38.3	94.5	.0185
AD -361	69.5	35.3	37.4	94.4	.0171
FAD-361	70.0	40.3	41.8	96.4	-
FD -361	66.5	54.6	55.2	99.0	.0505
ADS-167	65.2	34.7	37.1	92.5	.0168
AD -167	72.4	32.4	33.5	96.6	.0172
FAD-167	76.5	38.5	39.1	98.6	-
FD -167	76.7	57.3	58.3	98.3	.0437

* Reflectance, brightness and opacity are referred to MgO standard.

The scattering coefficient is an absolute value.

FIGURE 2

Results of Optical Measurements on Freeze-Dried and Air-Dried Paper.

Per cent Brightness, Printing Opacity and Scattering Coefficient

vs. Freeness

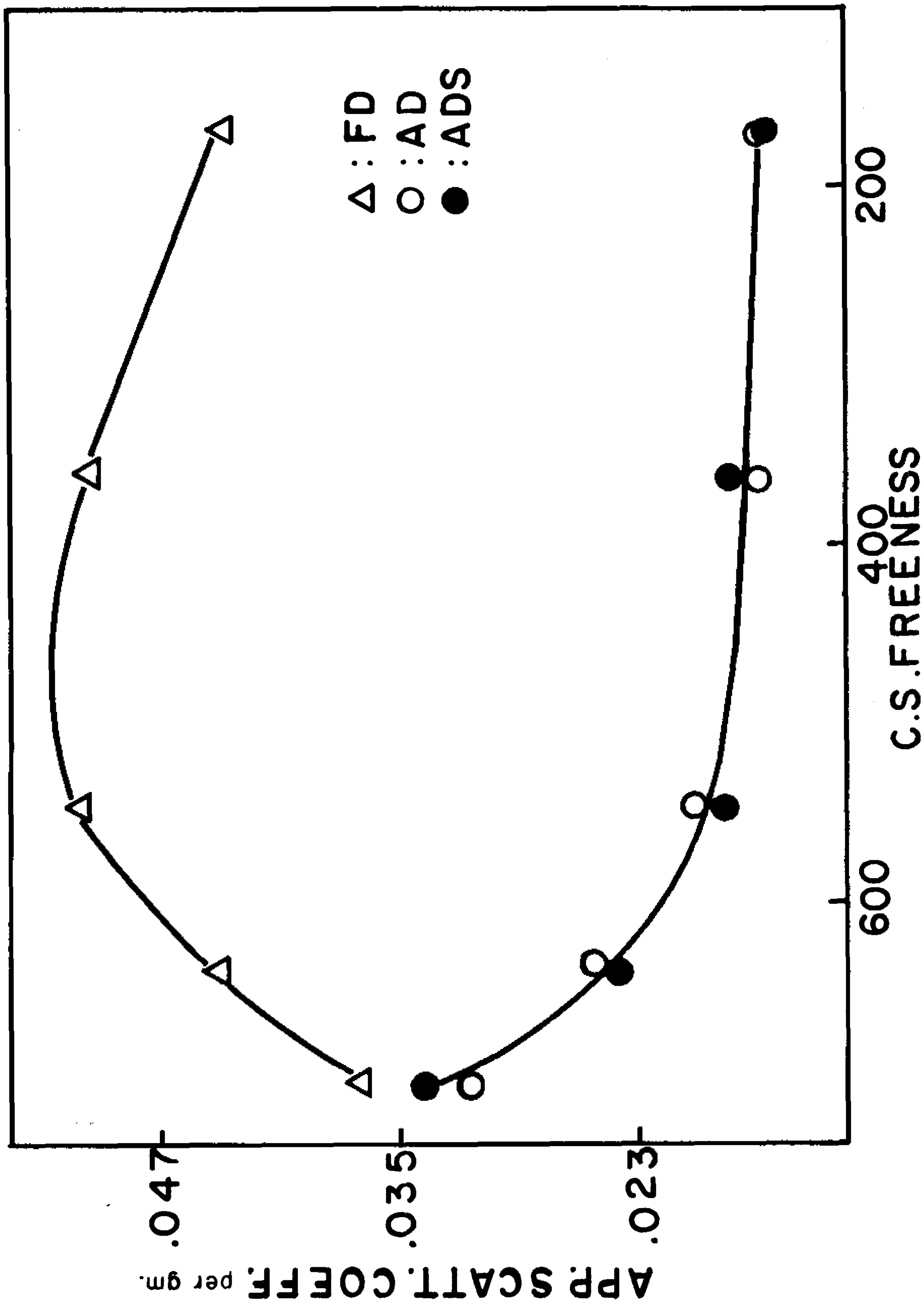
APP. SCATT. COEFF. per gm.
.047
.035
.023
C.S. FREENESS
600
400
200
Δ : FD
○ : AD
● : ADS

which is in accord with our previous conclusion that freeze-dried sheets possess a low degree of bonding.

C. Effect of Freeze-Drying on Paper Made from Alkali-Extracted Pulp

This experiment suggested itself quite naturally from the results of the preceding one. Freeze-dried sheets were indeed relatively unbonded but not completely so. Because of the well-known importance of hemicellulosic materials in promoting interfibre bonding, it was decided to determine what effect their removal would have on the diffuse network of interfibre bonds in freeze-dried paper.

1. Experimental

A sample of commercial unbleached kraft never dried pulp was beaten in a Valley laboratory beater to give five 55-gram samples which will henceforth be identified by their freeness.

a. Alkali Extraction

The extraction procedure was as follows: the wet pulp was formed into 8 pads of 5 grams each; a moisture determination on a control pad gave a close estimate of the total moisture held by the pads. This value was then used to calculate what weight of water had to be added to 1600 ml. of 26.3% NaOH in order to give a 17% by weight caustic soda solution when all moisture was taken into account. The amount of water to be added (generally 700 or 800 ml.) and the wet pads were placed in a 4-litre suction flask and the pulp deaerated. The flask was then clamped in a constant temperature water-bath maintained at 25.0 ± .1°C. along with a flask containing 1600 ml. of deaerated 26.3% caustic soda solution. When the two had attained the temperature of the bath, the caustic soda solution was added to the pulp and suction was immediately applied while the flask was momentarily removed from the bath and was given a vigorous shaking. The purpose of the suction was to maintain a relatively oxygen-free atmosphere over the alkali mixture to prevent oxidative degradation. Once evacuated, the flask was isolated from the aspirator pump by means of a pinchclamp and the extraction was allowed to proceed for one hour with shaking at fifteen-minute intervals.

After this period, the extracted pulp was rapidly filtered in a battery of Büchner funnels each covered with a 180-mesh stainless steel screen backed by a cotton cloth. Successive washings were carried out: twice with 17% NaOH to flush out any remaining alkali-soluble material, then with water, dilute acetic acid and finally water once more. The resulting slurry, which was barely acid, was disintegrated for 15-25 minutes in the British disintegrator to give a more uniform papermaking suspension by breaking up small fibre clots which tended to form during the washing procedure.

The per cent by weight of bone-dry material lost in each extraction was calculated from consistency measurements on the diluted stock before and after extraction.

It should be noted that the alkali concentration of 17% and the general procedure approximated Tappi Standard No. T 203 m-44 for the determination of alpha-cellulose, two important variations being: i) the samples of varying freeness were not allowed to dry before treatment with sodium hydroxide, ii) the extractions were carried out at 25.0°C instead of the recommended 20°C. The effect of these variations would seem to be considerable as evidenced by the results stated in Table V showing that increasing amounts of material were removed as the degree of beating increased. Although the division of cellulose into alpha, beta and gamma fractions on the basis of alkali solubility is purely empirical, it has been observed that this classification is only slightly affected by beating (8), hence the results of Table V are unusual both because of the variation with beating and because the normal value for an unbleached kraft (no account being taken of the lignin present) is from 8 to 12% (10).

TABLE V

Amount of Alkali-Soluble Material Removed from each Sample

Beating Time min.	Freeness Candn. Std.	% Loss on Dry Weight of Pulp
0	696	-
15	629	7.5
31	517	11.5
68	158	17.4
82	50	26.2

The interesting observation was made that all samples had approximately the same freeness after extraction and the value corresponded to that of an unbeaten sample. This corresponds to Giertz's (19) finding that a highly crystalline cellulose, even when extensively fibrillated, possesses very little "wetness".

b. Formation of Handsheets

From each sample the following sets of ten handsheets were formed in the same manner as described in section A.1; the H in the label refers to the extracted hemicellulose-free pulp:

i)	H•AD-k	alkali-treated pulp, air-dried on blotters
ii)	H•FD-k	alkali-treated pulp, freeze-dried

iii) AD-k air-dried on blotters

Difficulty was experienced in peeling off the wet H•AD-k and H•FD-k sheets from their ferroplates after wet-pressing. To overcome this difficulty, these sheets were covered with a filter paper so that the ferroplate was not in direct contact with the surface. The filter paper was easily removed after pressing without damage to the sheet.

The effect of freeze-drying and of hemicellulose removal was evaluated by comparing the results of Tappi Standard tests for the above sets. The same tests as outlined in section A.1 were carried out.

2. Results

Once again there were a number of differences immediately apparent between the H•AD and H•FD sets, the most important being the completely unbonded condition of the freeze-dried sheets. Set H•FD-696 was a gossamer-like felting of fibres without bonding or rigidity which could not even support its own weight. Individual fibres could be removed with tweezers without difficulty. With increased degree of beating, the H•FD sets increased in density and became progressively lighter in colour but were still completely unbonded. These changes were probably the results of fibrillation and cutting.

Handsheets H•AD were coarse and linen-like in appearance. Large-scale cockling was absent but their surfaces were very uneven.

Plate IV shows photomicrographs of H•AD-696, H•FD-696, AD-696 and of H•AD-353, H•FD-353, AD-353. It is interesting to compare the corresponding sheets made of extracted pulps where differences in density are quite apparent as well as the open structure of the freeze-dried sheets.

The results of the paper tests are recorded in Table VI. Because of the very large differences between sets, it was not deemed necessary to

PLATE IV

Photomicrographs of Handsheets from "Alkali-Extraction" Experiment

AD-696

AD-300

H·AD-696

H·AD-300

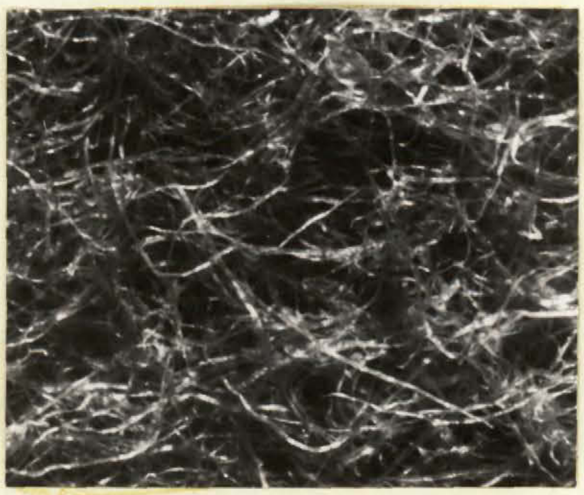

H·FD-696

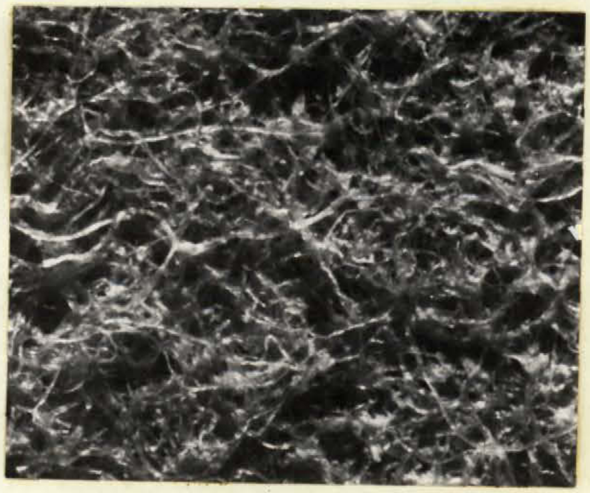

H·FD-300

TABLE VI

Results of Physical Tests for Sets AD, H•AD and H•FD

Treatment	Bulk cc/gm	Burst Factor	Tear Factor	Breaking Length	Stretch %	% Diam. Shrinkage
AD-696	1.84	.575	1.84	5640	4.98	2.2
H•AD-696	2.77	.079	0.827	1070	2.7	2.8
H•FD-696	5.32	.028	0.086	—	-	2.9
AD-629	1.60	.904	1.31	9040	5.95	2.8
H•AD-629	2.74	.0689	0.868	1350	2.68	3.3
H•FD-629	5.27	.0170	0.081	—	-	2.9
AD-517	1.77	1.04	1.37	9000	6.92	3.6
H•AD-517	2.37	.066	0.641	1102	3.56	4.9
H•FD-517	3.95	.0121	0.096	—	-	3.4
AD-353	1.54	1.07	1.36	9140	7.90	4.2
H•AD-353	2.41	.0822	0.646	1230	4.25	6.8
H•FD-353	3.82	.0183	0.117	—	-	3.6
AD-50	1.20	.934	1.40	6900	12.73	10.4
H.AD-50	2.12	.0861	.585	1240	4.86	12.9
H•FD-50	3.73	.0132	.157	—	-	4.4

calculate the standard deviation of the mean. Furthermore, the results for sets H•FD, except for diameter shrinkage and possibly bulk also, are simply orders of magnitude as these sheets could not be properly tested by the standard methods.

Figures 6 and 7 are plots of % diameter shrinkage and bulk respectively, vs. freeness.

3. Significance of Results

The effect of alkali-solubles or hemicelluloses, as we have defined them, on the strength characteristics of paper was reviewed in the introductory part and correlated with the surface tension theory. The present

FIGURES 6, 7

Per Cent Diameter Shrinkage and Bulk
vs. Freeness for AD, H•AD and H•FD

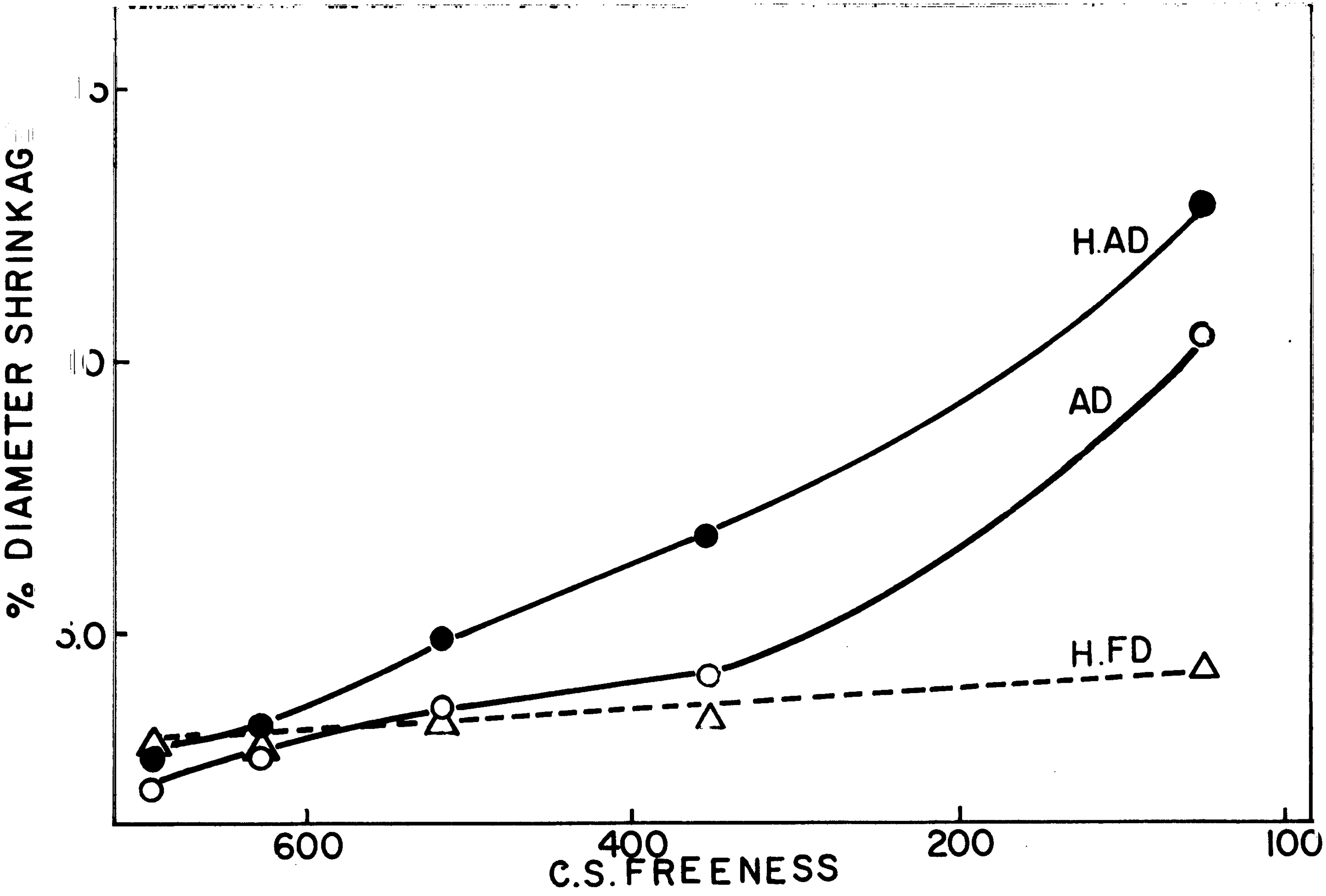
% DIAMETER SHRINKAG
15
10
5.0
H.AD
AD
H.FD
600
400
200
100
C.S. FREENESS

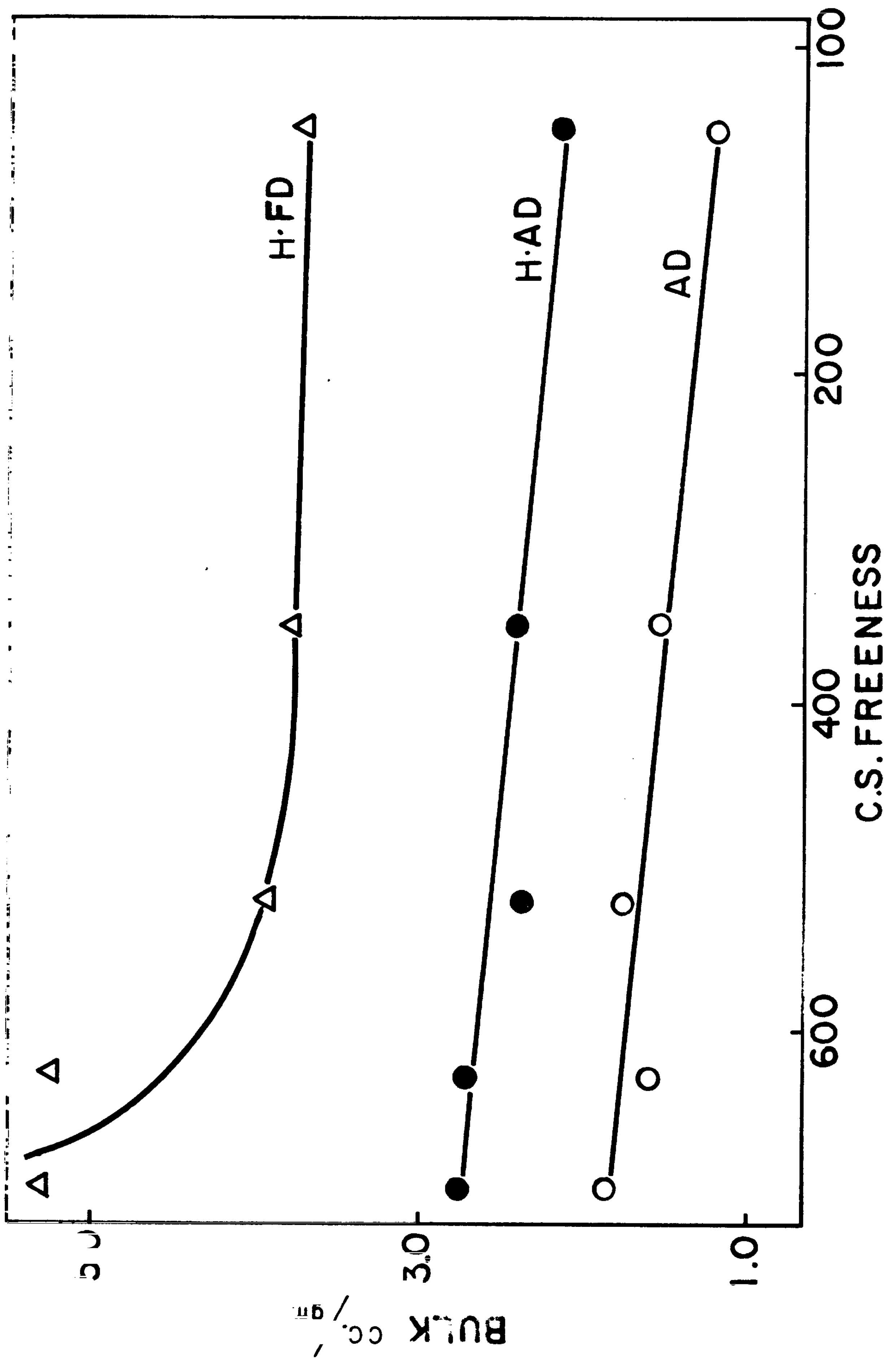
H·FD
H·AD
AD
100
200
400
600
C.S. FREENESS
1.0
3.0
BULK cc/gm

experiment provided a rather significant illustration of their importance. Whereas the freeze-dried handsheets, prepared in section A, possessed all the subjective properties of paper, extracted freeze-dried handsheets could not properly be called paper. The word "felt" better described them. It would appear that the superficial bonding which was present in the FD sheets was due to the ability of the hemicelluloses to make the fibre soft and plastic and to maintain on the fibre surface through their hydrating influence, a layer of "bound" (non-freezing) water. At points of close fibre-to-fibre contact (the more plastic the fibres the greater the degree of contact) this non-freezing water induced bonding according to the surface tension mechanism. Fibres of high alpha-cellulose content are relatively stiff and non-swelling (11) and their surface is deficient in those materials which promote solution. On the basis of the surface tension theory one would expect such fibres to be most unsuitable for papermaking and indeed they are.

A noteworthy fact is the greater diameter shrinkage of the H•AD sets relative to the AD sets as shown graphically in Figure 6. It would appear that the forces of surface tension are equally operative with extracted pulps. However, because of the greater rigidity of the fibres, compression occurs mainly in the lateral direction and only to a small degree perpendicular to sheet surface. Compactness in the latter direction corresponds to high density of bonding and is greatly dependent on fibre plasticity (cf. Figure 7).

While the removal of increasing amounts of material from each sample did not affect the significance of the results, nevertheless, the phenomenon is worthy of note. Although the method used was not designed for accurate measurements, the differences are such as to be out of the range of experimental error.

Unquestionably the use of an undried sample enhanced the reactivity of the beaten pulp over that of a dried sample (16). Furthermore, since beating promotes swelling (11, 12) which corresponds to large increases in total surface (13) then one should expect reactivity to increase with degree of beating. This appears to be particularly true of unpurified pulps, for Bryde and co-workers (14) observed significant increases in low molecular weight material when unbleached sulphite pulp was beaten. There is other evidence of increased reactivity resulting from beating of a pulp, but in all cases the pulp was not allowed to dry before measurements were carried out (17).

An accurate explanation of this phenomenon is dependent on a knowledge of the distribution and structure of hemicellulose in the fibre. In this regard, McKinney (15) puts forth the interesting hypothesis that the low reactivity of sulphate pulps is due to the formation of new bonds in the fibre during sulphate cooking. Hemicellulose-lignin linkages are broken in sulphate digestion and the hemicellulose groups linked up again with other parts of the hemicellulose. Possibly these new cross-links are sufficiently weak to be ruptured by mechanical action?

D. Cyclic Drying of Paper

It is general knowledge among papermakers that a strong paper cannot be made from an unbeaten pulp under normal conditions; even a beaten pulp, once dried, must be given mechanical treatment before it is again suitable for papermaking. The present experiment was designed to evaluate quantitatively the effect of repeated wetting and drying on the papermaking properties of pulp and also to compare the effect of air-drying and freeze-drying on these properties.

1. Experimental

The starting material for this experiment was an unbleached kraft pulp which had never been allowed to dry after "cooking". The pulp was beaten in a Valley laboratory beater to give six 60-gram samples which will henceforth be identified by their freeness.

From each sample three sets of ten handsheets were prepared. It was arranged that each sheet should undergo two formations on the wire of the sheet-machine, yet each set was made of fibres which had undergone a different number of wetting and drying cycles. Thus, from the fraction of freeness 528 the following sets of ten handsheets were prepared:

(AD)-528 After the wet fibre web had settled on the wire of the British sheetmaking machine, the drainage valve was closed and the fibres were diluted to full deckle, stirred and the sheet was reformed. Afterwards it was couched and pressed in the usual manner, then it was peeled off the ferroplate and was allowed to air-dry at 50% relative humidity and 73°F.

AD^2-528 After a single formation on the wire of the sheet-making machine the set was couched, pressed and dried as the previous set. When dry, the sheets were soaked in water for 24 hours, were disintegrated for ten minutes, and then were formed again. This set, therefore, underwent two wetting and drying cycles.

AD^4-528 The same procedure as outlined for AD^2-528 was followed except that, after the first cycle, the second and third cycles were accomplished by placing the dry sheets on a water surface for one minute during which time they were thoroughly wetted. After this wetting they were laid between wet blotters for 24 hours or more after which they were air-dried. The last cycle was carried out as described for AD^2-528. Samples 528, 375 and 265 were put through the above procedure.

From samples 644, 447 and 190, sets (AD)-k, FD•AD-k, FD^3•AD-k were prepared from each, where, as indicated in the markings, freeze-drying replaced all but the last drying cycle.

All sheets were tested as described in section B.1.

2. Results

a) Air-Drying Cycles

The results of the various tests are listed in Table VII and plotted against the number of drying cycles in Figure 3. The standard deviation of the mean for the values in Table VII, as well as those for Table VIII, which will follow, are of the same order of magnitude as those listed in Table II of section B.2, i.e. ± 0.7% for bulk and diameter shrinkage, ± 2% for burst, ± 4% for tear and ± 5% for tensile. These are maximum values.

TABLE VII

Results of Physical Tests for Sets (AD), AD^2, AD^4

Treatment	Bulk cc/gm	Burst Factor	Tear Factor	Breaking Length	Stretch %	% Diam. Shrinkage
(AD)-528	1.53	1.14	1.46	6860	6.5	3.7
AD2-528	1.48	.796	1.67	5860	5.6	2.7
AD^4-528	1.55	.622	2.05	5960	5.3	2.1
(AD)-375	1.50	1.19	1.50	8460	9.3	5.1
AD^2-375	1.45	.834	1.78	5280	6.1	4.0
AD^4-375	1.57	.680	2.22	5620	6.7	2.9
(AD)-265	1.41	1.14	1.43	5860	9.8	6.5
AD^2-265	1.42	.911	1.80	5720	8.2	4.4
AD^4-265	1.49	.701	1.81	5240	7.2	2.7

FIGURE 3

Results of Physical Tests for Air-Drying Cycles.

Test Value vs. Number of Cycles.

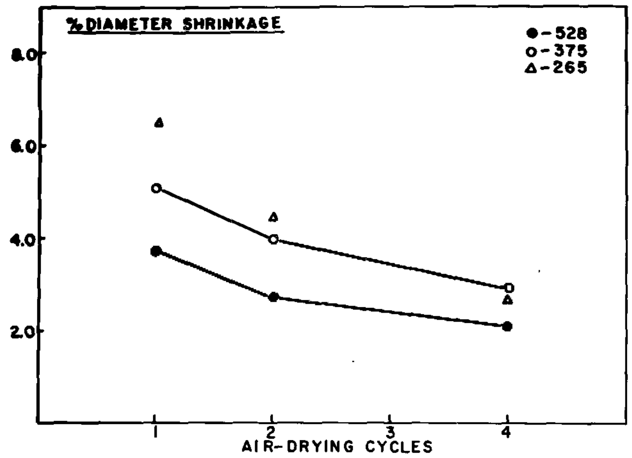
% DIAMETER SHRINKAGE
● - 528
○ - 375
△ - 265
8.0
6.0
4.0
2.0
1
2
3
4
AIR-DRYING CYCLES

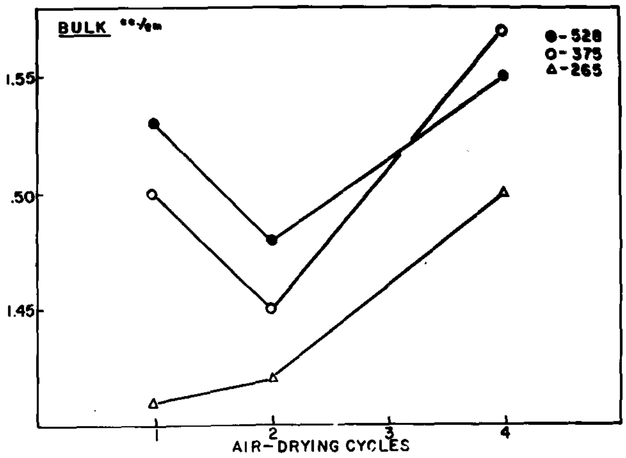
BULK cc/gm
● - 528
○ - 375
△ - 265
1.55
.50
1.45
1
2
3
4
AIR-DRYING CYCLES

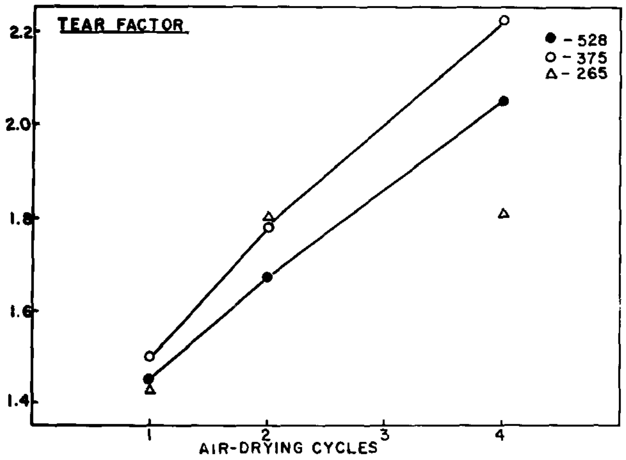
TEAR FACTOR
● - 528
○ - 375
△ - 265
2.2
2.0
1.8
1.6
1.4
1
2
3
4
AIR-DRYING CYCLES

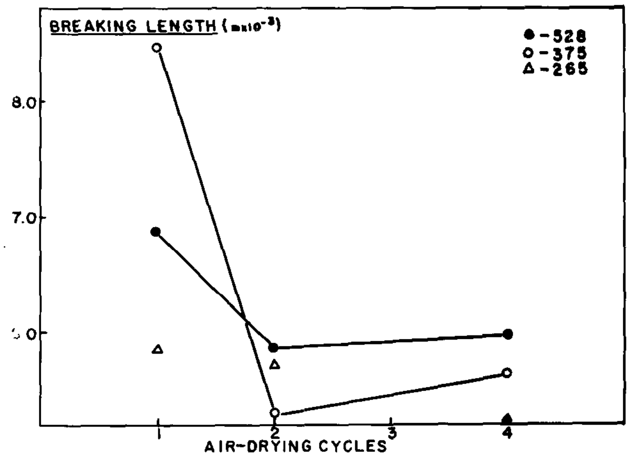
BREAKING LENGTH (m x 10⁻³)
● - 528
○ - 375
△ - 265
8.0
7.0
6.0
1
2
3
4
AIR-DRYING CYCLES

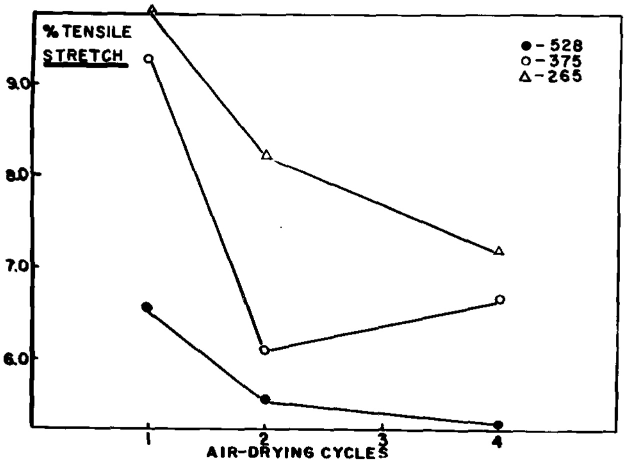
% TENSILE STRETCH
● - 528
○ - 375
△ - 265
9.0
8.0
7.0
6.0
1
2
3
4
AIR-DRYING CYCLES

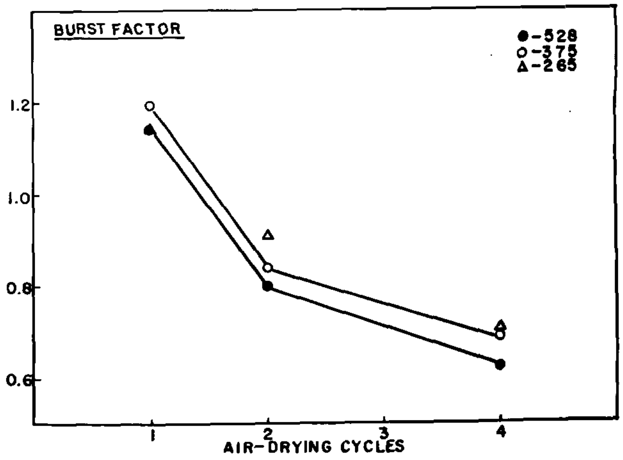
BURST FACTOR
● - 528
○ - 375
△ - 265
1.2
1.0
0.8
0.6
1
2
3
4
AIR-DRYING CYCLES

As expected, burst factor, tear factor and diameter shrinkage vary regularly with the number of cycles. The minimum in the bulk curves for samples 528 and 375 should be interpreted with care for, although the values are significant, the sheets of the first cycle were highly cockled relative to those of the second and fourth cycles. This would affect the thickness measurements to varying degrees and hence the bulk also. The slight rise in tensile and stretch values for samples 528 and 375 in going from cycle 2 to cycle 4 is significant but rather difficult to explain, since it must depend upon several factors.

b) Freeze-Drying Cycles

Table VIII shows the results of the various tests which are plotted against number of cycles in Figure 4.

TABLE VIII

Results of Physical Tests for Sets (AD), FD·AD and FD^3·AD

Treatment	Bulk cc/gm	Burst Factor	Tear Factor	Breaking Length	Stretch %	% Diam. Shrinkage
(AD)-644	1.59	.800	1.39	7900	-	2.8
FD·AD-644	1.58	.594	1.77	5650	3.9	1.7
FD^3·AD-644	1.76	.332	2.48	4520	2.8	1.3
(AD)-447	1.50	1.17	1.48	8100	-	3.9
FD·AD-447	1.52	.885	1.46	7550	6.0	2.7
FD^3·AD-447	1.62	.605	1.90	6390	4.8	2.2
(AD)-190	1.44	1.10	1.42	6100	-	7.5
FD·AD-190	1.45	.950	1.48	6470	7.3	4.5
FD^3·AD-190	1.48	.615	1.48	6800	5.7	2.7

The general trend of the results is the same as for the air-drying cycles, all test values vary regularly with degree of beating, except

FIGURE 4

Results of Physical Tests for Mixed Drying Cycles.

Test Values vs. Number of Cycles.

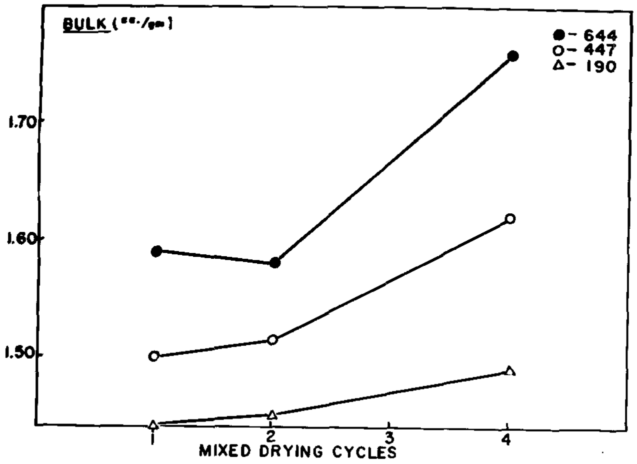
BULK (cc./gm)
●- 644
○- 447
△- 190
1.70
1.60
1.50
1
2
3
4
MIXED DRYING CYCLES

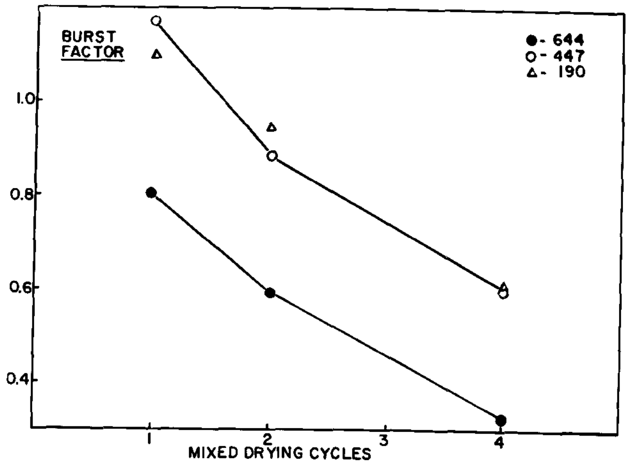
BURST FACTOR
●- 644
○- 447
△- 190
1.0
0.8
0.6
0.4
1
2
3
4
MIXED DRYING CYCLES

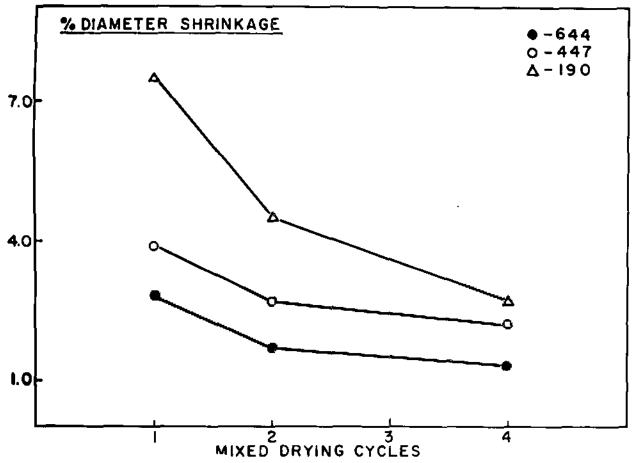
% DIAMETER SHRINKAGE
● -644
○ -447
△ -190
7.0
4.0
1.0
1
2
3
4
MIXED DRYING CYCLES

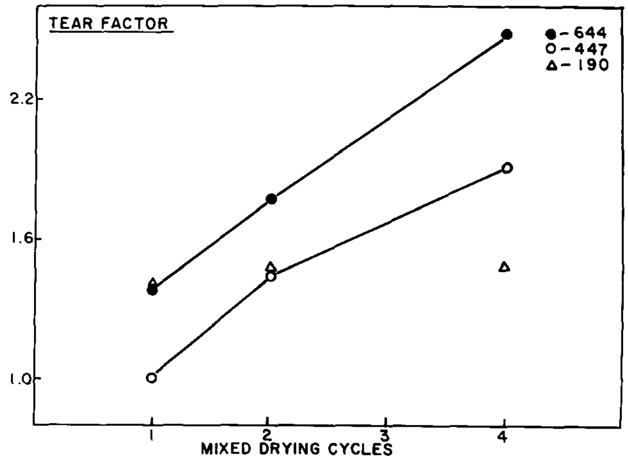
TEAR FACTOR
●-644
○-447
△-190
2.2
1.6
1.0
1
2
3
4
MIXED DRYING CYCLES

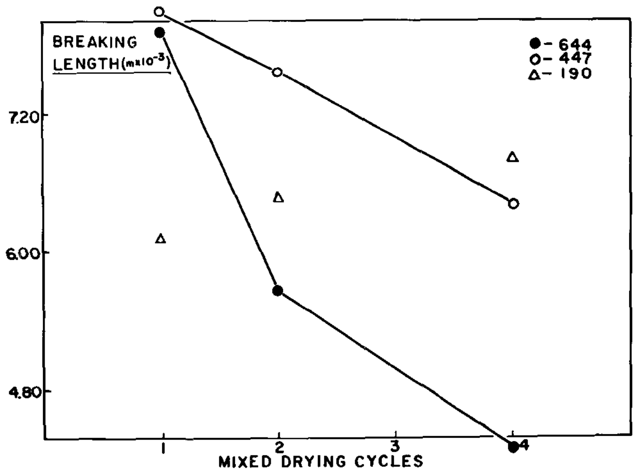
BREAKING LENGTH $(m \times 10^{-3})$
●- 644
○- 447
△- 190
7.20
6.00
4.80
1
2
3
4
MIXED DRYING CYCLES

for the tensile values of sample 190 which increase slightly with the number of cycles.

3. Significance of Results

Before discussing the above results it should be mentioned that, in general, the strength characteristics of most pulps show a sharp decline after 350 to 300 freeness. From this stage on, the adverse effects of beating on the fibre appear to prevail. With this fact in mind, the sometimes singular behaviour of the highly beaten samples 265 and 190 is not so unexpected. As mentioned previously, paper tests are complex functions of several variables each one of which will vary with drying, hence parallel behaviour at all degrees of beating is not to be expected. For this reason, in the following discussion, only the salient features of the results will be considered.

a. Cyclic Air-Drying

From the cyclic air-drying experiments a few generalizations may be made concerning the effect of drying on beaten fibres and on their papermaking properties. First of all, different degrees of beating leave a characteristic mark on the fibre which is not lost even after four drying cycles. The test values corresponding to each freeness remain distinct although the differences between the two samples may decrease or increase with the number of cycles. In a few cases, there is a crossing over of the curves.

Those physical properties which depend on density of bonding undergo large changes after the first cycle. This includes: tensile, burst and shrinkage. The reason for this may be twofold:

i) Irreversible bonding of fine fibrils to the parent fibre (18)

ii) Irreversible shrinkage or vitrification of the fibre (16).

from the available data it is impossible to distinguish between these two factors. More than likely they are related in the same way as swelling and surface area. The same properties, except tensile strength, show further decrease after four cycles.

It was mentioned in a preceding section that tear strength varies inversely as bonding density. In keeping with this generalization, the tear factor for samples 528 and 375 increases linearly with number of cycles.

The loss in swelling power of a cellulose fibre with the number of drying cycles is a well-established fact. The above data, therefore, would testify to the importance of swelling in promoting fibre-to-fibre bonds.

b. Relative Effect of Air-Drying and Freeze-Drying on the Papermaking Properties of Cellulose Fibres

One of the purposes of this experiment was to compare the effect of freeze-drying and air-drying on the papermaking properties of fibres. The comparison is best made by plotting curves of some particular property versus freeness at constant number of drying cycles. If difference in the drying procedure has no effect on the property, then all points should fall on the same curve regardless of how the cycles were carried out. If the opposite is true then there should be an AD^2 curve and an FD•AD curve. The appropriate data taken from Tables VII and VIII are shown in Figure 5.

The curves for diameter shrinkage, bulk, breaking length and tear factor point to the conclusion that freeze-drying has a distinct effect on the papermaking properties of the fibres. A similar plot for the samples which underwent four wetting and drying cycles gives curves which occupy the same positions relative to each other (with one exception) but

FIGURE 5

Results of Cyclic Drying Experiment Plotted vs. Freeness

at Constant Number of Cycles.

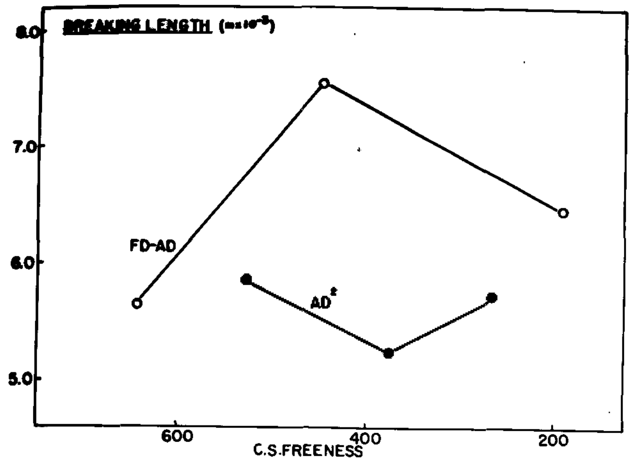
BREAKING LENGTH (m×10⁻³)
8.0
7.0
6.0
5.0
FD-AD
AD²
600
400
200
C.S.FREENESS

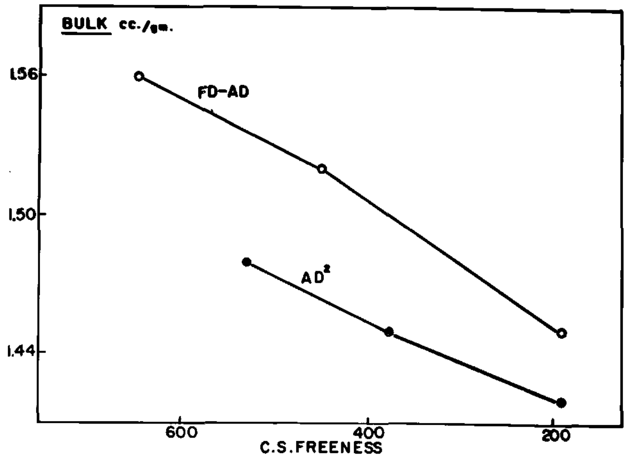
BULK cc./gm.
1.56
1.50
1.44
FD-AD
AD²
600
400
200
C.S.FREENESS

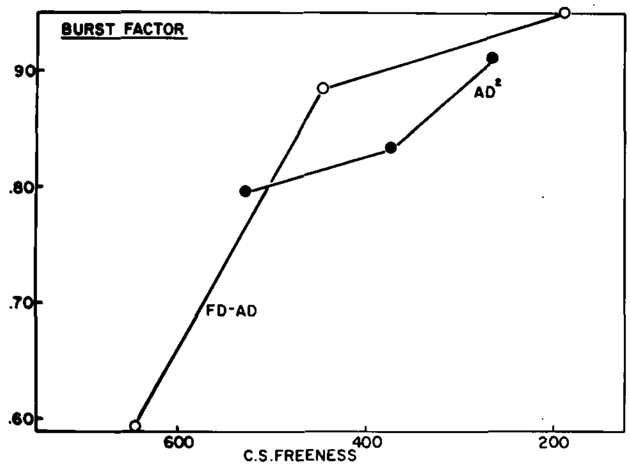
BURST FACTOR
.90
.80
.70
.60
AD²
FD-AD
600
400
200
C.S.FREENESS

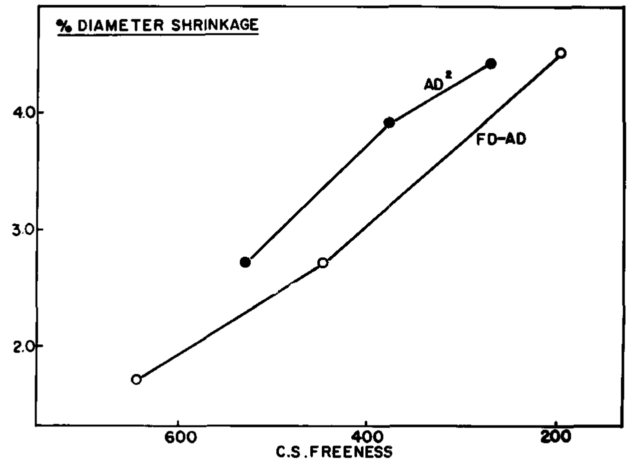
% DIAMETER SHRINKAGE
4.0
3.0
2.0
AD²
FD-AD
600
400
200
C.S.FREENESS

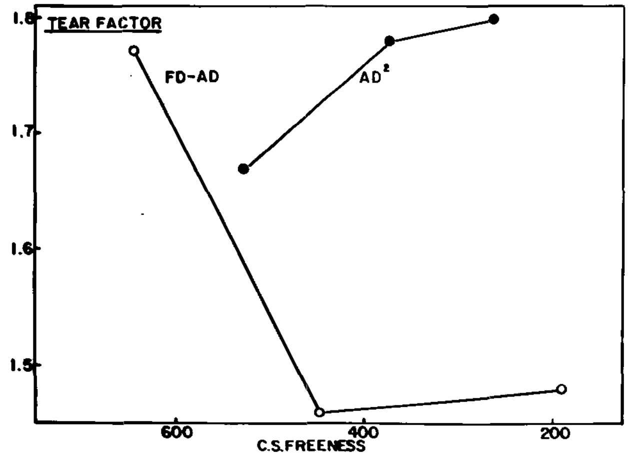
TEAR FACTOR
1.8
1.7
1.6
1.5
FD-AD
AD²
600
400
200
C.S.FREENESS

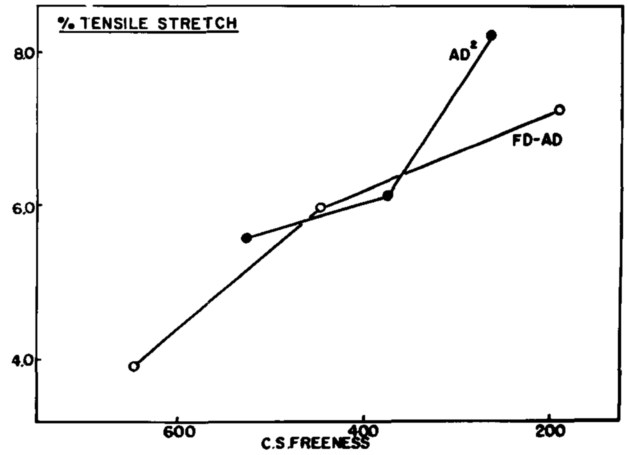
% TENSILE STRETCH
8.0
6.0
4.0
AD²
FD-AD
600
400
200
C.S.FREENESS

of different shape.

A careful examination of the AD^2 and FD•AD curves over the middle range of freeness values reveals the following:

(i) Freeze-dried pulp forms a bulkier sheet which shrinks less than paper made from air-dried pulp

(ii) Freeze-dried pulp gives sheets with higher tensile strength

(iii) Freeze-dried pulp gives sheets with lower tear strength.

Points (ii) and (iii) indicate a relatively high degree of bonding. In conjunction with this, point (i) is evidence that freeze-dried fibres are more rigid or less capable of swelling than air-dried fibres.

It will be recalled that it was concluded tentatively from the data of Table III in section B.3 that freezing at low temperature tended to increase the rigidity of the fibre.

It is particularly significant that the FD•AD samples should show a higher degree of bonding than AD^2 sheets but only after a certain amount of beating has occurred. This is explained as follows. Since freeze-drying does not favour interfibre bonding, fine fibrils will not be bonded irreversibly to the parent fibre. More generally, the fibre will possess greater external surface than if it had been air-dried. However, to promote extensive interfibre bonding, this factor must prevail over the effect of greater fibre rigidity. Thus, a certain minimum of surface development must be attained before FD•AD sheets show greater bonded area than AD^2 sheets.

From the data presented in this section, it may be concluded that freeze-drying has a distinct effect on the papermaking properties of the fibre compared to air-drying. The physical tests would indicate that freeze-drying does not promote shrinkage or loss of surface to the same extent as air-drying does. On the other hand, freeze-drying literally seemed to "freeze" the more open structure so that on reswelling in water, it did not attain the same degree of plasticity or swelling as an air-dried fibre.

III. Effect of Freeze-Drying on Cellulose Fibres

A. Preparation of Materials

The starting material in this part of the investigation was a bleached sulphite pulp in dry lap form. The sample was soaked for 48 hours in distilled water at room temperature after which it was disintegrated five minutes in the British disintegrator to bring about complete dispersion. The mixture was then divided into five portions which were dried as described below.

The first portion (AD) was allowed to air-dry at room temperature. The second portion (FD) was freeze-dried. The remaining portions were combined and the water was replaced with benzene by means of solvent exchange according to the method of Assaf, Haas and Purves (13). (It should be noted that the samples were not swollen in alkali). The swollen fibres, now moist with benzene. were again divided into three portions one of which, FDB. was freeze-dried. Another portion, ADB, was slowly air-dried in a desiccator over solid paraffin according to (13). Finally, the third fraction ADB' was allowed to stand in benzene for two weeks before being dried in the same way as ADB.

The purpose of this latter sample was to observe the effect of prolonged standing in a non-polar solvent on the physico-chemical properties of cellulose. It has been observed (20) that water-swollen cellophane, solvent-exchanged to benzene, undergoes slow deswelling on standing in benzene.

The dried samples were stored in a desiccator over P_2O_5 until used.

B. Determination of Sorption Isotherms

1. Experimental

A simple quartz spiral arrangement was used for determining the sorption isotherms of the samples described in the preceding section. The system is sketched in Figure 9. A is the sorption cell with the quartz spiral mounted on a crossbar. The vapour source, a saturated salt solution, was contained in tube B which was equipped with a magnetic stirrer C. The equilibrium vapour pressure was measured to 0.1 mm. in the U-tube mercury manometer D. Both vapour and sorption cells were kept in a thermostat at 25.00 ± .03°C. in the same water bath E.

The quartz spiral, having a diameter of 5/8 of an inch, was calibrated up to 150 mg. The spring constant was 0.0427 cm./mg. Measurements of the spiral extension were made with a cathetometer reading to ± 0.003 cm. The smallest spiral elongation due to sorption, which occurred at the lowest relative humidity, was of the order of 0.080 cm. Hence the error in these measurements, which decreased with increasing relative humidity, was approximately ± 3.0%.

Since the dried fibre samples were slightly matted it was possible to form them into small bundles which were attached to the spiral by means of fine nichrome wire. In this way larger samples (90 mg.) could be used than with the conventional quartz pan.

Water vapour was maintained at constant relative humidity by means of saturated salt solutions whose vapour pressures,which were determined by Wink and Sears (21) over a range of temperatures, are listed in Table IX. The vapour pressures of these solutions were found by Wink and Sears to be only slightly temperature dependent.

The observed vapour pressures were found to agree with the recorded values within a few tenths of a millimetre of mercury.

Points on the isotherm were determined by equilibrating the samples with the vapour of constant relative humidity. Equilibrium was considered to be attained when there was no change in weight over a period of 10 hours.

FIGURE 9

Apparatus for Determination of Adsorption Isotherms

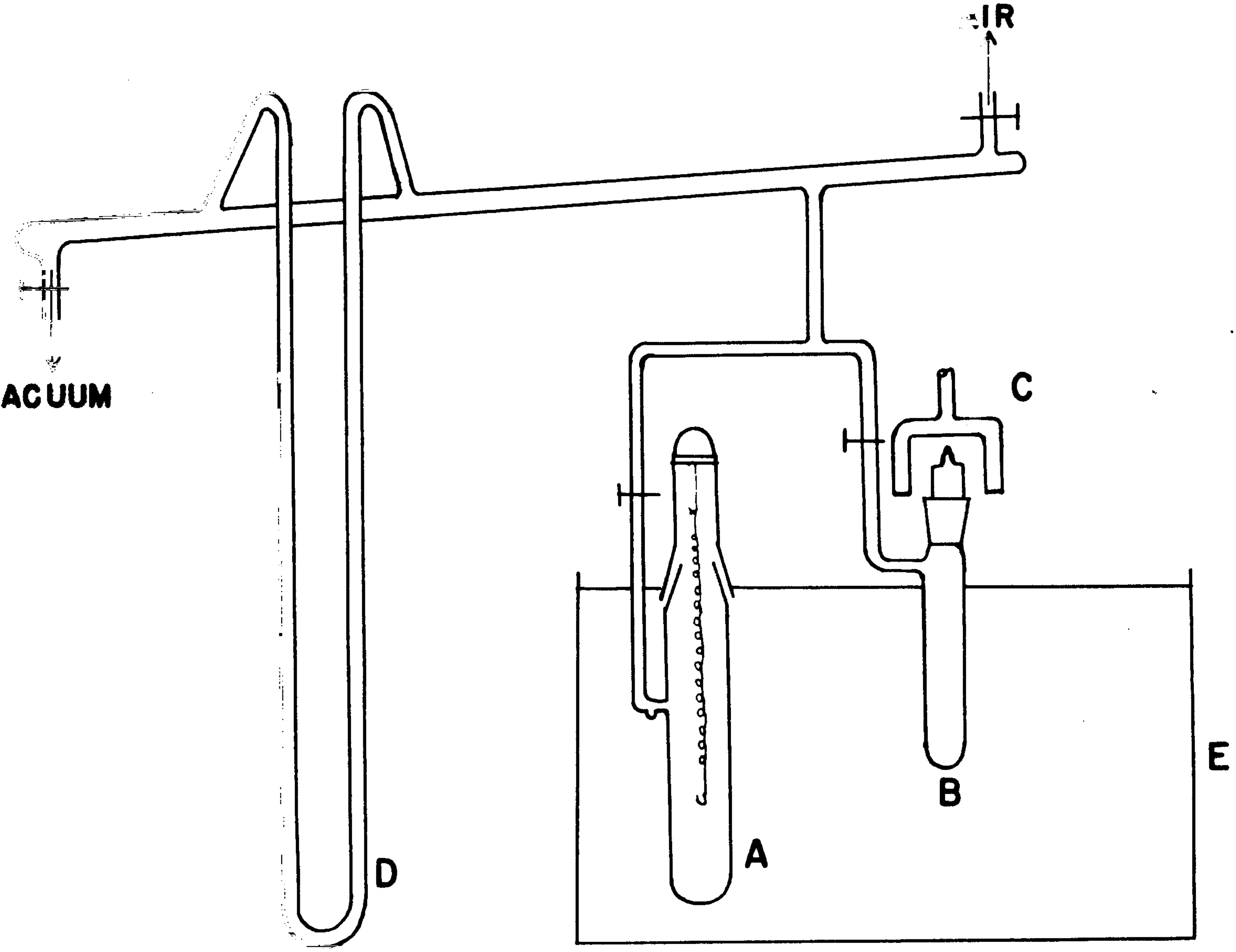

AIR
VACUUM
C
A
B
D
E

TABLE IX

Vapour Pressure and Per Cent Relative Humidity of Saturated Salt Solutions at 25.00 + .02°C.

Saturated Solution	Press. (mm. Hg)	% R.H.
Potassium Acetate	5.39	22.7
Potassium Carbonate	10.4	43.8
Sodium Nitrite	15.3	64.3
Sodium Chloride	17.9	75.4
Ammonium Sulphate	19.0	80.0
Potassium Chromate	20.5	86.4
Ammonium Dihydrogen Phosphate	22.0	92.7

It is to be noted that by using saturated salt solutions to maintain an atmosphere of constant relative humidity, the whole of the sample approaches equilibrium along the sorption branch of the isotherm hence hysteresis effects are avoided.

The dry weight of the sample was obtained by degassing to constant weight at a pressure of one micron of mercury.

. Results

The sorption data for each sample are listed in Table X and plotted against relative humidity in Figure 10.

. Significance of Results

The results of the sorption experiments confirm the observations made on paper where, similarly, the effects of air-drying and freeze-drying on paper strength were found to differ. The differences between the AD and

TABLE X

Sorption Data at 25.0°C. for Bleached Sulphite Cellulose Fibres Dried According to Various Methods

Sample	Description of Drying Method	% Relative Humidity	Regain gm/100 gm.
AD	Air-dried from water-swollen state	25.3	3.77
		44.2	5.64
		65.4	8.62
		79.3	12.0
FD	Freeze-dried from water-swollen state	20.9	3.58
		44.5	6.40
		66.6	8.70
		77.2	10.75
ADB	Water-swollen, solvent-exchanged and air-dried from benzene	21.9	4.21
		43.3	6.08
		64.0	7.80
		80.5	10.62
FDB	Water-swollen, solvent-exchanged and freeze-dried from benzene	20.9	2.96
		44.7	4.07
		66.1	4.73
		66.5*	4.70
		86.4*	8.66
ADB'	Water-swollen, solvent-exchanged, allowed to stand in benzene for two weeks and air-dried from benzene	22.8	1.80
		44.7	3.17
		64.9	4.63

---

* These points were obtained on a different sample, note good agreement at 66.1% and 66.5% relative humidity.

FIGURE 10.

Adsorption Isotherms at 25.0°C. for Bleached Sulphite Cellulose Fibres Dried According to Various Methods

AD: Air-dried from water-swollen state

FD: Freeze-dried from water-swollen state

ADB: Water-swollen, solvent-exchanged and air-dried from benzene

ADB': Water-swollen, solvent-exchanged, allowed to stand in benzene for two weeks and air-dried

FDB: Water-swollen, solvent-exchanged and freeze-dried from benzene.

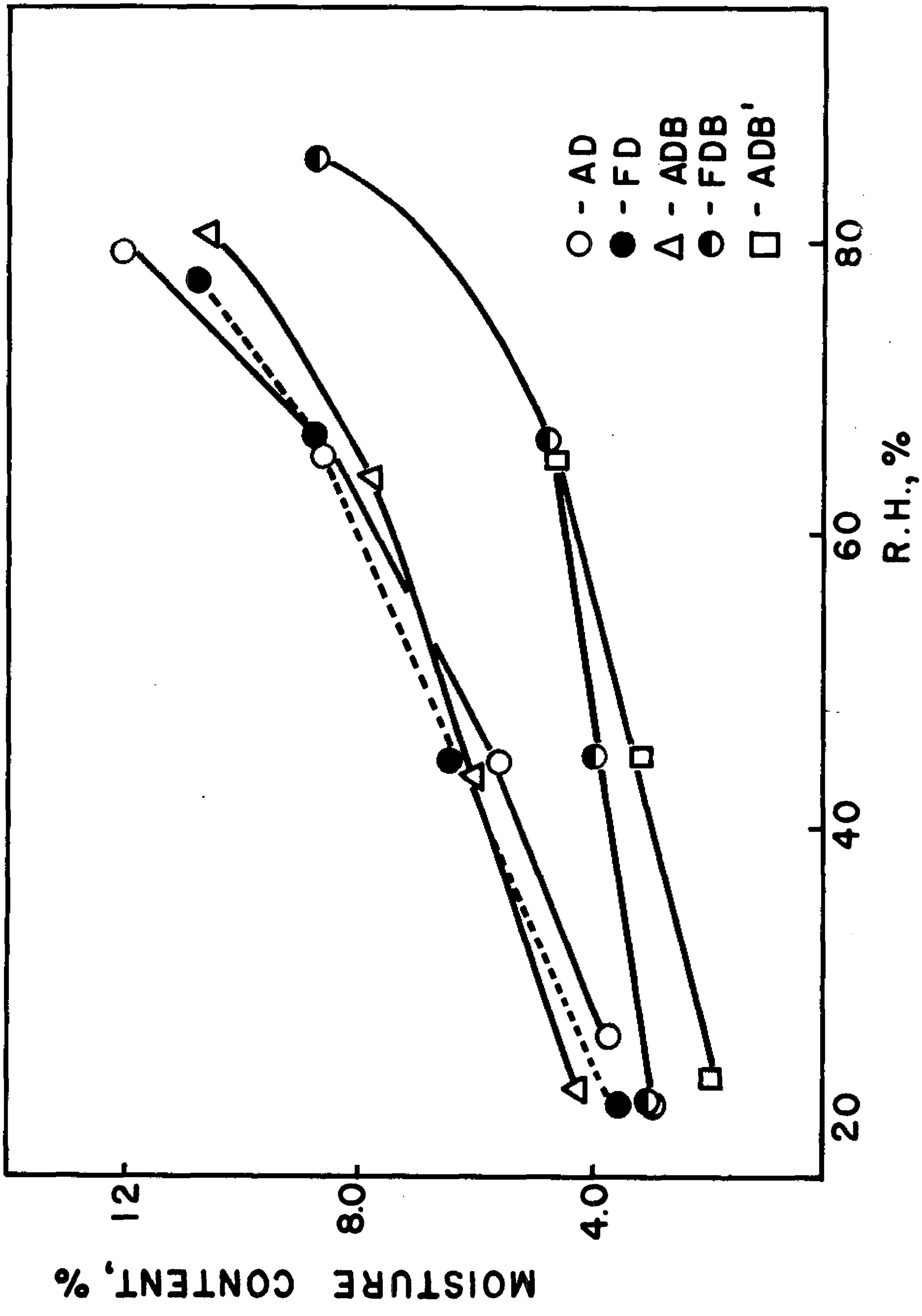
MOISTURE CONTENT, %
12
8.0
4.0
R.H., %
20
40
60
80
○ - AD
● - FD
△ - ADB
◐ - FDB
□ - ADB'

FD isotherms may be shown to be in qualitative agreement with the previous tentative conclusions that freeze-dried cellulose has greater surface area but less swelling power than air-dried cellulose.

According to the usual interpretation of the sigmoid isotherms for cellulose (62), the initial sorption up to about 30% r.h. is ascribed to strong hydrogen bonding of single molecules to the accessible hydroxyls i.e. surface adsorption. Between 30 and 50% there is gradual transition to the capillary condensation mechanism with accompanying swelling. Purves and co-workers (63) attribute sorption up to 10% r.h. to surface coverage of primary hydroxyls while in the region up to 50% r.h. surface adsorption on secondary hydroxyls is considered to occur with capillary condensation setting in afterwards. Thus the greater moisture take-up of the FD sample over the AD up to 60% r.h. may be attributed to its greater available surface. The crossing over of the curves beyond 60% r.h. results from the greater swelling capacity of the air-dried cellulose whereby its pore volume available for capillary condensation is substantially increased.

Although the concept of greater surface area for freeze-dried fibres follows naturally from the mechanism of the process, the reason for greater fibre rigidity and decreased swelling capacity is not immediately apparent. However, several investigators have shown (55, 64, 65, 66) that the degree of swelling of regenerated cellulosic fibres and the permeability of cellophane and other polymeric membranes may be controlled by varying the conditions of drying. Rapid dehydration at low relative humidity produces higher swelling and permeability than slow, careful drying at low temperatures and high relative humidity. Since freeze-drying corresponds to the latter conditions, a decrease in swelling capacity is not unexpected.

Hubert, Matthes and Weisbrod (64) have offered the following explanation for these phenomena. Assuming that shrinkage, which consists in the arrangement of the chains so as to mutually satisfy their secondary valences (formation of junction points), can only occur in the presence of a minimum quantity of water, and that the rate of dehydration is always greater than that of shrinking, then obviously the faster the rate of drying the less complete is the shrinkage. Every wetting and drying cycle produces a certain number (depending on the conditions of drying) of "water resistant" junction points which impose a permanent constraint on the swelling capacity of the fibre.

The properties of alkali-swollen solvent exchange-dried cellulose have been the subject of several investigations. It has been found that the reactivity (13) the surface area (58) and the water-binding capacity (59) of this material is greater than that of untreated cellulose. These properties are attributed to the non-polar nature of benzene which does not promote hydrogen bonding when it is removed.

In the present investigation the ADB sample was found to possess the highest regain of all in the low pressure region where surface adsorption predominates. However, at higher relative humidities where swelling power is important in determining the moisture regain, its isotherm falls below those of the AD and FD samples.

Sample ADB', which was given the same treatment as ADB, except that it was kept in benzene for two weeks before being dried, showed considerably less moisture take-up than ADB at all observed relative humidities. This is not inconsistent with the previously-mentioned observation of slow deswelling of solvent-exchanged cellophane on standing in benzene. This observation is very significant, for it illustrates the non-solvent property of benzene towards cellulose with the result that the chain molecules appear to be slowly "precipitated" out of solution with the formation of numerous junction points. Thus the extent to which the sorptive and swelling properties of the fibre are affected depends on the length of time it spends n contact with the benzene.

The non-solvent property of benzene towards cellulose is quite evident on comparing the soft, "spongy" feel of water-swollen cellophane with the stiff, hard feel of the benzene-saturated film.

In terms of the foregoing, the intermediate position of the FDB isotherm is easily explained. The combination low-temperature drying along with the non-solvent property of benzene, for it has been shown that at 0°C., solvent-exchanged cellulose has 36% non-freezing benzene (59), account for the substantial decrease in sorptive properties as compared to ADB.

A further complication in the interpretation of these isotherms is the likelihood of benzene being trapped within the fine structure and decreasing the area available for adsorption. This has been shown to occur 67, 68). Clearly this error is a function of the degree of collapse which occurs and is no doubt partly responsible for the extremely low regain of the ADB' and FDB samples.

The slow deswelling of solvent-exchanged cellulose on standing in benzene probably accounts for the difficulty which several workers (58, 59) have experienced in reproducing their results on different samples.

. Pore Volume, Pore Size and Pore Size Distribution in Air-Dried and Freeze-Dried Cellulose

. Introduction

The porosity of native cellulose is evident from its submicroscopic structure. The existence of pores in dry fibres has been confirmed by X-ray methods and electron microscopy (69). However, the size and distribution of the pore volume is not well-established. The experiments reported in this section, which were carried out by Mr. T.S. McKnight, constitute a novel approach to the study of the fine pores in cellulosic materials. The mercury porosimeter method of Ritter and Drake (70), which they applied to the study of the pores in solid sorbents, was applied to air-dried and freeze-dried cellulose fibres in order to detect changes in both the volume and size of microscopic and submicroscopic pores due to the difference in the method of drying.

Basically, the procedure* may be broken down into the following steps:

a) Determination of helium displacement density.

b) Determination of mercury density at a small known pressure.

c) Penetration of pores in the sample by mercury under pressure.

The helium and mercury densities of the samples and the pressures at which the mercury densities were determined are recorded in Table XI.

TABLE XI

Helium and Mercury Densities of Fibre Samples AD, FD and FDB.

Sample	Helium Density gm./cc.	Mercury Density gm./cc.	Mercury Density lb./sq. in.
AD	1.53	0.3536	16.2
FD	1.53	0.2964	17.0
FDB	1.53	0.2935	17.4

The results of Table XI were not unexpected. If helium penetrates pores of molecular dimensions, then it is doubtful that the various drying methods would bring about changes in the fine structure which would cause the helium density to vary. On the other hand, the mercury density of these

---

* For a detailed procedure, the reader is referred to Mr. T.S. McKnight's thesis (71).

slightly matted fibres depends on the interfibre pore sizes which have been shown to be larger for the freeze-dried samples.

From the difference between the helium and mercury densities the void volume available to the mercury, at pressures beyond that at which the mercury density was determined, may be calculated. From the decrease in void volume at each pressure, a pressure-volume curve may be constructed. Furthermore, from the relation

$$r = \frac{-2\sigma\cos\theta}{P} \qquad (1)$$

where: r is the radius of the pore

σ is the surface tension of mercury

P is the pressure on the mercury

θ is the angle of contact between mercury and cellulose

the pressure-volume curve may be converted to a radius-volume curve. Finally Ritter and Drake (70) have shown that the distribution function D(r) for the pore sizes is given by the equation:

$$D(r) = \frac{P}{r}\frac{dV}{dP}$$

where dV is the void volume penetrated by the mercury when a pressure increment dP is applied. From the slope of the pressure-volume plot and the corresponding radius, a pore size distribution curve may be constructed.

There are several possible sources of error which should be noted. First of all the contact angle, θ, in Equation (1) was assumed to be 140°. This angle represents the most commonly observed value for mercury on solid materials. Whatever error was involved in this assumption, and it is likely small, will not affect the relative character of the results for the different samples.

Secondly, Equation (1) states that the pressure required to fill a given pore is a measure of the size of the pore. However, Equation (1) was derived for pores of circular cross-section, it follows, that pore radii calculated from it represent average values and reveal nothing concerning the actual shape of the pores. Thirdly, Equation (1) only gives the radius of the opening to the pore. Thus the total volume of a bottle-shaped pore will appear as a contribution from pores whose radius is equivalent to that of the neck. No correction could be made for the compression factor introduced by the non-rigidity of the pore system.

. Results

The pressure-volume curves for samples AD, FD and FDB are shown in Figure 11. The three curves have very similar shape with most of the void volume being filled in the region from 0 to 1,000 p.s.i., the low pressure region as it will be referred to. The region from 1,000 to 15,000 p.s.i., the high pressure region, constitutes a relatively small fraction of the void volume. The relative position of the curves is according to the mercury densities. It is noteworthy that the void volumes of samples FDB and AD were completely filled at the maximum pressure which according to Equation 1) corresponds to a pore radius of 70 Å. The 8% difference between the void volume and the volume actually filled at 15,000 p.s.i. for sample FD is extremely high and undoubtedly is due to an error.

The low pressure region which includes pores up to 0.1 micron in radius. (these are roughly of the same order as the interfibre pores in filter paper (72)) is most naturally attributed to capillary spaces between fibres since the dry pads were very loosely packed. As expected the volume of such pores is greatest for the sample which was freeze-dried from benzene since a non-polar solvent does not produce "surface solution" of cellulose which is

FIGURE 11

Plot of Decrease in Void Volume, V, vs. Pressure, P, for Fibre Samples AD, FD and FDB.

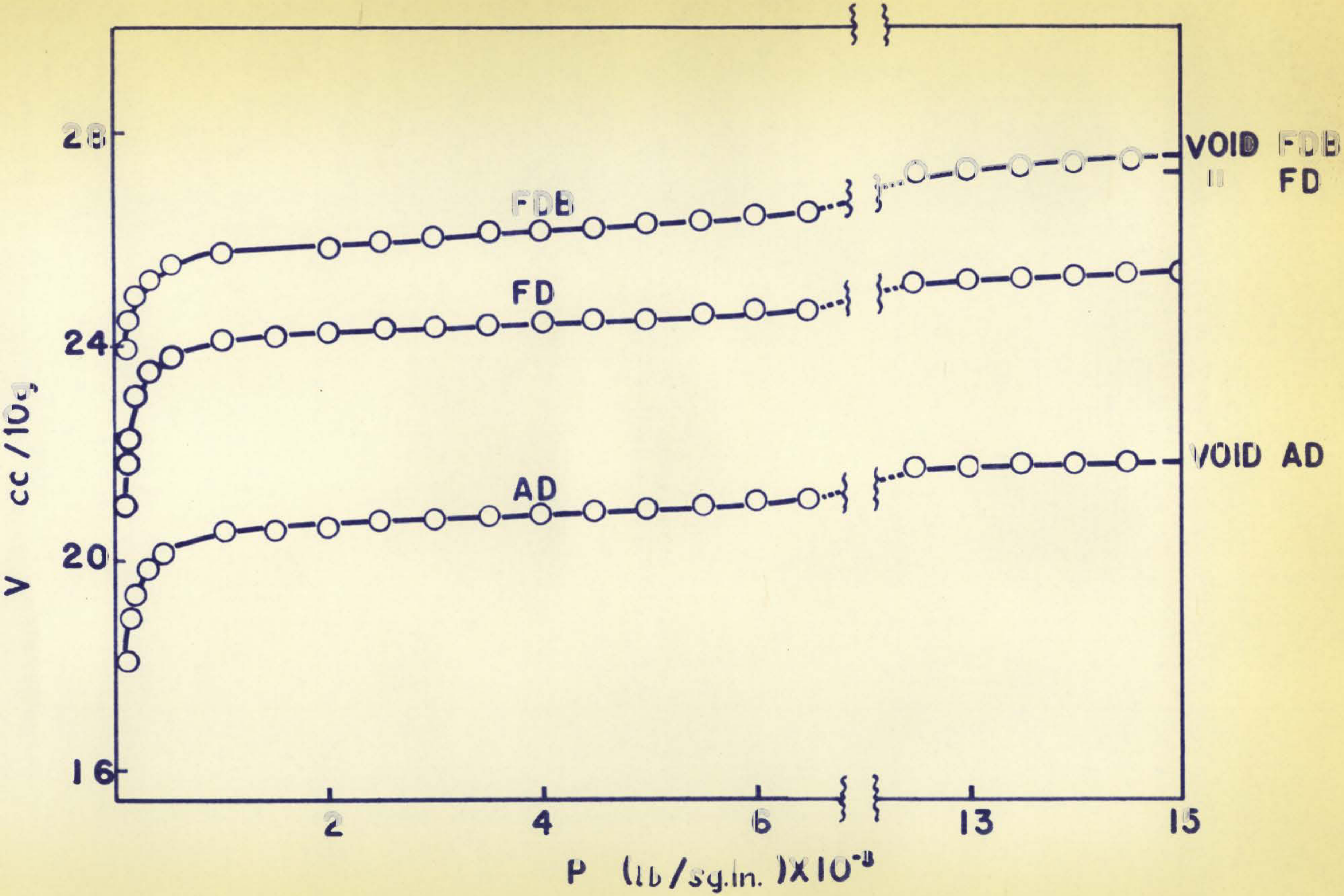
V cc/10g
28
24
20
16
FDB
FD
AD
VOID FDB
= FD
VOID AD
2
4
6
13
15
P (lb/sq.in.) X10^{-3}

mportant for the production of interfibre bonding. The results for samples D and AD are in agreement with the conclusions reached from the experiments n paper, viz. that freeze drying eliminates the factor responsible for the ntimate drawing together of fibres.

erhaps the more interesting part of these pressure-volume curves s the linear region from 1,000 to 15,000 p.s.i. Because of the sudden hange of slope just prior to this region, it is tempting to ascribe the ecrease in void volume within this range of pressures to penetration inside he fibres. although it appears likely that the fibre lumen was filled in he low pressure region.

t is very difficult to assign any particular dimensions to the umina of dried fibres. Within the wood the lumen varies considerably in ize in going from springwood to summerwood (73). Furthermore the tapered nds of the softwood tracheids add another uncertainty in the present case ince penetration only occurs at the pressure corresponding to the smallest pening. However, general considerations of fibre dimensions suggest that he lumina in dry fibres are of the order of 1 to 10 micron in diameter.

ssuming that the entire decrease in void volume in the high pressre range was due to penetration within the fibres, the calculated volume of ores per cc. of fibres are listed in Table XII. The true specific gravity f cellulose was taken as 1.53 gm./cc.

ABLE XII

olume of Pores per CC. of Fibres

ample	oid Volume cc./10 g. (from Fig. 11)	Pore Volume, % cc./cc. of fibres
DB	1.8	22
D	1.2	16
D	0.8	11

Hermans (74) quotes recorded values of the pore volume of native cellulose fibres ranging from 10 to 30%, hence the above assumption does not appear unreasonable.

Figure 12 shows the radius-volume curves. The almost linear portions which form the bulk of each curve correspond to the low pressure region and the rising sections at the ends correspond to the high pressure region. The significance of the different slopes of these curves is best understood from the pore size distribution curves in Figure 13. Thus, over the plotted low pressure range, sample FDB has the least number of pores of a given size. Since the area under the distribution curve must equal the total volume of pores, it follows that curve FDB must rise above the other two, at least in the high pressure region or in the early part of the low pressure region, or in both. The distribution was not worked out for the latter region but the high pressure region is shown on an enlarged scale in Figure 14 and curve FDB does fall above the other two.

Peaks, occurring at $r = 1$ micron, were found in all the distribution curves. It has been suggested that these maxima correspond to the lumina. While this is a possibility, no definite conclusions can be made.

Summarizing the conclusions from the preceding experimental data:

(i) Freeze-drying does not produce the same close fibre-to-fibre packing as air-drying.

(ii) Freeze-drying from water brings about denser packing than freeze-drying from benzene.

(iii) The intrafibre pore volume is in the order: FDB > FD > AD.

D. Microscopic Examination

Microscopic examination* of fibre samples was undertaken in order

---

* This examination was carried out by Mr. H.V. Green of Microscopy Section of the Pulp and Paper Research Institute of Canada.

IGURE 12

ecrease in Void Volume, V, vs. Radius r
or Fibre Samples AD, FD and FDB.

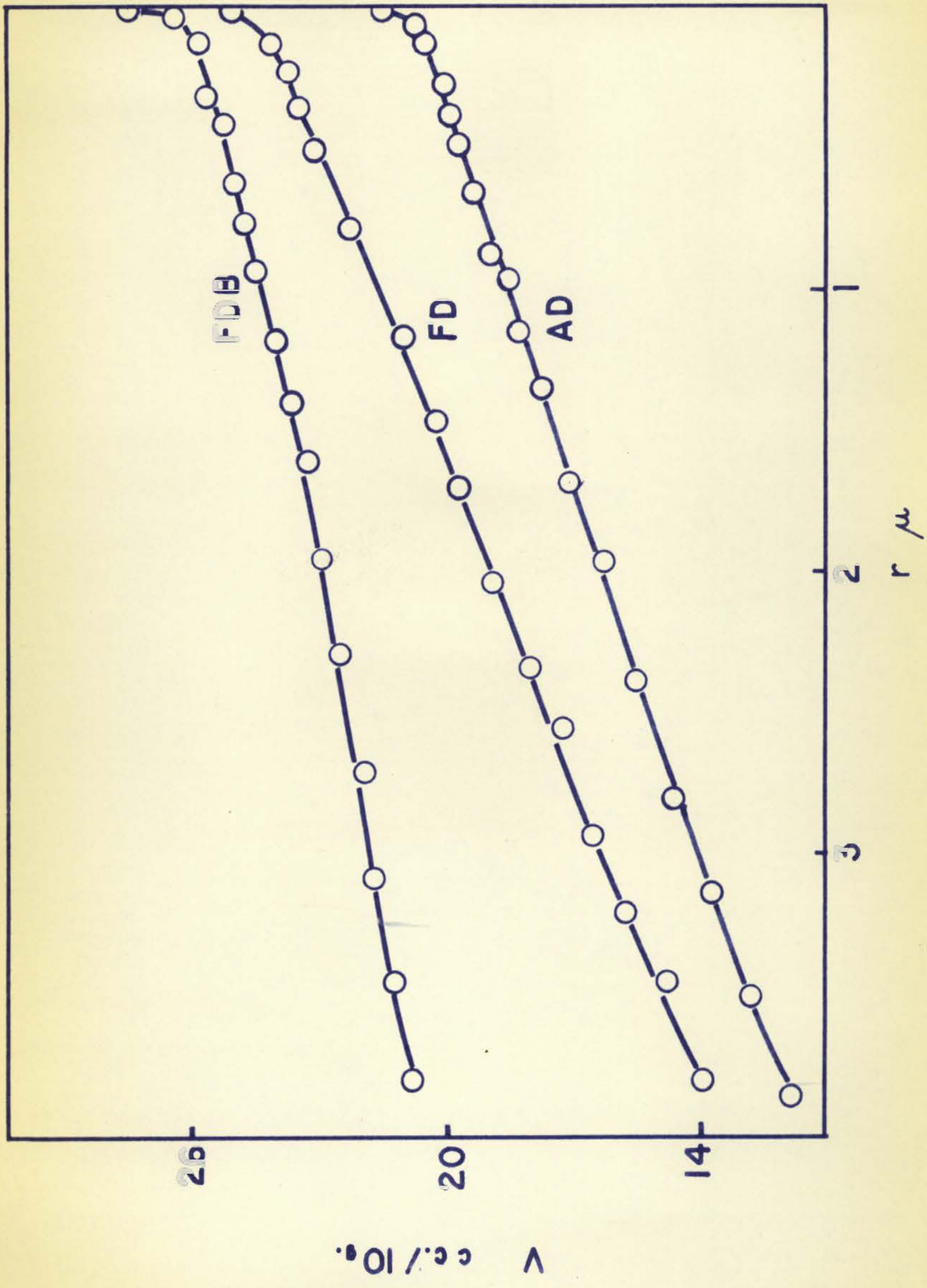
V c.c./10g.
26
20
14
r μ
1
2
3
FDB
FD
AD

FIGURE 13

Pore Size Distribution Function, D(r), vs.
Radius, r, for Fibre Samples AD, FD and FDB.

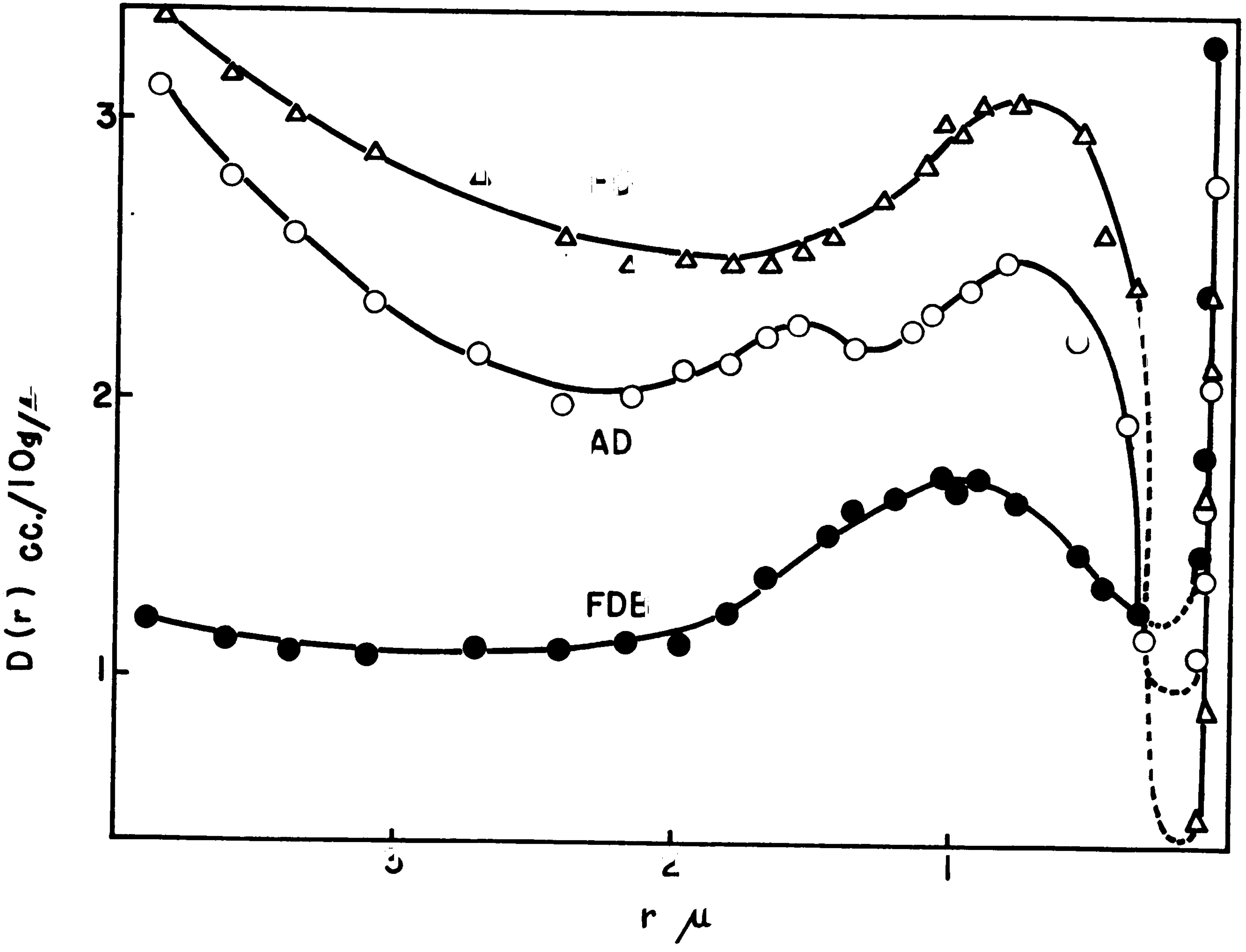
3
2
1
D (r) cc./10g/μ
AD
FDE
3
2
1
r μ

FIGURE 14

Pore Size Distribution Function, D(r), vs. Radius, r, for Fibre Samples AD, FD and FDB.
(High Pressure Region)

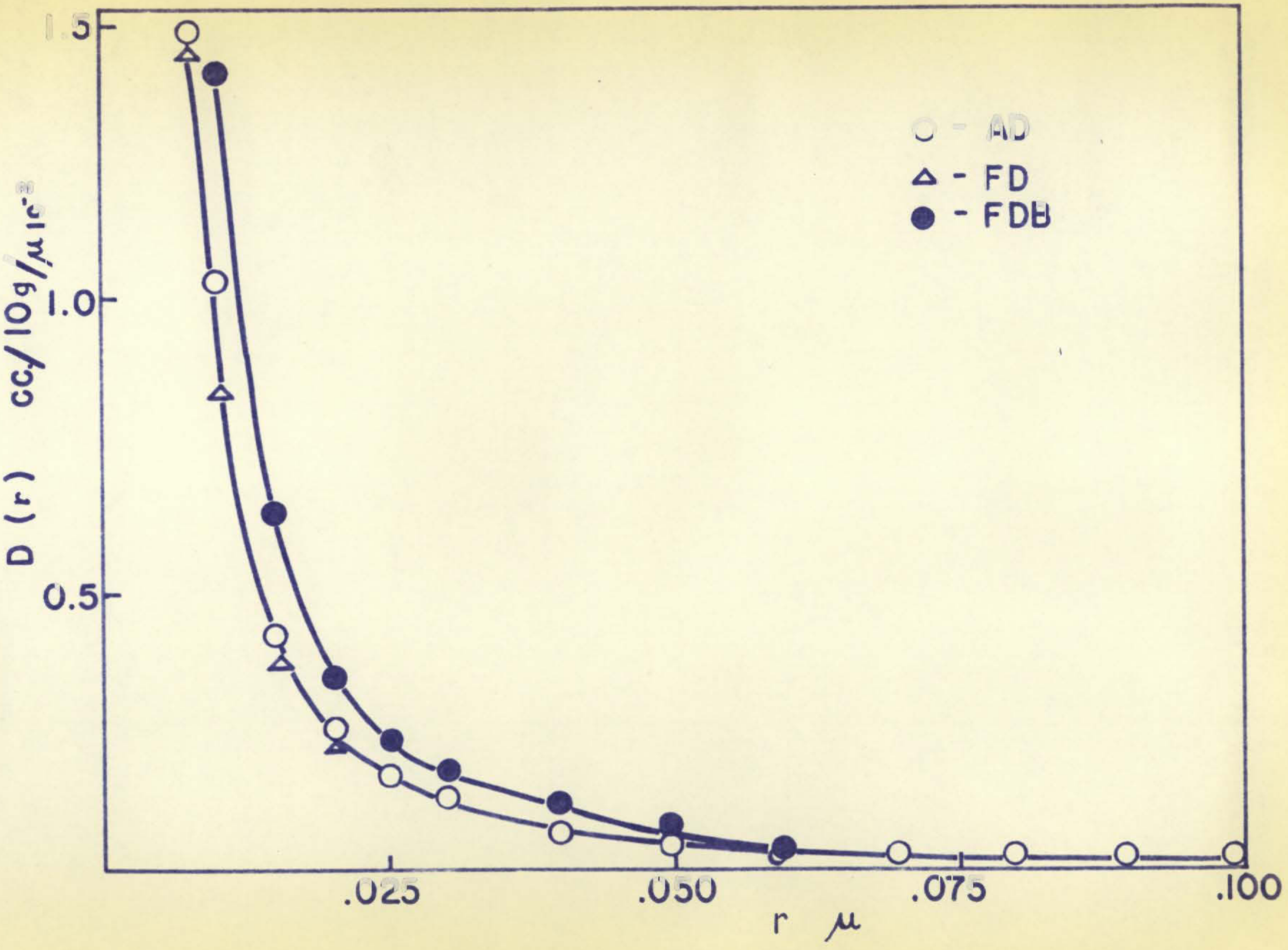
1.5
1.0
0.5
D (r) cc/10^9/$\mu 10^{-3}$
.025
.050
.075
.100
r μ
○ - AD
△ - FD
● - FDB

to detect any differences in their general appearance due to the various drying methods. The samples observed were AD, FD, FDB and also a sample of the original untreated pulp.

There seemed to be little or no difference in the appearance of these samples despite the various treatments. Samples FD and FDB showed a slight difference in the surface texture of the fibres. They seemed to show a tendency to split off short fibrils. While extensive conclusions are not warranted from a cursory examination such as this one, this latter observation does fall in line with the concept that freeze-drying keeps fibre elements apart so that the dry product has greater surface area.

IV. Application of Freeze-Drying to Paper Research

In this investigation the effect of freeze-drying on the physical properties of paper has been determined. Experimental results indicate that freeze-drying of standard handsheets allows only a minimum of bonding. Thus freeze-drying constitutes a valuable tool for workers who are interested in obtaining handsheets with all the subjective properties of paper except the extensive fibre-to-fibre bonding. The unbonded characteristic of freeze-dried paper is still more pronounced if the handsheet is not wet-pressed. Such handsheets are often required as unbonded references in measurements of the bonded area by optical methods. The unbonded reference sheet relates the absolute value of the surface area as determined by some independent method, e.g. the liquid permeability method (46) with the reflectance of the felted but unbonded pulp.

Freeze-drying may prove of great value in studying the kinetics of bonding in paper. This application is illustrated in the following experiment.

Twenty-six handsheets of 1.8 gms. each were formed of unbleached kraft pulp beaten to 300 freeness. The sheets were wet-pressed for 5 minutes. All sheets were laid on dry blotters which were arranged side by side on a laboratory bench. At zero time two sheets were frozen at -78°C. and placed in the desiccator within the frozen-food compartment, at the same time a section was taken from a control sheet and was placed in a covered weighing bottle and the diameter shrinkage of two control sheets was determined. The same procedure was carried out at various intervals for 160 minutes. Handsheets were labelled according to their time interval. Two handsheets, which were allowed to dry for 15 hours, were labelled ∞.

Reflectance measurements were carried out on all the dried sheets with a Steele opacimeter. The results of the experiment are recorded in Table XIII and plotted in Figure 15.

TABLE XIII

% Moisture Content, % Diameter Shrinkage, % Reflectance for Rate of Bonding Experiment.

Time of Sample mins.	Moisture Content %	Diameter Shrinkage %	Reflectance %
0	259	0	51.0
12	220	.31	49.6
25	183	.39	49.7
42	155	.47	47.4
70	69.7	.78	46.3
92	49.1	1.4	46.2
105	31.7	2.0	43.5
124	16.4	3.0	31.6
134	14.2	4.2	29.9
155	7.94	5.8	27.1
∞	5.28	7.1	26.1

Before discussing the results of this experiment it should be noted that the reflectance data and moisture determinations are average values

FIGURE 15

% Moisture Content, % Diameter Shrinkage and % Reflectance vs. Time for "Rate of Bonding Experiment".

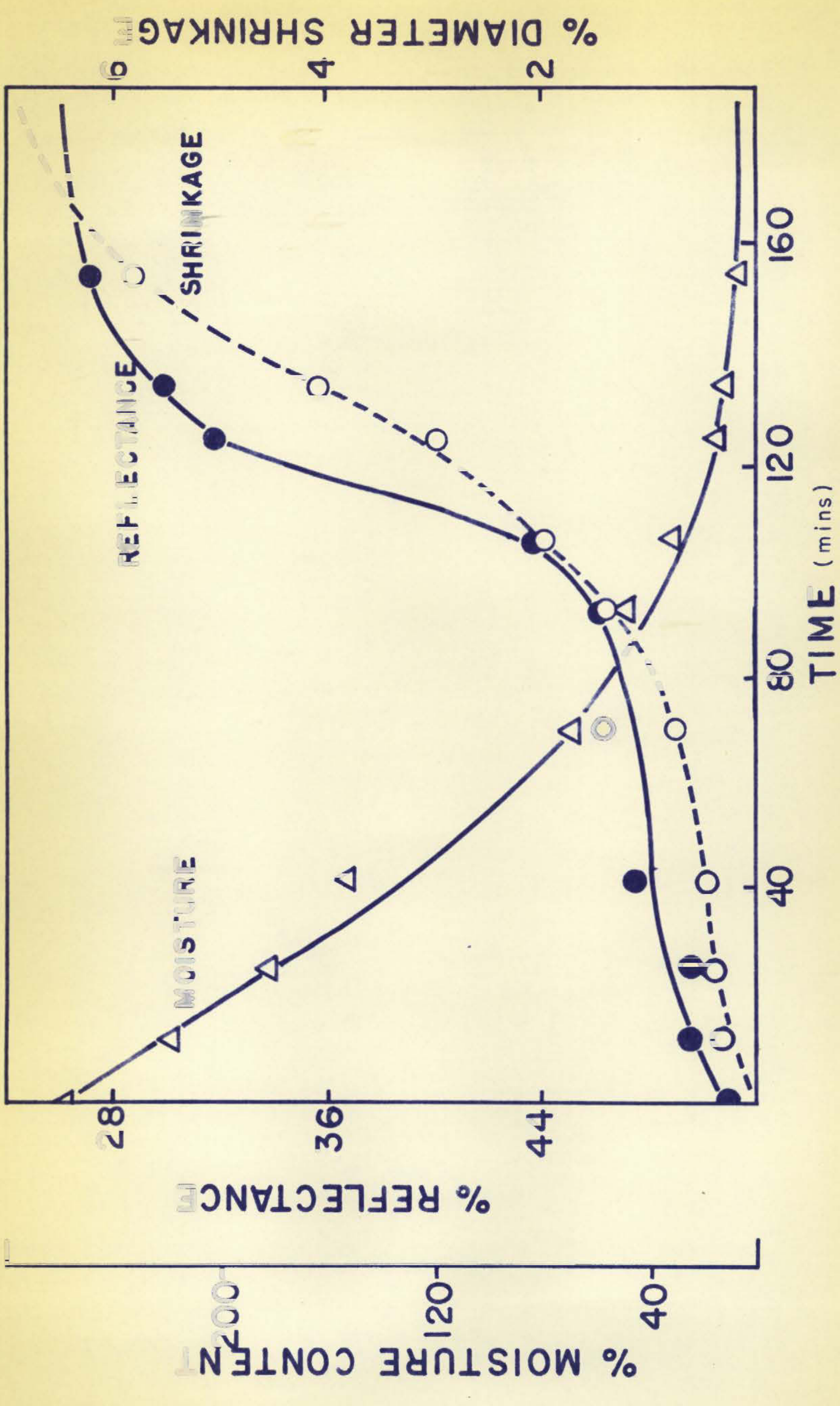
% DIAMETER SHRINKAGE
6
4
2
% REFLECTANCE
28
36
44
% MOISTURE CONTENT
200
120
40
TIME (mins)
40
80
120
160
REFLECTANCE
SHRINKAGE
MOISTURE

across the area of the sheets. For it is obvious that when a sheet is allowed free shrinkage it will curl and cockle so that the loss of moisture is not uniform across its diameter. However, if one considers the reflectance values as a rough measure of the degree of bonding (75) then the inflection points in the reflectance and shrinkage curves acquire new significance. indicating a close relationship between bonding and shrinkage. The most interesting feature of all is that the inflection points begin at an average moisture content of 45% which is very near the fibre saturation point. This may be interpreted as being in agreement with Campbell's theory that only when the liquid is present in very thin layers to the forces of surface tension become active. However, the simultaneous inflection points at such a low moisture content also suggest that part of the observed shrinkage was due to actual intercrystallization of fibres, surface tension being a necessary condition.

Maynard (76) reported an experiment similar to the preceding one in which the partially-dried sheets were washed free of water with some organic solvent. In this way the process of bonding was stopped at various stages. A plot of tear factor vs. time also showed an inflection point.

GENERAL DISCUSSION

The first aim of this investigation was to study the effect of freeze-drying on the physical properties of paper. The results presented show that the freeze-drying of paper results in a bulky product with relatively little strength and the general predictions of the Campbell theory concerning the mechanism of bonding were confirmed.

The "surface solution" idea, with regard to softwood pulp at least, may well give way to the more realistic concept of a hemicellulose gel which coats fibres and fibrils. The data clearly emphasize that bonding in paper is a complex phenomenon involving the participitation of many factors in a manner which is by no means well understood.

From the large differences observed between freeze-dried and air-dried paper and the effect of hemicellulose removal, the following mechanism for the formation of paper is proposed. Beating, after preliminary rupture of the primary wall, encourages cellulose-water interaction probably by loosening secondary valences within the amorphous regions thereby allowing greater water imbibition which results in an unravelling of the fibrillar structure. Swollen fibres are soft and plastic so that pressing causes them to flow and blend into a relatively homogeneous structure.

The role of the hemicelluloses is an important one in the swelling process. To use a topical analogy they may be regarded as a "fifth column" spreading disorder between the ranks of the highly crystalline microfibrils by attracting the invading water molecules. The hemicelluloses may be said to represent the swelling potential of the fibre. Their presence appears to be essential to the plasticization of the fibre which results from beating. From what is known of their distribution in the fibre, it may be concluded that the loosened fibrils are virtually coated with a highly swollen hemicellulose gel.

When drying occurs it is the shrinking of this highly swollen gel according to the mechanism proposed by Campbell which can result in a dense sheet. Essentially, the picture of a hemicellulose gel covering fibre elements is not different from the "surface solution" concept but it does provide a more reasonable explanation of the observed phenomena.

The above mechanism emphasizes the importance of swelling in developing paper strength as several investigators have recently observed 19, 47, 49). The importance of hemicellulosic components in swelling is appreciated but is definitely not understood. Their chemical nature, their structure, their distribution within the fibre and their colloidal properties are only beginning to receive attention (19, 39, 77, 78). Previous workers have generally been concerned with simple evaluation of the effect of alkali-soluble constituents on swelling or strength properties of various pulps.

From a comparison of the effects of freeze-drying and air-drying on the physical properties of paper and the sorptive properties of cellulose fibres it was concluded that freeze-dried material possessed greater surface area but less swelling capacity. The former conclusion is a common observation regarding the effect of freeze-drying on colloidal material (23) but the latter observation represents a phenomenon which is only imperfectly understood. The explanation that freeze-drying constitutes a mild drying method appears quite valid but it fails to distinguish between the effect of prolonged exposure to low temperature and the effect of slow drying. Slow drying of itself has been shown to procure a decrease in swelling capacity (55). A study of the effect of freezing on the swelling properties of cellulose should prove of value in this connection. Up to the present only cursory observations have been made (64, 79).

The slight increase in sorptive capacity of freeze-dried cellulose over the range of 20 to 60% relative humidity is of interest. The results of the experiments on paper suggest that it is due to an increase in surface while the porosimeter data suggest that it results from increased capillary condensation due to the larger pores which result from freeze-drying. Actually it is very difficult to correlate the sorption and porosimeter data since the pore sizes which were determined in the latter measurements correspond to relative humidities of 87 to 100% according to the Kelvin equation (62). Furthermore the effect of swelling on the pore size distribution of freeze-dried and air-dried fibres is a completely unknown factor. The presence of a relatively few extra junction points in freeze-dried cellulose as compared to air-dried cellulose could modify its swelling properties considerably.

An important feature of the porosimeter data is the peaks in all of the distribution curves at a pore radius of about 1 micron. It is well known that the moisture content of completely water-filled wood may amount to 200 or 300% of the oven-dry weight while the saturation sorption obtained by extrapolating the sorption isotherm from 99% relative humidity corresponds to 30 or 40% of the dry weight. Stamm (62) has suggested that this is due to the fact that there actually is a sharp upward break in the sorption curve just slightly below saturation. He attributes this to a break in the distribution of capillary sizes pointing out that gross microscopic fibre cavities reduce the relative vapour pressure by about .01% while the largest submicroscopic capillaries of the swollen cell wall, which are about 0.2 micron in diameter, will reduce it by about 1%. In view of this it appears likely that these very distinct peaks correspond to the gross fibre capillaries which would be predominantly fibre lumina. The Kelvin equation shows that a pore of 1 micron radius reduces the relative vapour pressure by 0.007%.

The results of the porosimeter experiments show clearly that freeze-drying increases the size of the inter- and intra-fibre pores.

SUGGESTIONS FOR FUTURE WORK

The pore size distributions obtained from mercury penetration data should be compared with values calculated, according to the Brunauer Emmett and Teller method, from desorption isotherms using a non-swelling gas, nitrogen or butane, at the boiling point.

The effect of freeze-drying and of simple freezing on the swelling and reactivity of cellulose fibres should be examined.

A study of the kinetics of deswelling of cellulose on standing in non-polar solvents should provide valuable information concerning the fine structure of cellulose fibres, particularly if correlated with different initial degrees of swelling and the amount of solvent which remains trapped within the dried fibre.

SUMMARY

A rapid and convenient method of freeze-drying cellulose fibre samples and laboratory handsheets has been developed. The method was applied to a study of the effect of drying by the sublimation of solid water, or freeze-drying, on the physical properties of paper made from unbleached kraft pulp and of bleached sulphite cellulose fibres.

It was found that freeze-dried paper was soft, bulky and possessed very little strength as compared to air-dried paper at the corresponding freeness. When an alkali-extracted pulp was formed into a handsheet and freeze-dried, the resultant product was completely unbonded.

The results of these experiments were correlated with the "surface tension theory" of paper strength proposed by Campbell. The application of freeze-drying to paper research was demonstrated by means of a simple experiment on the kinetics of bonding in paper.

To study the effect of freeze-drying on cellulose fibres, sorption isotherms were determined for samples of fibres which had been air-dried and freeze-dried. The results showed an increase in the sorptive properties of the fibres in the low pressure region but a decrease was noted in the high pressure region.

The effect of freeze-drying on the pore size distribution of paper was determined from mercury penetration measurements using a porosimeter. It was found that freeze-drying increased both the inter- and intra-fibre pore sizes of the fibres.

From the results of the investigation, it was concluded that freeze-drying produces an increase in the surface area of the fibre, but apparently it decreases its swelling capacity.

BIBLIOGRAPHY

1. Campbell, W.B. and Russell, J.K.; Forest Prod. Lab. Quart. Rev. No. 21, p. 24 (1935)

2. Van den Akker, J.A.; Tappi 33: 440 (1950)

3. Clark, J. d'A.; Proc. Techn. Sec. Paper Makers' Assoc. Grt. Brit. and Ireland 24: 30 (1943)

4. Casey, J.P.; "Pulp and Paper" Interscience Pub. N.Y. (1952)

5. Steele, F.A.; Paper Trade J. 101: 245 (1935)

6. Steele. F.A.; Paper Trade J. 100: 151 (1935)

7. Parsons, S.R. Paper Trade J. 115: 314 (1942)

8. Kress. O. and Bialchowsky, H.; Paper Trade J. 93: 219 (1931)

9. Curran, C.E., Simmonds, F.A. and Chang, H.M.; Ind. Eng. Chem. 23: 104 (1931)

10. Berzins, V.; Chem. Anal. Div. Pulp and Paper Research Inst. of Canada - Private Communication

11. Carroll, M.; Ph.D. Thesis, McGill University (1951)

12. Robertson, A.A. and Mason, S.G.; Pulp Paper Mag. Canada 50: 103 (1949)

13. Assaf, A.G., Haas, R.H. and Purves, C.B.; J.A.C.S. 66: 59 (1944)

14. Bryde, Ó, Elefsen, Ö and T.H. Smith; Tappi 36: 355 (1953)

15. McKinney, T.W.; Paper Trade J. 122: 58 (1946)

16. Jayme, G.; Cellulosechemie 21: 74 (1943)

17. Reference (4), p. 347

18. Clark, J. d'A.; Pulp and Paper Mag. Canada 44: 91 (1943)

19. Giertz, H.W.; Brit. Paper and Board Makers' Assoc. Proc. Techn. Sect. 33: 487 (1952)

20. Marchessault, R.H. and Mason, S.G,; Unpublished Data

21. Wink, W.A. and Sears, G.R.; Tappi 33: 96A (1950)

22. Campbell, W.B. Dept. of Interior, Canada; Forest Service - Bulletin 84

23. Flosdorf, E.W.; "Freeze-Drying" Reinhold Pub. Corp. New York (1949)

24. Kraemer, E.O.; Ind. Eng. Chem. 30: 1200 (1938)

25. Mark, H.; J. Phys. Chem. 44, 764 (1940)

26. Hermans, P.H.; "Physics and Chemistry of Cellulose Fibres", Elsevier Pub. Co., N.Y. (1949).

27. Howsmon, J.; Text. Res. J. 19: 152 (1949)

28. Hermans, P.H.; J. Text. Inst. 38: P. 63 (1947)

29. Nickerson, R.F.; Ind. Eng. Chem. 39: 1507 (1947)

30. Goldfinger, G., Mark, H., and Siggin, S.; Ind. Eng. Chem. 35: 1083 (19480

31. Frilette, V.J., Hanle, J. and Mark, H.; J.A.C.S. 70: 1107 (1948)

32. Ott, E.; "Frontiers in Colloid Science" ed. R. Burk, Interscience Pub. Corp. N.Y. (1950)

33. Ränby, B.G.; Tappi 35: 53 (1952)

34. Ränby, B.G.; Svensk Papperstidn. 55: 38 (1952)

35. Bailey, A.J.; Ind. Eng. Chem. Anal. Ed. 8: 52 (1936)

36. Tappi Standard T 203 m-44

37. Widerkehr, L.; Bull. Assoc. Tech. Ind. Pap. No. 3 (April 1948)

38. Ränby, B.G.; Far. Soc. Disc., No. 11: 158 (1951)

39. Simmons, J.R.; Brit. Paper and Board Makers' Assoc. Proc. Tech. Sect. 33: 513 (1952)

40. Roy, M.M.; J. Text. Inst. 44: T90 (1953)

41. Wise, L.E.; "Wood Chemistry" 2nd ed. vol. I p. 405, Reinhold Pub. Corp. N.Y. (1952)

42. Rance, H.F.; Brit. Paper and Board Makers' Assoc. Proc. Tech. Sect. 33: 544 (1952)

43. Rance, H.F.; Brit. Paper and Board Makers' Assoc. Proc. Tech. Sect. 32: 360 (1951)

44. Christensen, G.N. and Barkas, W.W.; Nature 171: 165 (1953)

45. Van Nederveen, G.; Paper-Maker 125: 8 (Mid Summer 1953)

46. Robertson, A.A.; Ph.D. Thesis, McGill University (1949)

47. Carroll, M. and Mason, S.G.; Can. J. Tech. 30: 321 (1952)

48. Alekseeva et al.; C.A. 46: 10618 (1952)

49. Borruso, D.; Industri Carta <u>6</u>: 7 (1952) (abstract)

50. Dixson, H.P.; Paper Trade J. <u>111</u>: 29 (1940)

51. Jayme, G.; Cellulosechemie <u>21</u>: 74 (1943)

52. Reference (26) p. 192

53. Barkas, W.W.; Trans. Far. Soc. <u>28</u>: 205 (1943)

54. Reference (26) p. 441

55. Kuzmak, J.M.; Ph.D. Thesis, McGill University (1953)

56. Brickman, W.J. Dunford, H.B., Tory, E.M., Morrison, J.L., Brown, K.R.; Can. J. Chem. <u>31</u>: 550 (1953)

57. Kistler, S.S.; J. Phys. Chem. <u>36</u>: 52 (1932)

58. Forziati, F.H., Brownell, R.M. and Hunt, C.M.; J. Res. Natl. Bur. Stds. <u>50</u>: 139 (1953)

59. Magne, F.C., Skau, E.L.; Text. Res. J. <u>22</u>: 748 (1952)

60. Reference (41) p. 117

61. Purves, C.B.; McGill University - Private Communication

62. Stamm, A.J.; p. 463, "Wood Chemistry" 1st ed., edited by L.E. Wise, Reinhold Pub. Corp. N.Y. (1946)

63. Assaf, H.G., Haas, R.H. and Purves, C.B.; J.A.C.S. <u>66</u>: 66 (1944)

64. Hubert, E., Matthes, A. and Weisbrod, K.; Kolloid Z. <u>98</u>: 193 (1942) cited by reference (26) p. 441

65. Jopling, D.W.; Research (sup.) <u>6</u>:275 (1953)

66. "Chemistry Research" p. 80 (1952)

67. Chem. Ztg. <u>77</u>, No. 12: 405-10 (June 20, 1953) Abstract

68. Coppick, C.S.; American Viscose Corp. - Private Communication

69. Reference (26) p. 31

70. Ritter, H.L. and Drake, L.C.; Ind. and Eng. Chem., Anal. ed. <u>17</u>: 782 (1945)

71. McKnight, T.S.; Ph.D. Thesis, McGill University (1954)

72. Peck, R.L. and McLean, D.A.; Ind. Eng. Chem., Anal. ed. <u>6</u>: 85 (1934)

73. Stamm, A.J. and Harris, E.E.; "Chemical Processing of Wood", Chemical Pub. Co., N.Y. (1953)

74. Reference (26) p. 210

75. Nordman, L., Gustafson, C. and Olafsson, G.; Finnish Paper and Timber J., No. 3 (1952)

76. Maynard, C.R.G.: Alex Pirie & Sons Ltd., England - Private Communication

77. Klauditz, W.; Holzforschung 5, 58 (1951) (abstract)

78. Imamura, R.; J. Soc. Text. Cell. Ind. 8: 445 (1952) (abstract)

79. Lauer, K.; Papier Fabrik. p. 268 (1944)

PART II

THE CAPILLARY FLOW OF LIQUIDS WITH ENTRAPPED AIR BUBBLES

INTRODUCTION

The flow of liquids through porous media is important in many processes, e.g. in the underground flow of water and petroleum, in filtration, in wetting and capillary rise of liquids and in the impregnation of wood with "cooking" liquor or preservatives. It has been shown that the presence of air bubbles significantly affects the rate of flow of liquids through porous media (9, 10, 11). The present investigation, although it was not directly undertaken to investigate the effect of air bubbles on any particular process, does offer fundamental information concerning the mechanism of flow of an entrapped air bubble in a cylindrical capillary tube and how its presence decreases the permeability of the passage.

The investigation reported in this thesis was concerned solely with bubbles which were large relative to the capillary diameter so that the entrapped air bubble approximately assumed the shape of the capillary tube, i.e. cylindrical. The term bubble length (l_b) refers to the end to end length of the cylindrical bubble.

I. Jamin Effect

The decrease in liquid permeability of porous media due to the presence of air bubbles has been traditionally ascribed to the well-known Jamin effect (12). This theory, which arose as the result of certain observations made by Jamin (16) almost a hundred years ago, simply states that if within a capillary there are arranged, alternately, drops of liquid and bubbles of gas, then a pressure exerted at one end of the tube causes adjustment of the menisci between liquid and gas so that each drop of liquid transmits less pressure than it receives. The resistance offered by such a system (Jamin's tube) is inversely proportional to the diameter of the tube and directly proportional to the length of the tube and the number of liquid drop-gas bubble sequences.

Accordingly, a Jamin's tube should support a positive hydrostatic pressure. Smith and Crane (13) reported such an observation with a capillary tube whose walls had been contaminated with a solution of oleic acid in benzene. When the capillary was carefully cleaned no Jamin effect was observed. Smith and Crane concluded that there is no Jamin effect in cylindrical tubes when perfect wetting liquids are used. When there is only partial wetting, and hysteretic contact angles are present, there will be a definite effect.

II. Liquid Film Surrounding a Moving Bubble

The concept of a liquid film surrounding a cylindrical air bubble moving in a capillary tube was put forth by Fairbrother and Stubbs (1) who observed that the rate of flow calculated from the measured bubble velocity, U_b, was greater than the true rate. From their measurements, they concluded that there is a film of liquid between a moving bubble and the walls of the tube whose thickness $\underline{\chi}$ is given empirically by

$$\chi = \frac{r}{2}\sqrt{\frac{U_b \eta}{\sigma}} \tag{1}$$

$\underline{r}$ being the radius of the capillary, η and σ the viscosity and surface tension of the liquid, respectively.

According to this concept, which was confirmed experimentally in this investigation, a moving bubble bypasses a certain quantity of liquid as it flows. The volume depending on the thickness of the liquid film.

The existence of a liquid film surrounding a stationary air bubble had been established previously by the conductivity measurements of Vaillant 14). His results, however, are significant only as to order of magnitude since he does not specify how long he allowed the bubble to stand before making a measurement. It will be shown later that the thickness of the film around a stationary bubble varies with time.

Elton (7) and Derjaguin (8) measured the thickness of the liquid film between an air bubble and a smooth surface against which the bubble was pressed. Elton (7) showed that liquid was slowly squeezed out of the film due to the excess pressure inside the bubble and that the rate of decrease of film thickness could be predicted from the laws of viscous flow.

II. Hydraulic Resistance of an Air Bubble

iefer and Mason (15) used a capillary tube with an enclosed air bubble as a flowmeter for the measurement of electro-osmotic flow. $F_{obs.}$, through pads of cellulose fibres. The principle of this method is illustrated in Fig. 1. The true electro-osmotic speed, V_t, through the pad, D, is measured by the apparent velocity of flow, V_a, of the liquid through the capillary tube. AA, as indicated by the linear speed, $\underline{U_b}$, of the air bubble, B. which is contained in the capillary.

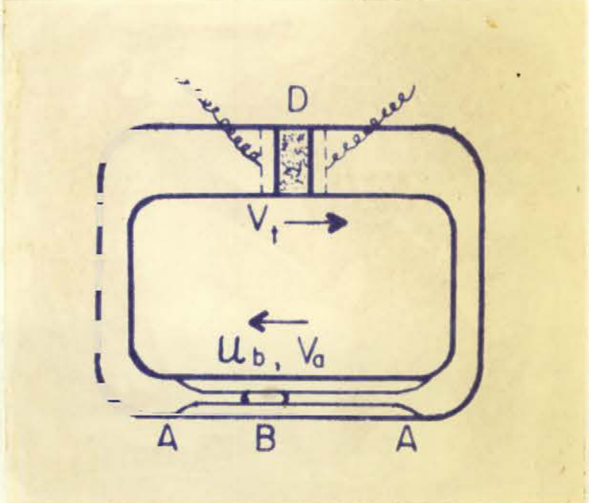

Figure 1.

In using a bubble flowmeter in this way the hydrodynamic resistance of the flowmeter capillary must be negligible compared with that of the pad otherwise a "back-flow" will occur through the pad and the observed flow will represent only part of the total electro-osmotic flow.

Biefer and Mason corrected for "back-flow" through the pad as follows. Using the quantity

$$\phi = \frac{Q\eta}{P} \qquad (2)$$

as a measure of liquid permeability where Q is the rate of viscous flow of a fluid of viscosity η under a pressure head P, the true rate of electro-osmotic flow was calculated from

$$F = F_{obs.} \left(1 + \frac{\phi_p}{\phi_c}\right) \qquad (3)$$

where the subscripts p and c designate the pad and capillary respectively.

The quantity ϕ_p was obtained directly from permeability measurements while in the initial treatment of the experimental data ϕ_c was calculated from the Poiseuille equation.

Experimentally, they observed variations in $F_{obs.}$ with bubble length which they attributed to a real decrease in capillary permeability due to the presence of an air bubble. Their experimental data suggested also that the capillary permeability increased with increasing bubble velocity. Making the assumption that the bubble moves as a solid plug i.e. the velocity gradient is confined to the film around the bubble and is zero inside the bubble, they proceeded to calculate the hydraulic resistance of the bubble as follows.

If it be assumed that there is a pressure drop P_b across the bubble, then there is a force $P_b \pi r^2$ causing the bubble to move in a plug type flow at a velocity $\underline{U_b}$. Assuming that there is a layer of liquid of thickness, χ, between the bubble and the walls of the capillary and that χ/r is small then there is a velocity gradient $\underline{U_b/\chi}$ across the liquid layer and the frictional force opposing the bubble motion is $\eta \frac{U_b}{\chi} 2\pi r \ell_b$. At equilibrium flow

$$U_b = \frac{P_b \chi r}{2 \eta \ell_b} \tag{4}$$

Where the observed flow through the capillary is Q volume units per unit time then

$$Q = U_b \pi r^2 = \frac{\pi P_b \chi r^3}{2 \eta \ell_b} \tag{5}$$

and the pressure necessary to cause bubble motion is

$$P_b = \frac{2 \eta \ell_b Q}{\pi \chi r^3} \tag{6}$$

Adding this pressure to the pressure $\underline{P_o}$ which is necessary to overcome the normal resistance to flow of the capillary tube, it is readily shown that

$$\phi_c = \frac{Q\eta}{P} = \frac{1}{\frac{2\ell_b}{\pi \chi r^3} + \frac{1}{\phi_o}} \tag{7}$$

where P is the total pressure drop across the capillary

ϕ_o is the permeability of the capillary tube without a bubble

Substituting for $\underline{\chi}$ from Equation (1), they obtained

$$\phi_c = \frac{1}{\left(\frac{4\ell_b}{\pi r^4}\sqrt{\frac{\sigma}{U_b \eta}} + \frac{1}{\phi_o}\right)} \tag{8}$$

It follows from Equation (8) that ϕ_c (i) is lower than the Poiseuille value; (ii) decreases with increasing bubble length; and (iii) increases with increasing bubble velocity. This qualitatively explained the observed variations in $F_{obs.}$ with bubble velocity and bubble length.

It was the object of the experimental work to be presented in the following section to confirm quantitatively Equation (7).

EXPERIMENTAL AND RESULTS

I. Scope of the Investigation

The experimental work which follows is divided into two parts. The first part deals with experiments which were carried out with a modified bubble flowmeter. With this apparatus all the quantities on the right and the left hand side of Equation (7), except the film thickness, $\underline{\tau}$, could be determined in a single run. From the measured data, values of the thickness of the liquid film, surrounding a moving air bubble were calculated.

The second part deals with the development and application of an electrolytic conductance method for the measurement of the film thickness surrounding a moving or a stationary air bubble.

Measured values of $\underline{\tau}$ for moving bubbles were correlated with the calculated values.

Finally, the "conductance method" provided valuable information concerning the factors which govern the thickness of the liquid film surrounding a moving bubble, hence the permeability of the capillary which contains it. This information was obtained by observing the effect of capillary diameter, bubble length, viscosity and surface tension of the medium on the film thickness. The effect of the same variables on the rate of change of film thickness with time, for a stationary air bubble, was also investigated.

II. Inclined Bubble Flowmeter

A. Description and Operation

The effect of an entrapped air bubble on the capillary permeability was demonstrated in the following manner. To the end of a capillary tube 80 cms. in length a "U"-shaped reservoir was sealed (cf. Figure 2). The average radius of the capillary tube which was determined from the length and

FIGURE 2

Inclined Capillary Flowmeter and Support

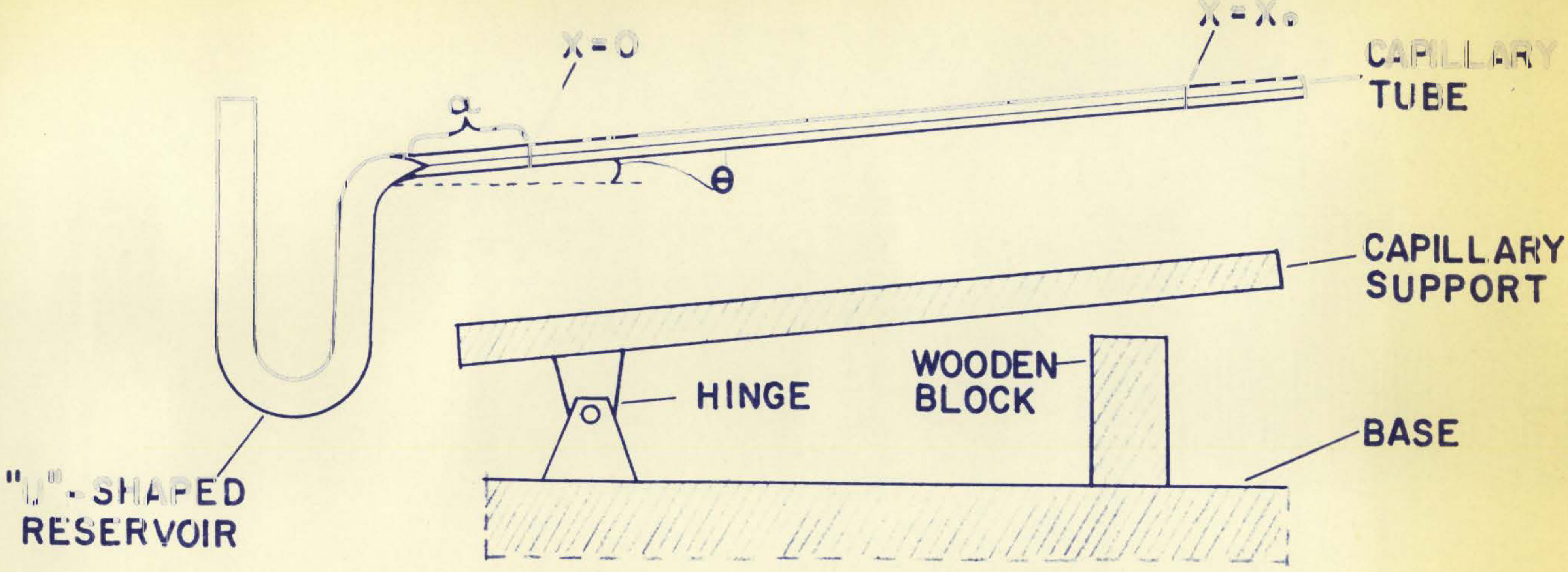
X = X₀
X = 0
a
θ
CAPILLARY TUBE
CAPILLARY SUPPORT
HINGE
WOODEN BLOCK
BASE
"U"-SHAPED RESERVOIR

weight of a mercury thread, was 0.0742 cm. The capillary tube was clamped at intervals along its length into a uniform groove running lengthwise along the surface of a hardwood board which will be referred to as the capillary support. The "U"-shaped reservoir projected out at one end of the board, which end was fixed by means of a hinge to a wooden base. A part of the capillary (6 cm.) also projected out at the other end. By placing wooden blocks between the capillary support and the base, any desired inclination of the capillary could be obtained.

The inclination of the capillary was measured by means of a sensitive clinometer which allowed angular measurements to be made to ± 3'. The clinometer was placed on the capillary support parallel to the capillary tube and the inclination of the support was measured. Measurements were made at three different positions along the length of the support. Small variations of the measured angle with position of the clinometer along the support were observed so that the average values reported in the following data are accurate to ± 5'.

It is to be noted that the "U"-shaped reservoir was arranged at an angle slightly greater than 90° to the capillary tube so that only when the inclination of the latter was 1 or 2 dgreees were the parallel arms of the reservoir vertical. Since the maximum inclination of the capillary tube was never more than 3°22', it was assumed in all calculations that the arms of the reservoir were vertical.

To operate the inclined flowmeter, the reservoir was filled with water until the meniscus in the capillary tube reached the fixed mark $X = 0$ (Figure 2) which will be called the position of rest, or equilibrium position. The distance from $X = 0$ to the point where the capillary was sealed to the reservoir will be referred to as a. The height of the meniscus in the capillary tube was always greater than the corresponding liquid level in the other arm of the reservoir due to the effect of capillary rise. By referring all measurements to the point $X = 0$, the capillarity effect is automatically cancelled.

The following symbols will be employed in all references to the inclined flowmeter:

X = distance between meniscus and its position of rest in the capillary tube

a = length of liquid in capillary when the meniscus is at its equilibrium position

t_b = time of flow of meniscus over distance (X_o-X) with entrapped air bubble

t_o = time of flow of meniscus over distance (X_o-X), no bubble present

A_1 = cross-sectional area of capillary

A_2 = cross-sectional area of reservoir

r = radius of capillary

θ = the angle of inclination of the capillary to the horizontal

The rate of flow through the capillary tube, with or without an air bubble, was measured by drawing the meniscus up to a point 7 or 8 cms. past the mark on the capillary tube corresponding to X_o by means of a light suction applied at the end of the tube. The suction was released and the time of flow, t_o or t_b, of the meniscus between the fixed marks X_o and X was recorded. From t_o or t_b the corresponding volume rate of flow Q_o or Q_b was calculated from the following equation

$$Q = \frac{(X_o-X)\pi r^2}{t} = \pi r^2 v \qquad (9)$$

The meniscus was drawn past the mark X_o first of all to eliminate any acceleration effects which, however, were shown to be negligible and secondly as a matter of convenience in making the measurements.

To insert an air bubble into the apparatus, use was made of flexible polyethylene tubing attached to a hypodermic syringe. The tubing was pushed through the reservoir up to the edge of the capillary and a bubble of desired size was released into the capillary by ejecting air from the syringe.

It should be noted that the insertion of an air bubble always caused the meniscus to rise above its position of rest by a distance which was approximately equal to the length of the bubble. This effect was cancelled by withdrawing liquid from the reservoir, by means of a syringe, until the meniscus was again equilibrated at $X = 0$. It should be noted, also, that the rate of approach of the meniscus to the position of rest ($X = 0$) was exceedingly slow, particularly with an entrapped bubble, at all inclinations used in this investigation. It was difficult, therefore, to adjust the meniscus to the fixed equilibrium mark to better than ± 3 mm. The equilibrium position was checked before and after each measurement of t_o and t_b, and any deviation greater than ± 3 mm. was considered to invalidate the measurement.

According to the conception of a liquid film surrounding the moving air bubble, as proposed by Fairbrother and Stubbs (1), it may seem at first sight that the distance between the bubble and the meniscus should have increased as flow occurred. With the inclined flowmeter, it was difficult to detect changes in this distance of less than 1 or 2 mm. with any amount of accuracy and no changes greater than this were observed. Furthermore, the presence of a falling meniscus in the inclined capillary meant that a thin film of liquid was left on the wall, the volume of which, conceivably, may have been as large as the volume of liquid which the bubble by-passed. In the results which follow the measured velocity of the meniscus will be referred to as U_b or U_0, depending on whether or not an air bubble was present.

In order to calculate the permeability, ψ, it was necessary to derive an expression for the mean effective pressure, P, while the meniscus travelled over the distance (X_0-X). The derivation of this quantity, which is given by Equation (10) below, is outlined in Appendix A.

$$P = \frac{(X_0-X)\ (\sin\theta + \frac{r_1}{r_2})\rho\, g}{\ln \frac{X_0}{X}} \qquad (10)$$

Experience showed that measurements which involved the slow movement of a meniscus and a long air bubble in a capillary tube were very dependent on the cleanliness of the latter. Accordingly, the capillary tube was thoroughly cleaned with hot detergent solution and hot chromic acid before each experiment. Because of the method of operation which allowed unpurified laboratory air to come in contact with the inside walls of the tube, it happened, not infrequently, that the cleaning procedure had to be repeated after a few measurements had been made because the results became erratic.

3. Free Liquid Flow

The equation governing the rate of flow through the inclined flowmeter, without an entrapped air bubble and neglecting inertia effects, can be deduced from Poiseuille's law:

$$-dV = \frac{\pi r^4 P}{8 \eta L}\ dt \qquad (11)$$

where: $\frac{-dV}{dt}$ is the instantaneous volume rate of flow through the capillary

r is the radius of the capillary tube

P is the instantaneous value of the pressure drop across the capillary

η is the viscosity of the liquid

L is the length of liquid in the capillary tube at any instant

g is the acceleration due to gravity

ρ is the density of the liquid

Since,

$$P = g\rho X \sin\theta + g\rho X \frac{A_1}{A_2}, \qquad (12)$$

$$-dV = A_1 dX = \pi r^2 dX \qquad (13)$$

and

$$L = a + X \qquad (14)$$

then substituting for P, -dV and L in Equation (11) and rearranging

$$\pi\, dX = \pi \frac{r^2 \rho g X}{8\,(a+X)} \left(\sin\theta + \frac{A_1}{A_2}\right) dt \qquad (15)$$

integrating

$$\int_{X}^{X_o} \frac{(a+X)dX}{X} = \frac{r^2 \rho g}{8\eta} \left(\sin\theta + \frac{A_1}{A_2}\right) \int_{o}^{t} dt \qquad (16)$$

which gives

$$(X_o - X) + a \ln \frac{X_o}{X} = \frac{r^2 \rho g}{8\eta} \left(\sin\theta + \frac{A_1}{A_2}\right) t_o \qquad (17)$$

Equation (17) was tested experimentally by observing the value of $\underline{t_o}$ over $(X_o - X)$ at various values of $\underline{a}$ while all other quantities remained constant. Table I shows the observed values of $\underline{t_o}$ and those calculated from Equation (17) at different $\underline{a}$. Similarly Table II shows the observed and calculated values of $\underline{t_o}$ for different values of $\underline{\theta}$, all other quantities in Equation (17) being constant.

Measured values of r, θ, X_o and X were used in the calculations.

TABLE I

Observed and Calculated Values of t_o for Different "a"

θ = 1°10' T = 23.0°C.; (X_o-X) = 30 cm.; X_o/X = 2.

a(cm.)	t_o (obs.)	t_o (calc.)	t_o (obs.)/ t_o (calc.)
2.2	8.1	7.99	1.0
5.3	8.6	8.64	1.0
7.7	9.0	9.12	.99
10.2	9.6	9.70	.99
13.3	10.4	10.5	.992

TABLE II

Observed and Calculated Values of t_o for Different θ

a = 7 cm.; T = 23.0°C.; (X_o-X) = 30 cm.; X_o/X = 2.

θ°	t_o (obs.)	t_o (calc.)	t_o (obs.)/t_o (calc.)
33'	11.2	11.2	1.00
56'	9.6	9.7	.99
1°10'	9.0	8.98	1.0
1°39'	7.7	7.79	.99
2°6'	6.9	6.94	1.0

These results indicate that at small inclinations, flow through the capillary tube is laminar and according to Poiseuille's law. It was necessary to establish this fact since laminar flow is an implicit assumption in the derivation of Equation (7).

C. Equivalent Capillary Length

Given the necessary data, χ, may be calculated readily from Equation (7). An alternative method of calculating χ, which is both simpler than the use of Equation (7) and at the same time illustrative of the resistance to flow caused by an entrapped air bubble, is the following. It involves the definition of l_b', the equivalent capillary length of a bubble of length l_b. By this we mean the length of capillary tubing which filled completely with liquid offers the same resistance to flow as the bubble. Then from Equation (6) and Poiseuille's equation we have:

$$\frac{2\eta l_b Q}{\pi \chi r^3} = \frac{8 Q \eta l_b'}{\pi r^4} \tag{18}$$

whence

$$l_b' = l_b \left(\frac{r}{4\chi}\right) \tag{19}$$

Furthermore it may be shown (cf. Appendix B)

$$(l_b' - l_b) = B \frac{\left[\sin\theta + A_1/A_2\right]}{\eta} (t_b - t_o) \tag{20}$$

where

$$B = \frac{\rho g r^2}{8 \ln \frac{X_o}{X}} \tag{21}$$

Thus l_b' is easily derived from the measured values of t_b and t_o and from Equation (19) χ may be calculated.

The quantity $l_b'/l_b = f$ is defined as the "bubble resistance factor". It is a measure of the resistance to flow per unit length of the bubble.

D. Flow with an Entrapped Air Bubble

The decrease in permeability of a capillary tube due to the presence of an entrapped air bubble was determined by making measurements, at fixed θ, of t_o and t_b for several bubble lengths. From the measured quantities, ϕ_o and ϕ_c were calculated according to Equation (2), P being given by Equation (10). The observations are recorded in Table III along with the permeability values ϕ_o and ϕ_c, the film thickness calculated from Equation (19) and the bubble resistance factor, f.

TABLE III

Data Relating to Flow with an Entrapped Air Bubble

A. $X = 30.2$ cm. $\theta = 35'$ $\phi_o = 2.4 \times 10^{-7}$ cc.
$X_o = 60.2$ cm. $P = 1920$ dynes/$_{cm}2$ $T = 24.0$°C.

l_b cm.	U_b cm./sec.	$\phi_c \times 10^7$ cc.	$\chi \times 10^4$ cm.	f
.56	2.34	1.96	8.7	21.4
.67	2.26	1.89	8.16	21.1
1.10	2.00	1.68	9.27	20.0

B. $X = 31.0$ cm. $\theta = 58'$ $\phi_o = 2.4 \times 10^{-7}$ cc.
$X_o = 61.0$ cm. $P = 2240$ dynes/$_{cm}2$ $T = 24.0$°C.

l_b cm.	U_b cm./sec.	$\phi_c \times 10^7$ cc.	$\chi \times 10^4$ cm.	f
.36	3.03	2.18	11.1	16.8
.57	2.75	1.98	9.16	20.2
.75	2.54	1.83	8.55	21.7
1.10	2.26	1.62	8.40	22.1

C. X = 30.2 cm. θ = 1°7' ϕ_o = 2.4 x 10^{-7} cc.
X_o = 60.2 cm. P = 2320 dynes/cm^2 T = 24.0°C.

l_b cm.	U_b cm./sec.	$\phi_c \times 10^7$ cc.	$\chi \times 10^4$ cm.	f
.37	3.12	2.16	10.4	17.9
.62	2.94	2.04	11.4	16.3
1.20	2.34	1.64	8.92	20.8

D. X = 30.2 cm. θ = 1°39' ϕ_o = 2.26 x 10^{-7} cc.
X_o = 60.2 cm. P = 2720 dynes/cm^2 T = 25.2°C.

l_b cm.	U_b cm./sec.	$\phi_c \times 10^7$ cc.	$\chi \times 10^4$ cm.	f
.48	3.57	2.04	15.1	12.3
.66	3.38	1.90	13.3	14.0
.84	3.17	1.82	11.9	15.5
1.00	2.94	1.68	10.2	18.1
1.11	2.76	1.58	9.02	20.4

E. X = 30.2 cm. θ = 2°10' ϕ_o = 2.4 x 10^{-7} cc.
X_o = 60.2 cm. P = 3100 dynes/cm^2 T = 27.2°C.

l_b cm.	U_b cm./sec.	$\phi_c \times 10^7$ cc.	$\chi \times 10^4$ cm.	f
.53	4.42	2.12	14.0	13.3
.76	4.06	1.95	11.6	16.0
.87	3.85	1.85	10.4	17.9
1.15	3.49	1.67	9.62	18.4

F. X = 30.2 cm. θ = 2°51' ϕ_o = 2.3 x 10^{-7} cc.
X_o = 60.2 cm. P = 3620 dynes/cm^2 T = 26.7°C

l_b cm.	U_b cm./sec.	$\phi_c \times 10^7$ cc.	$\chi \times 10^4$ cm.	f
.65	5.01	2.08	21.4	8.70
.85	4.69	1.94	16.3	11.3
.95	4.48	1.86	14.0	13.2
1.03	4.35	1.81	13.2	14.0

G. $X = 30.2$ cm. $\theta = 3°22'$ $\phi_o = 2.13 \times 10^{-7}$ cc.
$X_o = 60.2$ cm. $P = 4280$ dynes/cm^2 $T = 27.3$°C.

l_b cm.	U_b cm./sec.	$\phi_c \times 10^7$ cc.	$\tau \times 10^4$ cm.	f
.58	5.66	1.96	19.9	9.34
.76	5.26	1.82	14.5	12.8
.90	5.09	1.76	14.0	13.2
1.40	4.19	1.45	10.2	18.2

The data clearly show that the presence of an entrapped air bubble decreases the permeability of the capillary tube. The decrease being from 10 to 30% depending on the velocity and length of the bubble.

Admittedly as the data are presented, it is difficult to separate the contribution of bubble velocity and bubble length; this was a limitation which could not be overcome. However, by comparing results for the same $\underline{l_b}$ but different $\underline{U_b}$, and vice versa, it may be concluded that decrease in permeability is greater the longer the bubble and the smaller the velocity. This is in qualitative accord with Equation (8). By the same method, the film thickness appears to be mainly a function of bubble velocity which is the prediction of the empirical Equation (1).

The bubble resistance factor is a measure of the resistance to flow per unit bubble length. Since $\underline{f}$ is an inverse function of τ (Eq. 19) it must vary inversely as $\underline{U_b}$. The values of $\underline{f}$ are themselves worthy of note. Thus in the present case, a bubble of unit length offers the same resistance to flow as a 10 to 20 cm. length of capillary, depending on its velocity.

The relation between $\underline{U_b}$ and $\underline{f}$ or $\underline{U_b}$ and $\underline{\tau}$ is not unexpected. Since the tangential drag on the bubble increases with bubble velocity, the bubble tends to increase its axis ratio with velocity so as to assume the shape of minimum hydrodynamic resistance. This results in a large percentage increase in film thickness with a consequent decrease in f.

The effect of bubble velocity on the thickness of the liquid film was investigated systematically by the conductance method reported in the following section. In this way the calculated τ reported in Table III were checked by direct measurement.

III. Conductance Method

A. Theoretical Considerations

The electrical resistance of a capillary tube filled with liquid will be increased by the presence of an air bubble sufficiently large to assume the cylindrical shape of the capillary tube. If, however, the air bubble is surrounded by a thin liquid film, then the electrical resistance will not become infinite. Furthermore, if it is assumed that the thin liquid film has the same specific conductivity as the bulk liquid then quite evidently the thickness of the liquid film may be calculated from the increase in resistance due to the entrapped air bubble.

Thus the electrical resistance of a capillary tube filled with liquid is:

$$R_o = \frac{1}{k} \frac{L}{r^2} \qquad (22)$$

where R_o is the electrical resistance

k is the specific conductivity of the liquid

L is the length of the capillary tube

r is the radius of the capillary tube

With an entrapped air bubble which for simplification is assumed to be cylindrical:

$$R_b = \frac{1}{k\pi}\left(\frac{L - \ell_b}{r^2} + \frac{\ell_b}{2r\tau}\right) \qquad (23)$$

where ℓ_b is the length of the bubble

τ is the thickness of the liquid film

If τ is small relative to r then

$$\tau = \frac{\ell_b}{2\pi rk\ (R_b - R_o)} \qquad (24)$$

If the resistance of the capillary tube with and without the bubble is measured, then τ may be calculated. The advantage of the conductance method is that it affords a direct measure of the instantaneous film thickness around the bubble.

This method might be objected to on the basis that in a thin film of aqueous electrolyte a considerable part of the current is carried along the walls of the capillary tube. However, if surface conductance is a factor in these measurements it should be detected by carrying out measurements at several electrolyte concentrations (2). If τ proves to be independent of electrolyte concentration, then it may be concluded that surface conductance is of minor importance.

B. Experimental

1. Method and General Procedure

Measurements of the thickness of the liquid film around an air bubble moving at constant speed in a capillary tube were made using the cell sketched in Figure 3. A constant head of liquid was maintained at the inlet by the overflow tube (A) while the actual rate of flow through the detachable capillary tube (D) was regulated by an adjustable pinchclamp at (G).

Conductance measurements were made by the direct current (d.c.)

FIGURE 3

Conductance Cell for Measurement of the Film Thickness
Surrounding a Moving Air Bubble.

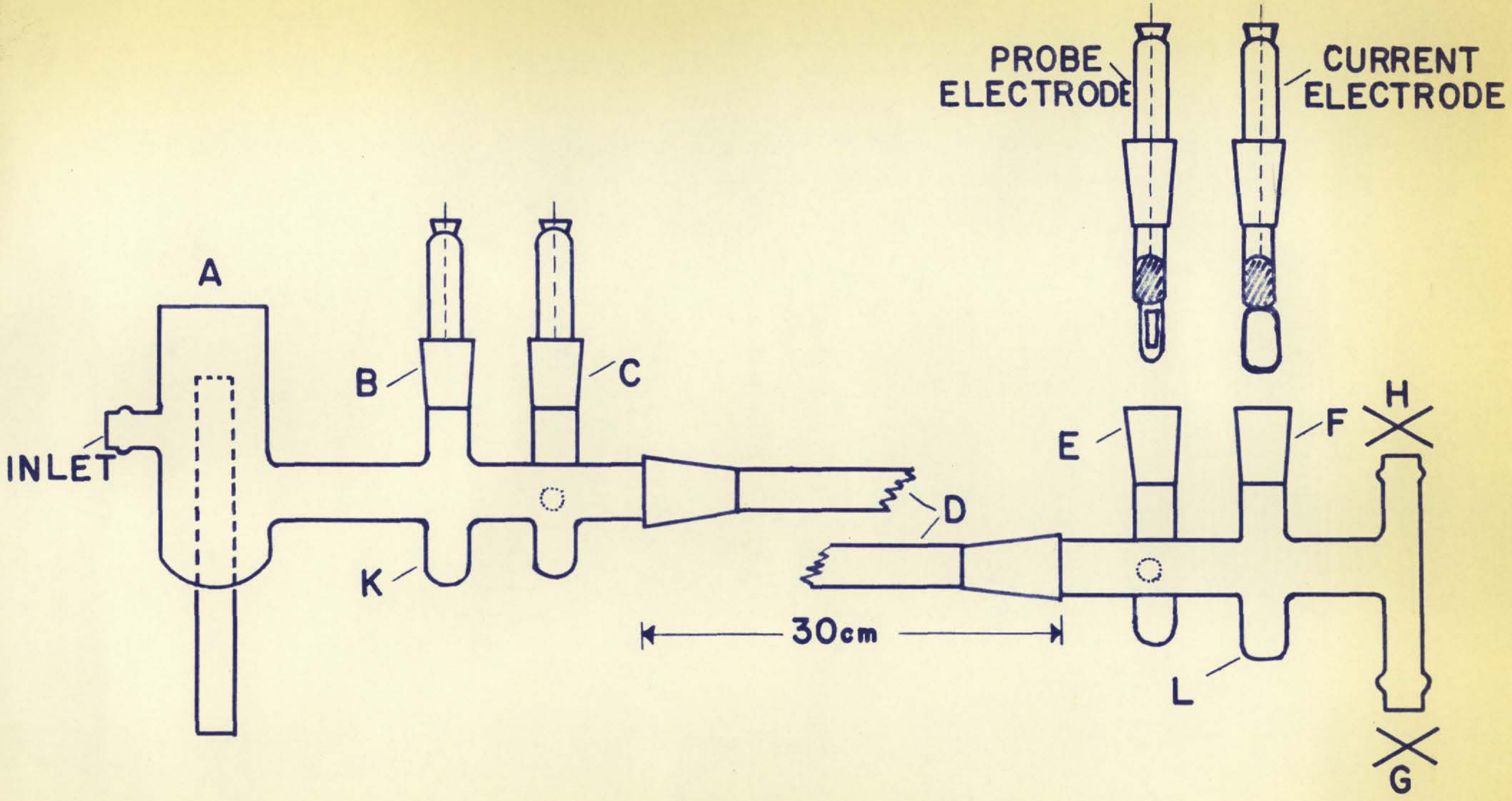
PROBE ELECTRODE
CURRENT ELECTRODE
A
B
C
INLET
K
D
30cm
E
F
H
L
G

method of Gunning and Gordon (3). Two silver-silver chloride electrodes which were inserted at B and F, carried the direct current to the potassium chloride solution while the potential drop across two silver-silver chloride probes inserted at C and E was measured. The value of the d.c. current was determined by measuring the potential drop across a standard resistor which was in the circuit. From the voltage drop across the probes and the current, the resistance of the column of liquid with and without an entrapped air bubble was obtained. The film thickness $\underline{t}$ was calculated from Equation (24).

The actual procedure was the following: with the electrodes in position, the cell completely filled with liquid and pinchclamp G closed so that no flow occurred, a bubble was inserted in the capillary tube by means of the long flexible polyethylene tubing which was pushed into the cell through the overflow tube. Then the length of the stationary bubble was measured to ± 0.5 mm. by means of a graduated scale. (Due to a slow movement of the bubble, it was not possible to use a cathetometer). Pinchclamp G was opened slightly and the bubble began to move in the tube. The current electrodes were connected to a six-volt battery through a 1-megohm resistor in series with a shielded decade resistor, R_s, which could be carried from 0 to 100,000 ohms (cf. Figure 4). The megohm resistor served to keep current variations to a minimum.

As the front end of the bubble passed a fixed mark at the centre of the tube, a Brush (model BL-211) recording oscillograph (R.O.) with coupled d.c. amplifier (model BL-935) which was recording a reference voltage was switched across the probes. Thus the potential drop across the probes (V_b) was continuously recorded until the bubble reached a second fixed mark on the capillary tube and the R.O. was switched across the standard resistor R_s to record its potential drop (V_{R_s}) while the bubble continued its steady course. Finally, the R.O. was switched back to the reference voltage. The

FIGURE 4

Working Circuit for Measurements of the Film Thickness
Surrounding Moving Bubbles

Sample Section of Oscillograph
Chart with Recorded Voltages.

WORKING CIRCUIT

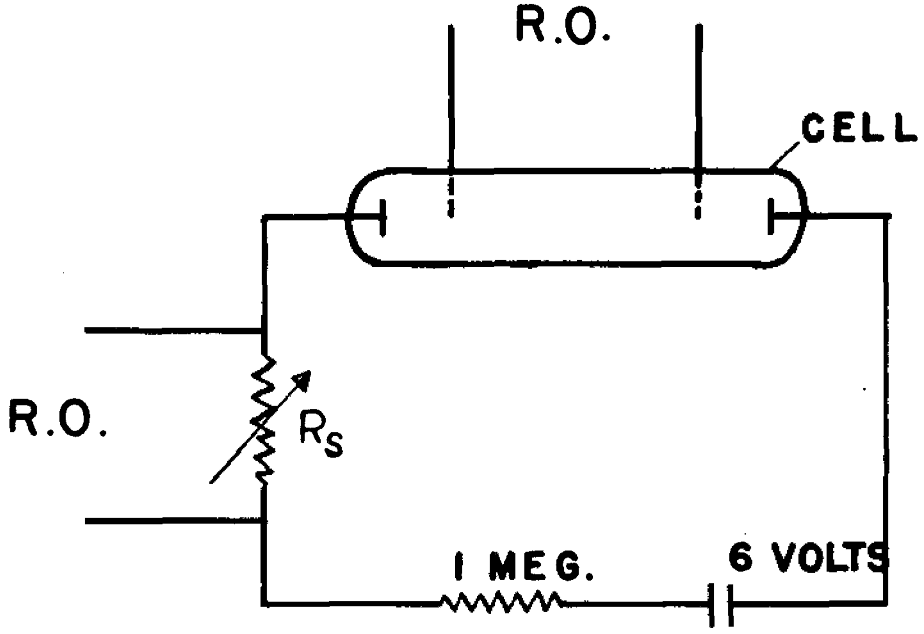

SCHEMATIC APPEARANCE OF R.O. CHART

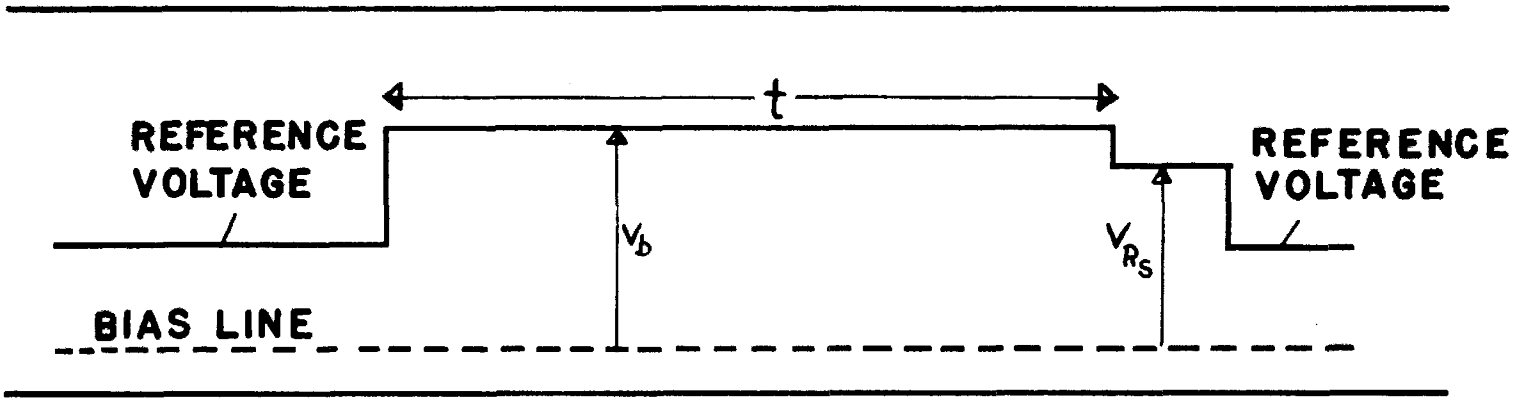

time constant of the toggle switches was such that the biased needle of the oscillograph could not respond to the point of zero input voltage, as the recorder was switched from one circuit to another.

The fixed distance over which measurements were made varied in length from 3.0 to 10.0 cms. depending on the velocity of the bubble.

As the bubble neared the end of the capillary tube, pinchclamp H was opened just enough so that the flow of liquid from a reservoir above caused the bubble to reverse its direction. When it had reached the other end of the capillary, H was closed; G was adjusted to give a new bubble velocity and the potential measurements were repeated.

By this procedure the film thicknesses corresponding to several different velocities were determined for each bubble. The effects of bubble length, capillary radius, surface tension and liquid viscosity on the thickness of the liquid film were studied.

The recording oscillograph was a valuable tool throughout this investigation. It served the following purposes:

(1) It acted as a stopwatch. Since the chart motor moved at a constant known speed, the length of the line traced by the pen while the bubble travelled over the fixed distance could be translated into the time of flow over that distance.

(2) It showed any variation in film thickness as the bubble moved between the fixed marks which indicated that τ and $\underline{U_b}$ had not reached their equilibrium values. This seemed to occur particularly at higher $\underline{U_b}$ and depended on the film thickness as the bubble began to move. Only equilibrium measurements were considered in this investigation.

(3) Finally, the oscillograph recorded automatically and accurately the potential drop across the probes with and without a bubble and across the standard resistor.

2. Electrodes and Cell

A current electrode is sketched in Figure 3. The electrode was made by sealing the pointed end of a heavy platinum foil, 0.5 cm. x 1 cm., to a 3 cm. length of 0.6 cm. o.d. "Nonex Brand" tubing. The Nonex tube was then sealed to the small end of a $\frac{12}{30}$ ₮ joint. Electrical contact with the platinum foil was made by means of a small column of mercury.

The probe electrodes, one of which is illustrated in Figure 3, also were constructed in the same way as the current electrodes, except that the platinum foil was only 0.15 cm. x 0.7 cm. and was completely backed with Nonex glass.

A small, narrow probe is necessary for the measurement of electrolytic conductance by the d.c. method. Theoretically, the probe should be a point since any size it has will cause a sensible ohmic drop across it. In practice, this shows up as a change in the apparent resistance with change of current.

The point feature of the probes is further accentuated by offsetting the probe chambers from the current path (cf. Figure 3). The chambers are joined to the cell by means of constricted necks. When in position,the current electrodes dip into the wells at K and L in Figure 3 in order to prevent the products of electrolysis from contaminating the main body of solution.

The electrodes were made reversible with respect to chloride ions by silvering and then chloridizing according to the method of Gunning and Gordon (3).

In practice a small difference in potential always exists between electrodes. In the present investigation, the residual potential between the probes varied from 0.0005 v. to 0.001 v. Generally, it was negligible compared to the measured values. Nevertheless, it was always checked before and after each series of measurements on a potentiometer and a correction was applied to V_b if the average value was significant.

To check the reliability of the d.c. method in a cell of such large cell constant, the following measurements were performed. A solution of recrystallized KCl having a specific conductivity k = 0.00141 ohm^{-1} cm^{-1} (4) at 25.0°C. was made up. The electrodes and probes were allowed to stand in the solution for one hour after which the cell was rinsed twice and then filled with the solution. The potential drop across the probes and across the standard resistor was measured on a "Type K" Leeds & Northrup potentiometer for both directions of the current. A large decade resistor variable in 10^5 ohm steps was included in the circuit to vary the current. The mean values of the voltage drop across the probes (V_o) and the currents are recorded in Table IV along with the calculated values of R_o, the resistance of the solution.

TABLE IV

Potential Drop Across Probes and Resistance of Solution at Different Currents for KCl Solution of k = 0.00141 $w^{-1}cm^{-1}$(at 25.0°C.)

V_o volts	$I \times 10^6$ amps	$R_o \times 10^{-5}$ ohms	T °C.
.88153	3.1116	2.8345	26.7
.82021	2.9093	2.8196	
.76783	2.0615	2.8144	
.72142	2.5655	2.8083	
.68032	2.4255	2.8010	
.64360	2.3021	2.7957	27.7

The slight variation in R_o with current is most probably accounted for by the temperature change during the measurements.

From the known specific conductance of the potassium chloride solution at 25.0°C. a cell constant was calculated by applying a correction of 2% per degree to the R_o value at 27.7°C. The cell constant so obtained was 413.

Another KCl solution consisting of 3.7236 gms. in 500 ml. of solution was made up and the results recorded in Table V were obtained.

TABLE V

Potential Drop Across Probes and Resistance of Solution at Different Currents

V_o volts	$I \times 10^6$ amps	$R_o \times 10^{-4}$ ohms	T °C
.07953	2.651	3.119	26.9
.08922	2.974	3.118	26.9
.09476	3.159	3.120	26.8
.10162	3.3873	3.1296	26.7
.11759	3.9197	3.1253	26.8
.13929	4.6430	3.1208	26.9

The constancy of R_o over the current range is more than satisfactory. From Jones and Prendergast (5) the specific conductivity of a solution of 3.7167 gms. KCl/500 gms. solution is 0.012886 $\text{ohms}^{-1}\ \text{cm}^{-1}$ at 25.0°C. Correcting the mean value of R_o from Table V to 25°C, the calculated specific conductivity using the previously determined cell constant was 0.0128 $\text{ohm}^{-1}\text{cm}^{-1}$.

Since the range of currents used in the present investigation was approximately 2 to 6 x 10^{-6} amps it was concluded from the above data that Ohm's law applied over the range of currents used and the d.c. method gave a reliable measure of the resistance between the probes.

C. Treatment of Observations on Moving Bubbles

Aside from the preliminary calibrating of the R.O., the measurement of the potential drop across the probes and the measurement of bubble length, all other data were recorded on the oscillograph chart during a series of measurements on a given bubble.

Figure 4 shows how the measured quantities appeared on the chart. From the length of the line corresponding to V_b and the chart speed (0.5 cm./sec.) the time of flow t was calculated. V_b and V_{Rs} were obtained by adding the pulses to the bias voltage. V_b was corrected for the potential difference across the probes to give V_b corr. Figure 5 shows a typical set of data, in this case belonging to run No. 42. Column 2 corresponds to the length of capillary over which the measurements were made.

D. Results with Moving Bubble

The empirical equation of Fairbrother and Stubbs:

$$\tau = \frac{r}{2}\sqrt{\frac{U_b \eta}{\sigma}} \qquad (1)$$

predicts that for a given liquid at constant temperature a plot of the film thickness versus U_b should yield a straight line. The results which follow do not confirm this relationship. However, over the velocity range covered in these experiments it was possible to draw a straight line through the experimental points the slope of which proved useful for characterizing the effect of the different variables on the thickness of the liquid film. The slope of this line is merely of qualitative significance.

The important data for each run are summarized in Table VI.

The second column in Table VI gives the liquid medium in which the experiment was carried out; it is understood that the appropriate amount of potassium chloride was dissolved in the medium to give it the specific cond-

FIGURE 5

Sample "Record Chart" of Data Obtained from a Single Run.

Run No. 42

Calibration Constant = 0.004175 volts/mm

Potential Drop across probes = 0.00094 v.

V_o (mean) = 0.06988 v.; V_{Rs} = 0.06207 v.;

R_s = 10,000 ohm; R_o = 11,430 ohm.

$k = \frac{413}{11,430} = 0.0365$ ohm^{-1} cm^{-1}.

r = 0.143 cm. λ_b = 0.880 cm. T = -°C.

t sec.	Dist. cm.	U_b cm/sec	R_s ohm	V_{Rs} v.	V_b v.	$V_b$corr. v.	R_s ohm	(R_b-R_o) ohm	x 10^4 cm.
13.2	8	.606	55,000	.3097	.2462	.2471	43,880	32,450	8.27
12.1	"	.661	"	.3097	.2412	.2421	43,000	31,570	8.50
9.70	"	.825	"	.3138	.2274	.2283	40,010	28,580	9.39
11.8	"	.677	"	.3117	.2388	.2397	42,290	32,860	8.70
8.00	"	1.00	"	.3121	.2131	.2140	37,710	26,280	10.2
12.6	"	6.34	"	.3096	.2465	.2550	45,300	33,870	7.92
29.0	"	.276	40,000	.2253	.3576	.3585	63,640	52,210	5.14
25.9	"	.308	"	.2250	.3343	.3352	59,590	48,160	5.57
21.0	"	.380	"	.2275	.3101	.3110	54,680	43,250	6.20
16.9	"	.472	"	.2265	.2805	.2814	49,690	38,260	7.02

TABLE VI

Results of Conductance Method Applied to Moving Bubbles

Run No.	Liquid Medium	T °C.	k ω^{-1} cm^{-1}	l_b cm.	r cm.	σ (bub-liq.) dynes/cm.	η c.p.	$d\psi/d\sqrt{U_b}$ x 10^4 $(\text{cm}\cdot\text{sec.})^{\frac{1}{2}}$
30	20% aqueous glycerol	25.0	0.0276	0.41	0.143	72.4	1.54	50.0
31	"	"	"	0.50	"	"	"	37.4
32	"	27.0	0.0287	0.60	"	"	1.60	27.3
33	"	"	"	0.77	"	"	"	20.5
34	"	"	"	0.93	"	"	"	19.6
35	water	27.0	0.0575	0.42	0.143	74.6	0.854	18.6
36	"	"	"	0.52	"	"	"	15.4
37	"	"	"	0.67	"	"	"	12.6
38	"	"	"	0.79	"	"	"	11.8
40	water	26.2	0.0575	0.26	0.143	74.8	0.872	0
41	water	26.8	0.0126	0.74	0.143	74.6	0.859	12.7
42	"	-	0.0365	0.88	"	-	-	11.0
43	0.5% aqueous diglycol laurate	25.0	0.6164	1.09	0.143	26.5	0.894	23.2
44	water	25.5	0.0216	0.87	0.0771	74.9	0.885	8.6
45	"	25.3	"	0.66	"	"	0.889	8.9
46	"	26.0	"	0.42	"	74.8	0.874	11.3
47	water with benzene bubble	23.7	0.0224	0.80	0.0771	35	0.920	10.0
48	" " " "	"	"	1.11	"	35	"	10.0
49	water with n-hexane bubble	24.0	"	0.88	"	51	0.914	9.0

uctivity recorded in column four. Specific conductivity was calculated from the measured value of R_o and the cell constant.

It should be noted that runs No. 47, 48 and 49 were carried out with liquid bubbles which were immiscible with water and had essentially zero conductance. Values of the surface tension, σ, for these runs correspond to the values found in the literature for the liquid-liquid interfacial tension. Other values of σ in Table VI correspond to the air-water interface and were also obtained from the literature, except for the 0.5% aqueous solution of diglycol laurate used in run No. 43. The surface tension and viscosity of this solution were measured at 25.0°C.

The effect of electrolytes on the surface tension and viscosity of water is small (6). In the present investigation, it was of the same order as the errors due to temperature fluctuations, hence it was ignored.

Some of the plots from which the recorded slopes were taken will be given in the following pages as the effect of the different variables on film thickness is demonstrated.

1. Effect of Bubble Velocity

Figure 6 shows the data of run No. 42 with film thickness plotted against the square root of bubble velocity. It was from such a plot that the slopes recorded in Table VI were obtained.

The broken line corresponds to the Fairbrother and Stubbs relation. Thus, at the same velocity, a greater film thickness is predicted by these measurements.

Unfortunately, it was not possible to control the flow rate so as to work at U_b less than 0.1 cm./sec. The fact that the straight line extrapolates to positive values of U_b suggests: (a) at low bubble velocities the liquid film surrounding the bubble breaks, or (b) the straight line bends

FIGURE 6

Plot of Film Thickness, η, vs. $\sqrt{U_b}$ for the Data of Run No. 42.

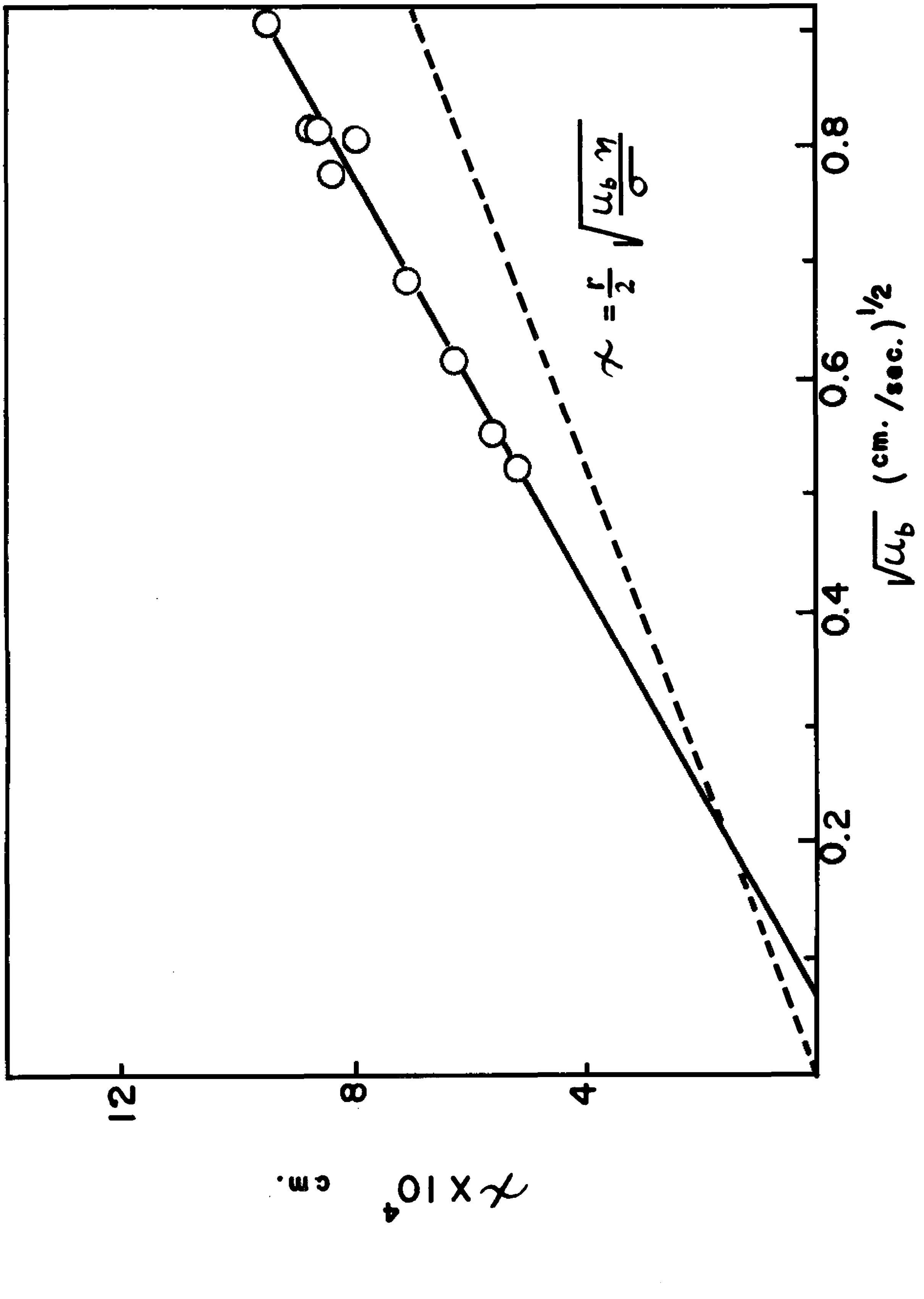
$\chi \times 10^4$ cm.
12
8
4
0.2
0.4
0.6
0.8
$\sqrt{u_b}$ (cm./sec.)$^{1/2}$
$\chi = \frac{r}{2}\sqrt{\frac{u_b \eta}{\sigma}}$

slightly to intersect the ordinate at positive values of $\underline{\chi}$. To study the state of the liquid film surrounding a stationary air bubble was the object of experiments to be reported in a later section.

2. Effect of Bubble Length

Fairbrother and Stubbs mention that their relationship only applies for bubbles whose length is at least one and one half times the diameter of the capillary. Otherwise the slope of the χ vs. $\sqrt{U_b}$ plot becomes a function of bubble length. The same behaviour was observed in the present investigation. This is illustrated in Figure 7 where the data of runs No. 30 and 33 are plotted. The shorter the bubble the greater the slope.

The relationship between slope and bubble length is shown in Figure 8. Curve I is for runs No. 44 to 46 which were carried out in a capillary of 0.0771 cm. radius. Curves II and III were obtained in a capillary tube of 0.143 cm. radius but at different liquid viscosities. It appears that the critical bubble length, beyond which the slope of the $\underline{\chi}$ vs. $\sqrt{U_b}$ line is independent of $\underline{l_b}$, depends on the viscosity as well as the capillary diameter. Other experiments suggest that surface tension is a factor also. From the data, it may be concluded that comparison of the effect of viscosity and capillary diameter on the slope must not be made at bubble lengths less than 0.8 cm. It will be assumed that the same precaution applies regarding all other variables.

In respect to the relationship between bubble length and slope, run No. 40 is of special interest. In this run the bubble length was less than the diameter of the capillary tube so that a definite gap existed between the underside of the bubble and the capillary wall. Under this condition not only was the electrical resistance, R_b, independent of bubble

FIGURE 7

Plots of Film Thickness, τ, vs. $\sqrt{U_b}$ for Runs No. 30 (ℓ_b = 0.41 cm.) and No. 33 (ℓ_b = 0.77 cm.).

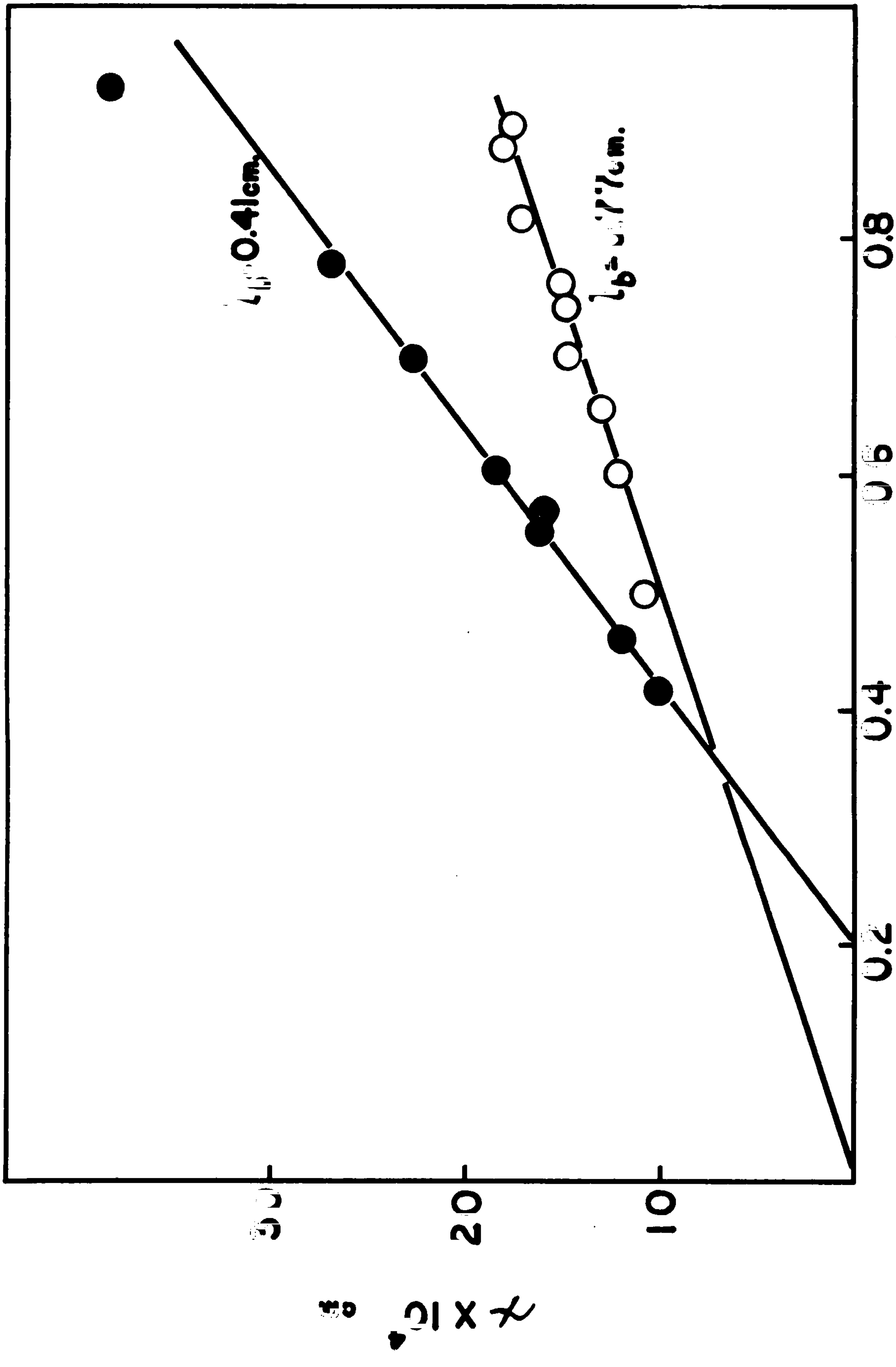
l_b= 0.41cm.
l_b= 0.177cm.
$\varkappa \times 10^4$ cm.
30
20
10
0.2
0.4
0.6
0.8
$\sqrt{u_b}$ (cm. /sec.)$^{1/2}$

FIGURE 8

Plots of Slope vs. Bubble Length, ℓ_b, for Runs:

I: Nos. 44 to 46 r = 0.0771 cm., in water

II: Nos. 35 to 38,41,42 r = 0.143 cm., " "

III: Nos. 30 to 34 r = 0.143 cm., in 20% aqueous glycerol solution

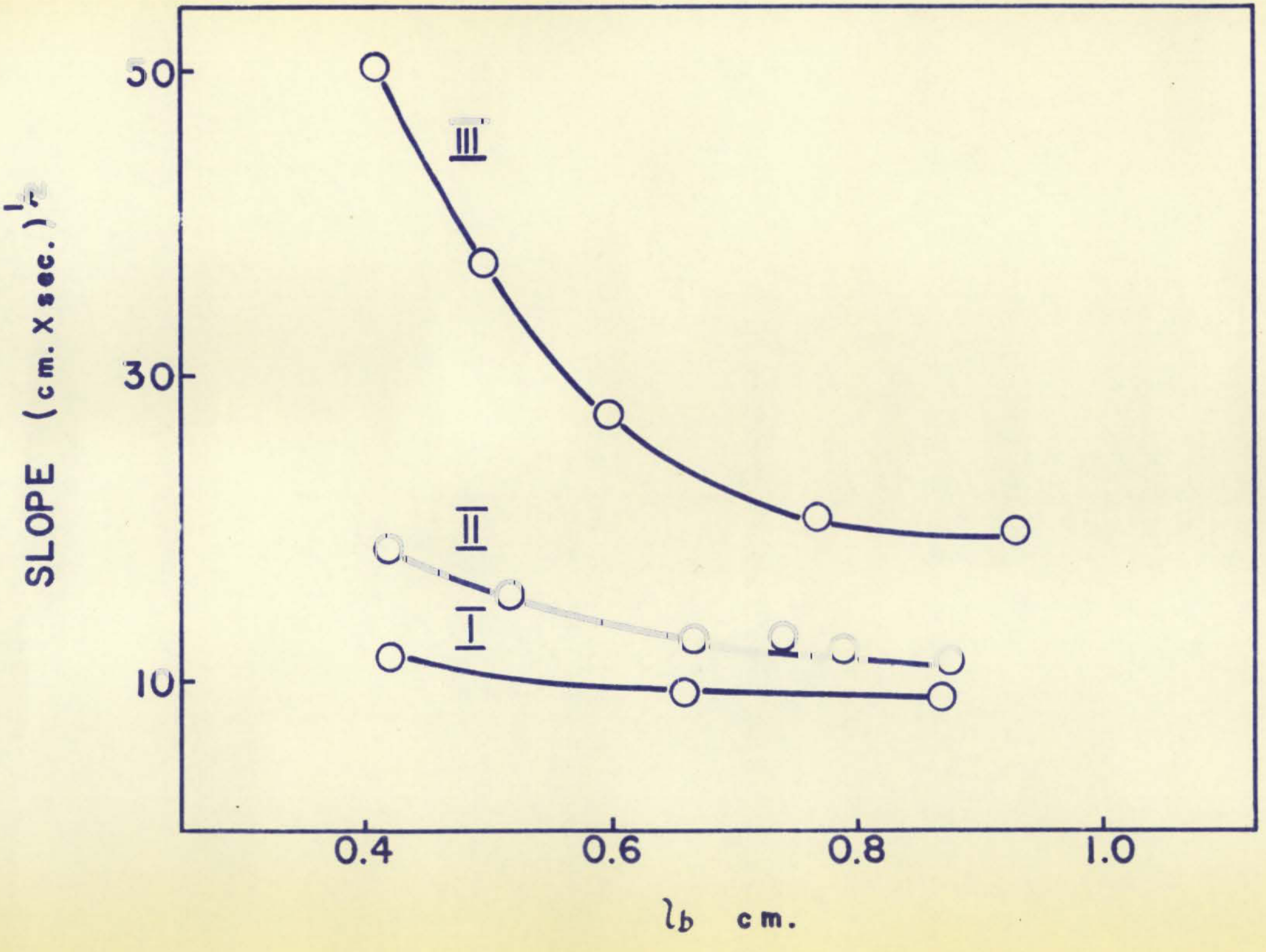
SLOPE (cm. x sec.)$^{-\frac{1}{2}}$
50
30
10
0.4
0.6
0.8
1.0
l_b cm.
III
II
I

velocity, it was independent of the bubble, i.e. R_b was almost identical with R_o. While this was an extreme case, it serves to illustrate that for short bubbles the cylindrical approximation is invalid.

The effect of buoyancy on the shape of the bubble is illustrated in Plates I and II.

From curve II, Figure 8, it may be concluded that surface conductance was of minor importance in carrying the current across the liquid film. This follows, because runs No. 41 and 42 which were carried out at different electrolyte concentrations nevertheless fall on the same curve as runs 35 to 38 which were made at yet another concentration of electrolyte. The overall variation in specific conductivity was from 0.0126 up to 0.0575 $\text{ohms}^{-1}\ \text{cm}^{-1}$.

3. Effect of Surface Tension and Capillary Radius

The effect of surface tension and capillary radius on the liquid film is shown in Figure 9 where runs No. 43 and 44 are plotted. The dotted line represents No. 42 which is included as a reference.

The major differences between Nos. 43 and 42 was in surface tension. The latter run was carried out in pure water while the former was carried out in a 5% diglycol laurate solution which had a surface tension of 26.5 dynes per centimetre. Thus a decrease in surface tension of the medium brings about an increase in the film thickness. Conversely, a decrease in capillary radius caused a decrease in film thickness as shown by No. 44 where the radius of the tube was only one half the radius of the capillary used in run No. 42.

The variation in slope due to surface tension is approximately as predicted by Fairbrother and Stubbs' relation. The variation in slope with capillary radius was only one half the predicted amount.

PLATE I

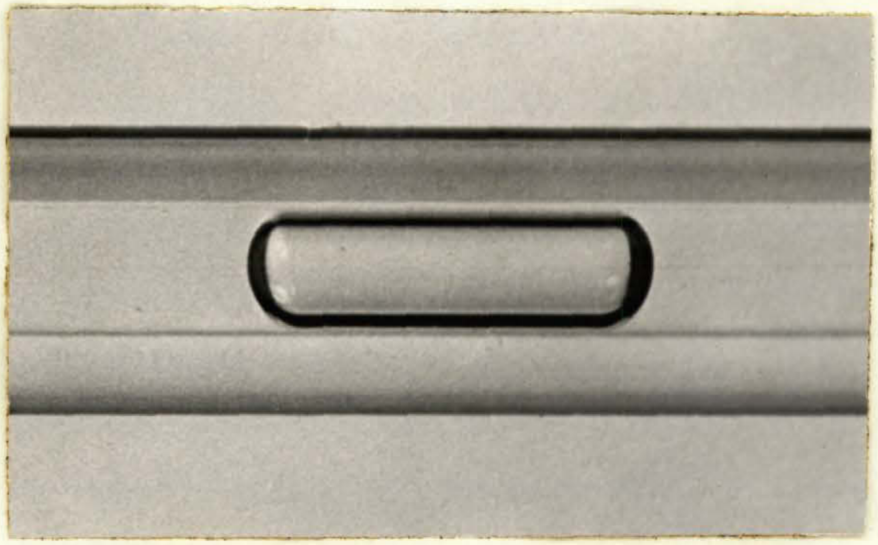

Photoflash of Stationary Bubble: $l_b = 1.2$ cm.; $r = 0.143$ cm.

PLATE II

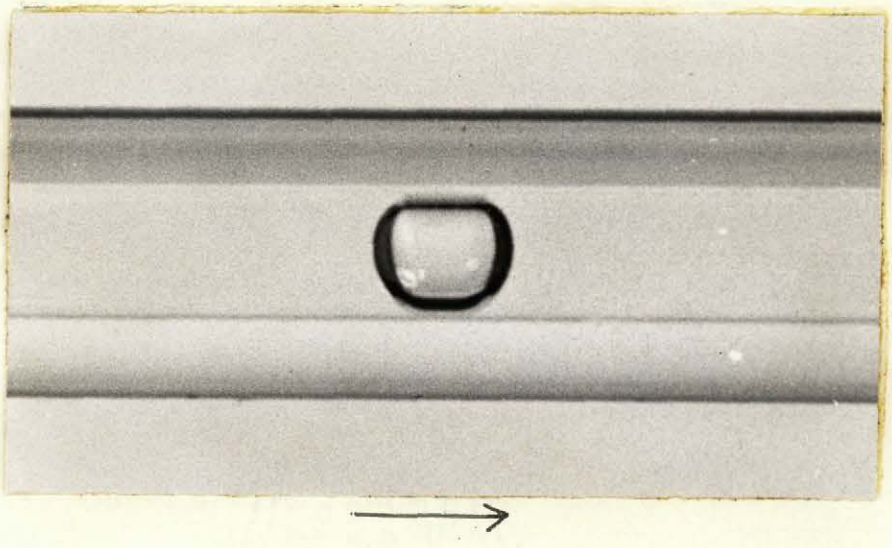

Photoflash of Moving Bubble: $l_b = 0.45$ cm.; $r = 0.143$ cm.

$U_b = 0.22$ cm./sec.,

FIGURE 9

Plots of Film Thickness, χ, vs. $\sqrt{U_b}$ for Runs:

No. 43: 0.5% Aqueous Diglycol Laurate Solution, $r = 0.143$ cm.

No. 44: Water, $r = 0.0771$ cm.

(No. 42: Water, $r = 0.143$ cm.)

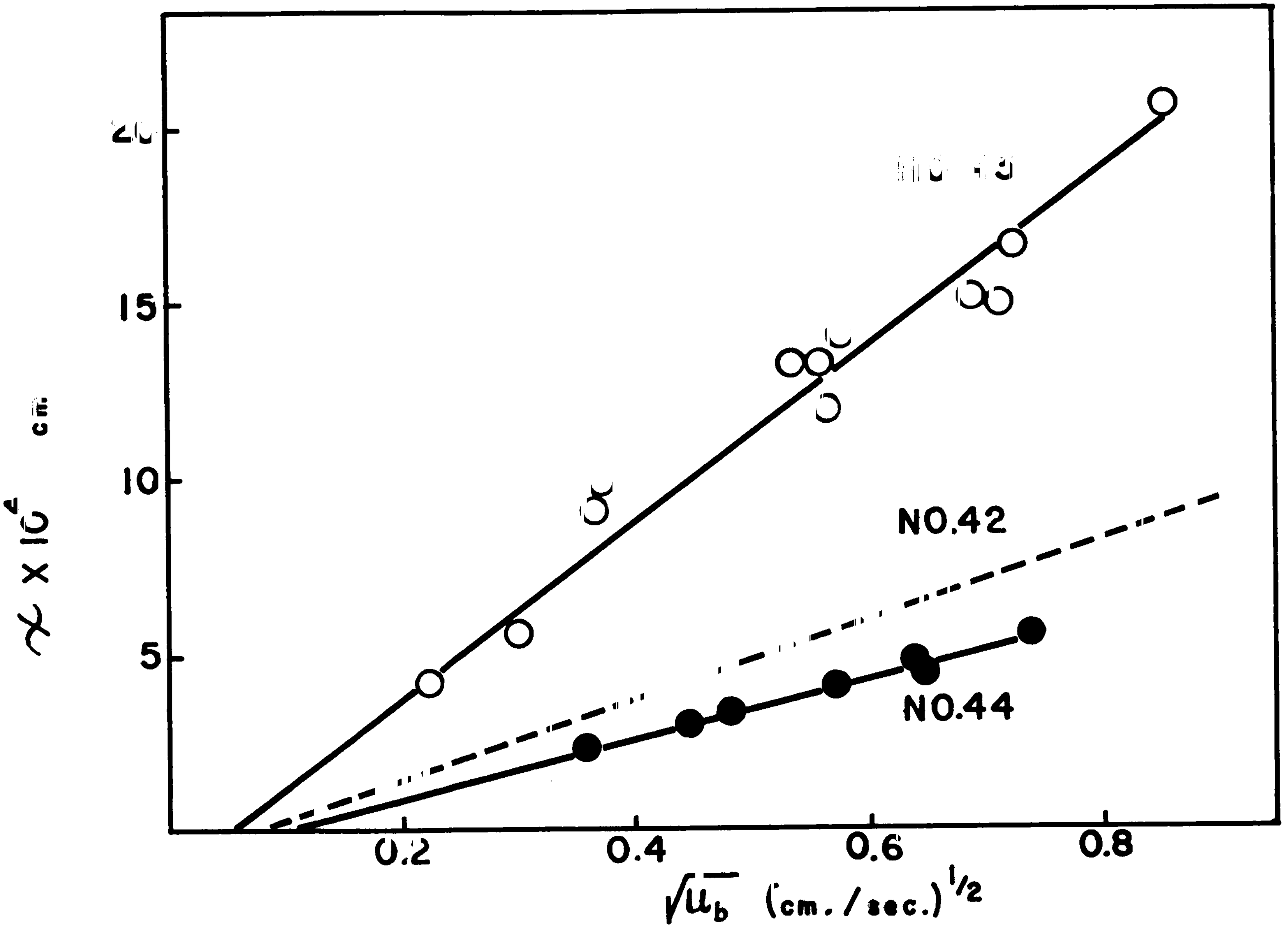
NO.43
NO.42
NO.44
$x \times 10^4$ cm
5
10
15
20
0.2
0.4
0.6
0.8
$\sqrt{u_b}$ (cm./sec.)$^{1/2}$

Surface tension may be considered as a restoring force which represents the bubble's resistance to deformation and accordingly its resistance to increase of film thickness with velocity. Similarly, the curvature of the menisci at the ends of the bubble, which is determined by the capillary radius, represents the bubble's capacity to resist deformation. The smaller the radius of curvature the smaller the film thickness at a given velocity and for a given liquid.

The effect of interfacial tension on the slope of the $\underline{\tau}$ vs. $\sqrt{U_b}$ curve is again illustrated by Figure 10 where the lines corresponding to runs No. 44, 47 and 50 are ordered according to their bubble-liquid interfacial tensions.

4. Effect of Viscosity

The equation of Fairbrother and Stubbs predicts an increase in slope of the $\underline{\tau}$ vs. $\sqrt{U_b}$ plot due to an increase in viscosity of the medium. Figure 11 shows a plot of the data for runs No. 33 and 38 where the former was carried out in a 20% aqueous glycerol solution whose viscosity was 1.60 c.p. but whose surface tension was only slightly different than that of pure water. Run No. 33 was carried out in water of viscosity 0.854 c.p. The increase in viscosity brought about a twofold increase in slope which is considerably more than predicted by the Fairbrother and Stubbs equation.

E. Stationary Bubble

Conductance measurements on moving bubbles did not give any indication as to whether the liquid film persisted when the bubble was stationary. However, it was to be concluded from the work of Elton (7) and Derjaguin (8) that the film would persist for some time at least while the excess pressure within the bubble gradually "squeezed" liquid out of the film. The following data deal with the rate at which the liquid film

FIGURE 10

Plots of Film Thickness, χ, vs. $\sqrt{U_b}$ for Runs of Varying Bubble-Liquid Interfacial Tension

No. 44 - Air bubble in water, interfacial tension: 74.9 dynes/cm.

No. 47 - Benzene bubble in water, " " : 35 "

No. 49 - n-Hexane " " " " " : 51 "

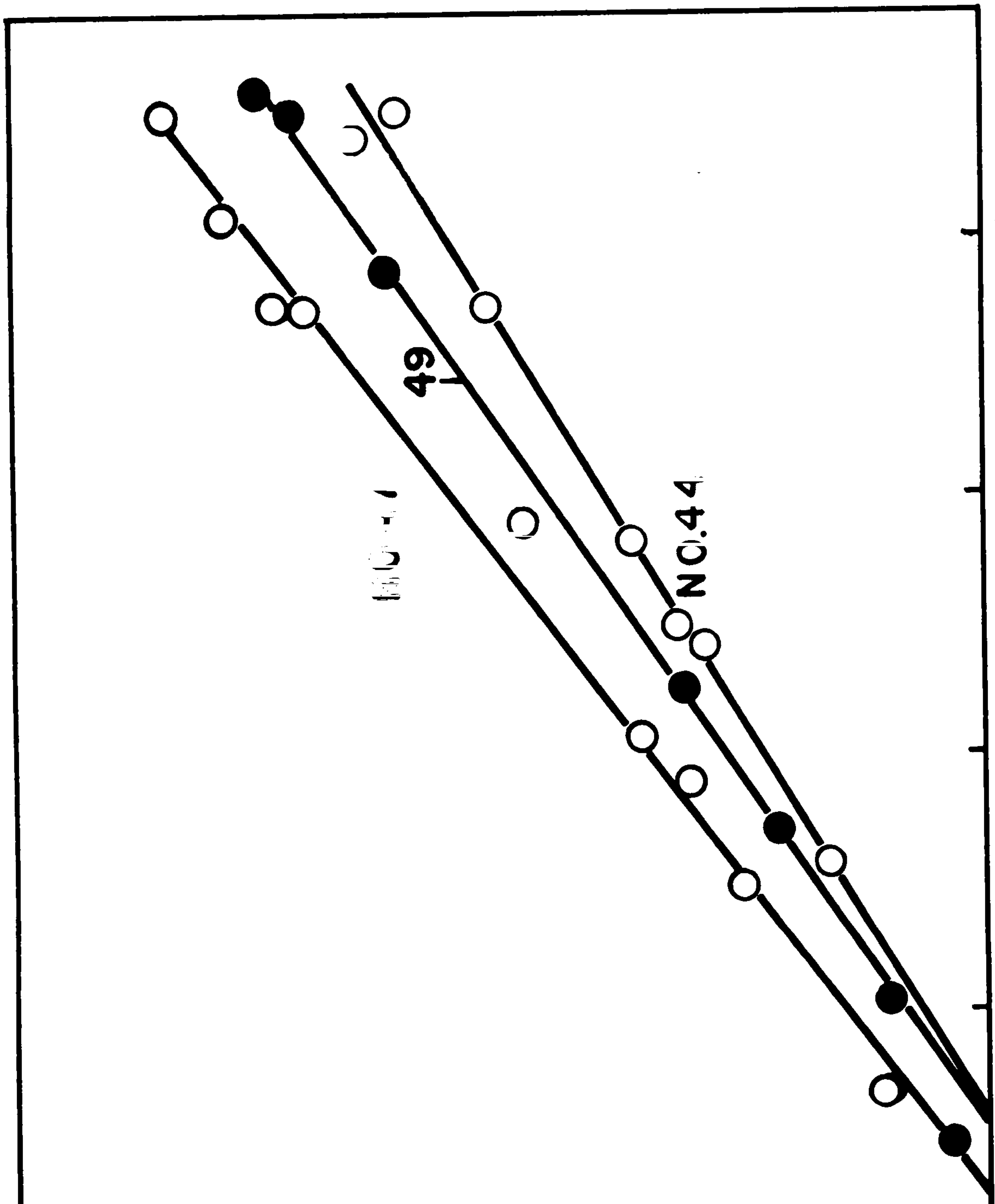

$x \times 10^4$ cm
5.5
4.5
3.5
2.5
1.5
0.3
0.4
0.5
0.6
$\sqrt{u_b}$ (cm./sec.)$^{1/2}$
NO.41
49
NO.44

FIGURE 11

Plots of Film Thickness.χ, vs.$\sqrt{U_b}$ for Runs:

No. 33: Water, viscosity: 0.854 c.p.

No. 38: 20% Aqueous Glycerol Solution,
viscosity: 1.60 c.p.

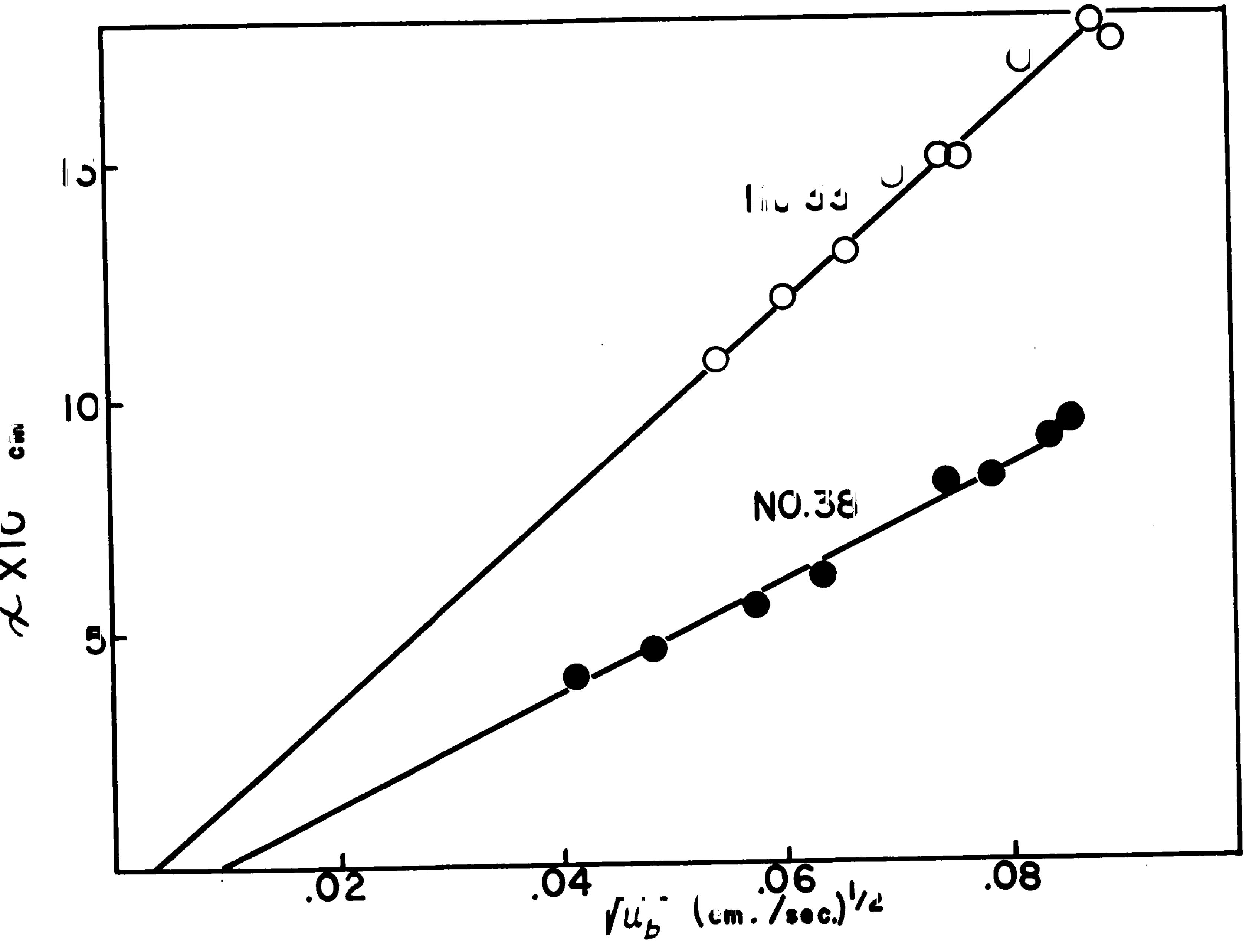
NO.39
NO.38
$\alpha \times 10^{4}$ cm
5
10
15
.02
.04
.06
.08
$\sqrt{u_b}$ (cm./sec.)$^{1/2}$

surrounding a cylindrical, capillary-entrapped air bubble decreases in thickness and the factors which influence this rate.

1. Theoretical Considerations

Before proceeding to the experimental results, it will be useful to consider theoretically the process whereby liquid is forced out of the film.

Let ℓ_b be the length of a long air bubble which is entrapped in a liquid-filled capillary tube of radius r. Furthermore, let the bubble be sufficiently long that it may be approximated by a cylinder of radius r. If it be considered that the excess pressure inside the bubble acting on its surface causes a pressure gradient in the liquid film which is maximum at the centre of the bubble film and zero at the edges, then flow will occur from the centre of the film to the outside edges. If it be assumed further that the flow is viscous, then it may be shown (Appendix C) that

$$t = k\left[\frac{1}{\chi^2} - \frac{1}{\chi_0^2}\right] \qquad (25)$$

where χ is the film thickness at any time t, χ_0 is the film thickness at "zero" time and

$$k = \frac{\eta \ell_b^2}{(P_1 + \frac{\sigma}{r})} \qquad (26)$$

P_1 being the pressure outside the film which was always constant, η and σ being the viscosity and surface tension of the liquid respectively. Thus a plot of $1/\chi^2$ vs. t should be linear if the proposed mechanism applies.

Equation (25) has the same form as the equation derived by Reynolds n 1886 for the approach of two plane parallel discs. It should be mphasized, however, that the above equation is based on the assumption hat the bubble is a rigid cylinder and hence that the film thickness is niform along its length. It will be shown later that this assumption is ot strictly valid, hence the above equation is mainly of qualitative ignificance. In this respect, it will be shown that the effect of ubble length, capillary radius, viscosity and surface tension on the ate of decrease of film thickness is qualitatively predicted by Equation 25).

. Apparatus and Procedure

onductance measurements with stationary bubbles were made with he simple capillary cell sketched in Figure 12. To each end of the apillary tube, A, which was 9 cms. in length, a $\overset{T}{S}$ $\frac{12}{30}$ ground glass oint was sealed. To the side of joint E an ordinary 3 mm. bore stopcock ith an extended right angle arm was sealed. To the end of joint D, a -mm. bore capillary stopcock, B, was attached. Two such cells were constructed. one with average capillary radius, 0.104 cm., and the other 0.152 m. as determined from the length and weight of mercury which filled the ube.

ith stopcock B closed and C open, the cell was filled with lectrolyte solution then the current electrodes, described in a preceding ection. were inserted, as shown, at D and E and the resistance, R_0, of he solution was measured on a portable a.c. bridge. It should be mentioned t this point that simultaneous measurements of the film thickness surrounding a moving bubble by the a.c. and d.c. methods yielded approximately the ame value. Thus. the a.c. method which is used purely as a matter of onvenience. in this case, may be considered as reliable as the d.c. method.

FIGURE 12

Capillary Cell for Measurement of the Film Thickness Surrounding a Stationary Air Bubble.

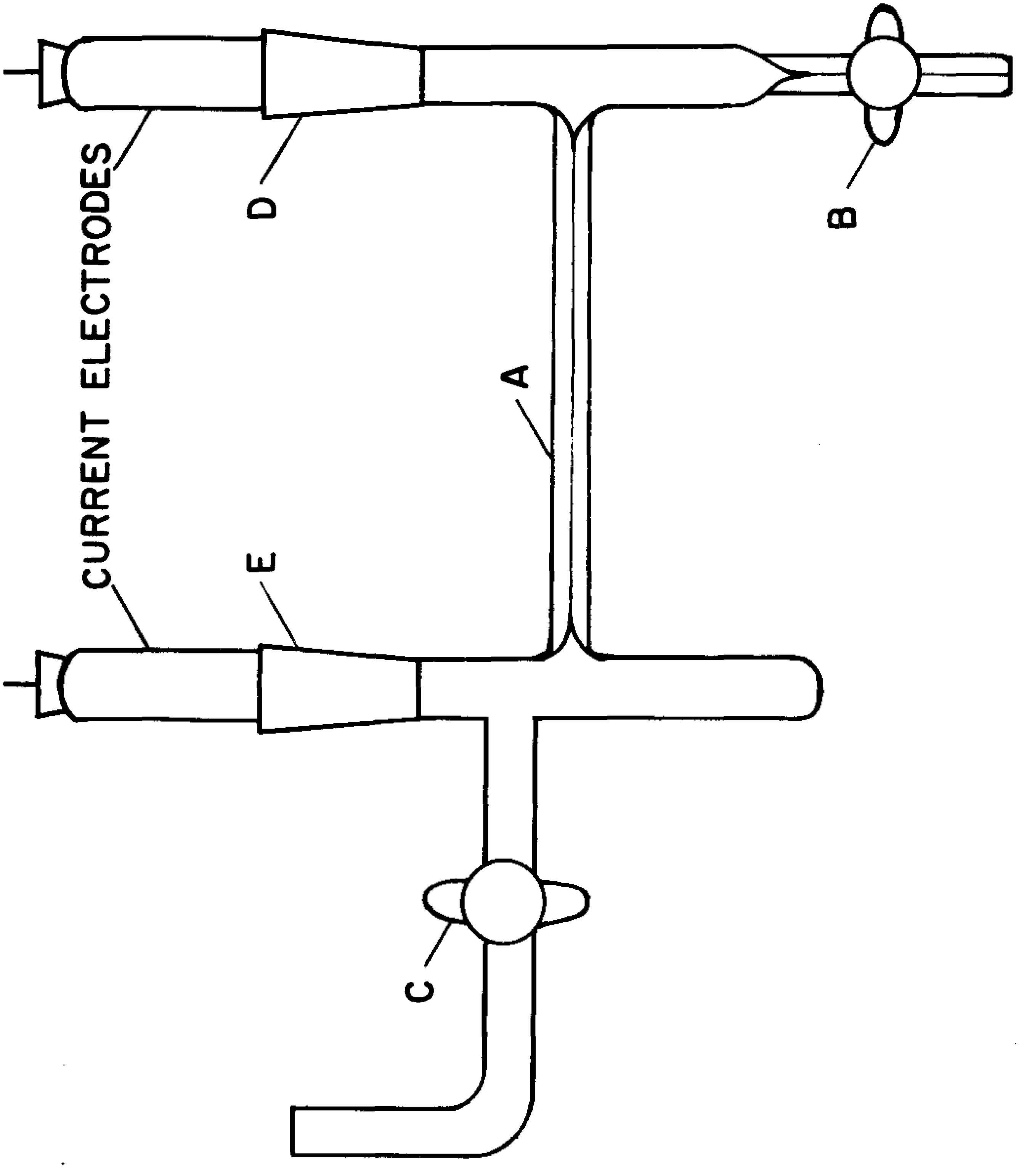
CURRENT ELECTRODES
D
B
A
E
C

After measuring R_o, stopcock C was closed and electrode E was removed to allow a bubble to be inserted at the end of the capillary tube. Electrode E was put back in place, stopcock C was opened, then stopcock B just sufficiently to bring the bubble slowly to a fixed mark at the centre of the tube. B and C were quickly closed and measurements of R_o were made on the a.c. bridge and the time was recorded from the first measurement. At the end of a run λ_b was measured on a cathetometer.

Because of its simplicity, it was possible to keep the capillary cells in an air bath, thermostated at 27.5 ± 0.2°C. Measurements were made from outside the bath. The cells were rinsed with warm cleaning solution, boiled in detergent solution then rinsed in hot distilled water before being used.

The thickness of the liquid film was calculated from Equation 24).

. Results

Table VII records the pertinent data for the several experiments which will be discussed in the following pages.

Figure 13 shows a plot of R_b vs. time for run 4A. The shape of this curve is typical for all the runs on stationary bubbles. The rapid change in film thickness recorded in the first few minutes is probably due to a rapid readjustment in the shape of the bubble which tends to be slightly bullet-nosed during flow (9). This factor will be discussed later. The period of rapid change is followed by an almost linear portion which continues up to 400 minutes after which the curve again changes its slope. Measurements on this particular bubble were continued up to 1500 minutes at which point $R_b = 16.0 \times 10^6$ and was still increasing although at a considerably lessened rate. Figure 14 shows how the film thickness cal-

TABLE VII

Data Pertaining to Measurements on Stationary Bubbles

Run No.	Liquid Medium	T °C.	k $ohm^{-1}\ cm^{-1}$	l_b cm.	r cm.	η c.p.	σ ([illegible]) dynes/cm.
4A	water	27.5	0.0121	1.938	0.104	0.844	74.6
6A	"	"	"	1.380	"	"	"
7A	"	"	0.0532	1.320	"	"	"
8A	"	"	0.0510	1.990	"	"	"
9A	"	"	"	2.540	"	"	"
10B	"	"	"	1.906	0.152	"	"
12A	20% aqueous glycerol	"	0.0510	1.946	0.104	1.51	72.6
13A	0.5% aqueous diglycol laurate	"	0.0532	1.938	"	0.844	26.4

FIGURE 13

Plot of the Resistance, R_b, of a Capillary Tube Containing a Stationary Air Bubble vs. Time for Run 4A.

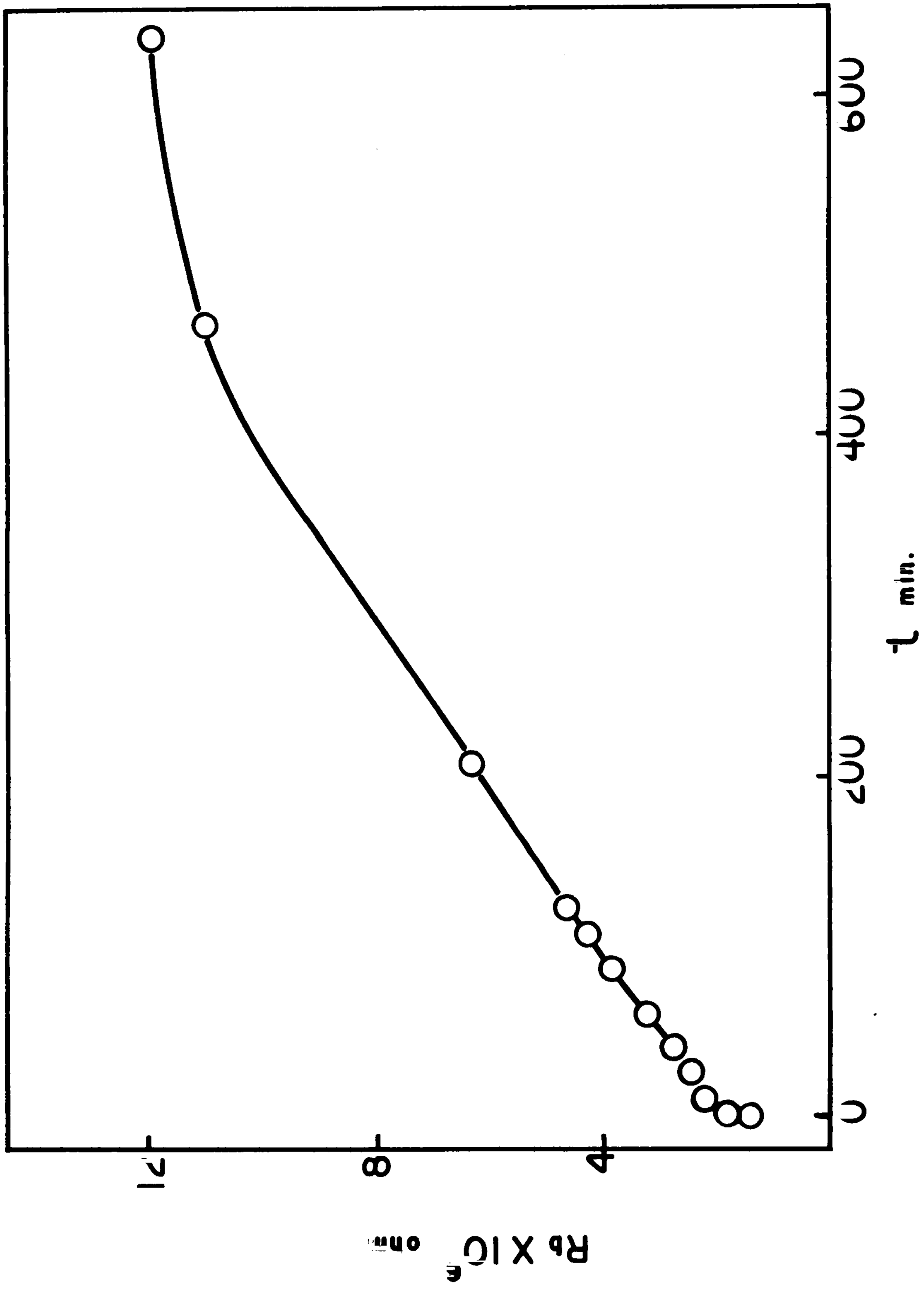
Rb X 10⁶ ohm
4
8
12
0
200
400
600
t min.

FIGURE 14

Plot of Film Thickness, γ, Surrounding a Stationary Air Bubble vs. Time for Run 4A.

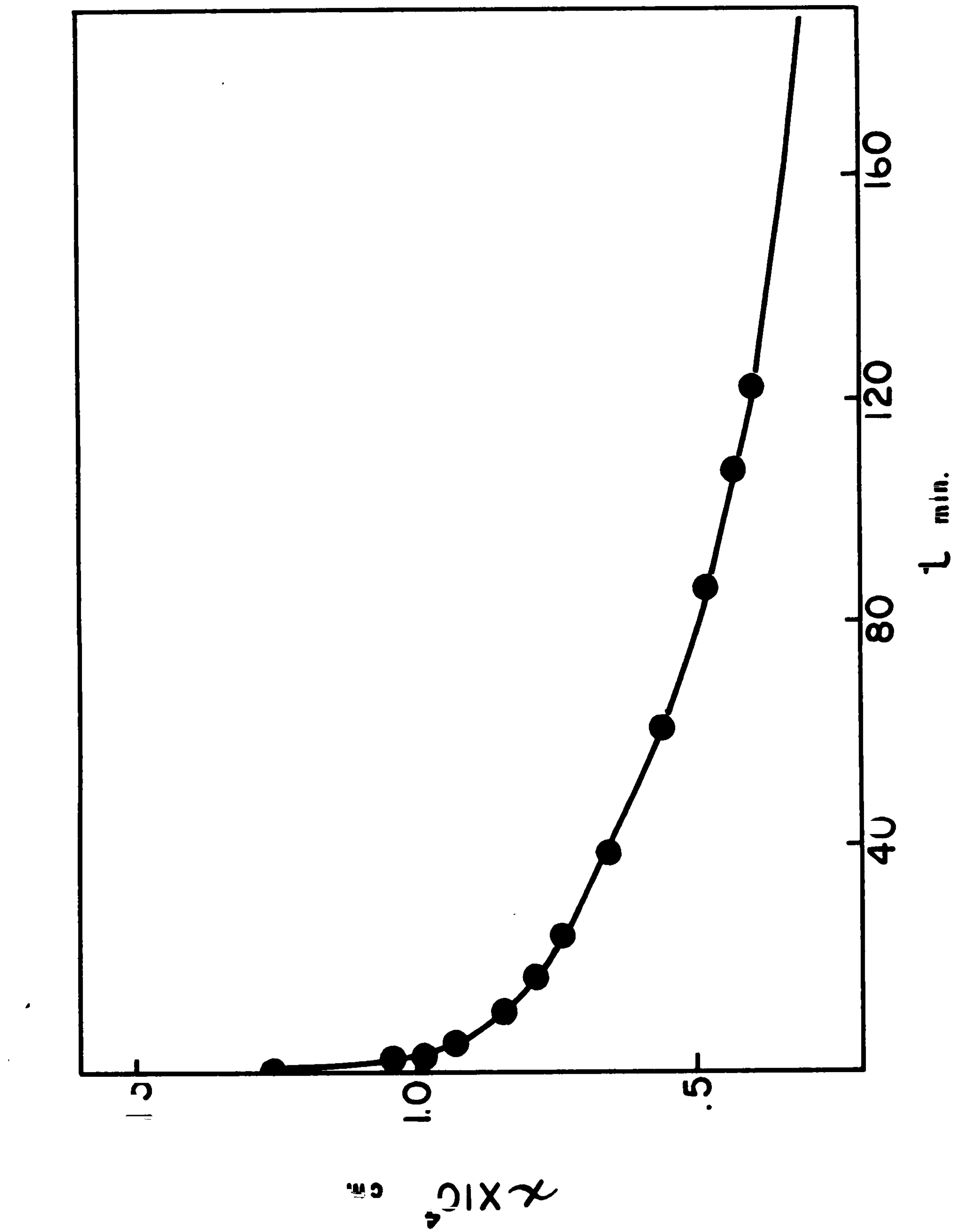

1.5
1.0
.5
40
80
120
160
t min.
$x \times 10^4$ cm.

ulated from R_b decreases with time. It is to be noted that after 75 nutes $\gamma = 0.5$ micron which is approximately a twentyfold decrease from he values obtained for moving bubbles. Equation (25) predicts a value r about 1 micron. After 1500 minutes, $\gamma = 0.112 \times 10^{-4}$ cm. and interstingly enough, the calculated value is roughly 0.2×10^{-4} cm.

Run 6A, where the variables were similar to run 4A was carried n for 7,000 minutes at which time the film thickness was 0.0925 micron. quation (25), under these conditions, predicts a value of 0.01 micron, e. 100 Å. It is obvious that Equation (25) which is based on the ssumption of normal viscous flow no longer applies and one must assume ther that the film has an abnormally high viscosity or that the conductnce method ceases to be valid in this range. The only certain conclusion hat may be drawn is that a liquid film is still present.

A plot of the data for run 4A according to Equation (25) yields he curve drawn in Figure 15 which shows definite departure from the predcted linearity. Some of the assumptions involved in the derivation of quation (25) would appear to be invalid. However, the effect of the ifferent variables on the rate of change of film thickness can be evaluated y comparing the slope of such plots over the first 60 to 80 minutes. In igure 16, such a plot is shown for runs 7A, 8A and 9A which differed only n bubble length. The variation in slope with bubble length is qualitatvely according to Equation (25). The greater the bubble the slower the ate of drainage from the film.

Figure 17 is a similar plot for runs 8A and 10B which were carried ut in capillary tubes of different diameter. Finally, Figure 18 shows he effect of viscosity and surface tension. Run 12A was carried out in 20% glycerol solution which has twice the viscosity of water, but only lightly different surface tension. The broken line is the corresponding

FIGURE 15

Plot of $\frac{1}{\chi^2}$, vs. Time for the Data of Run 4A.

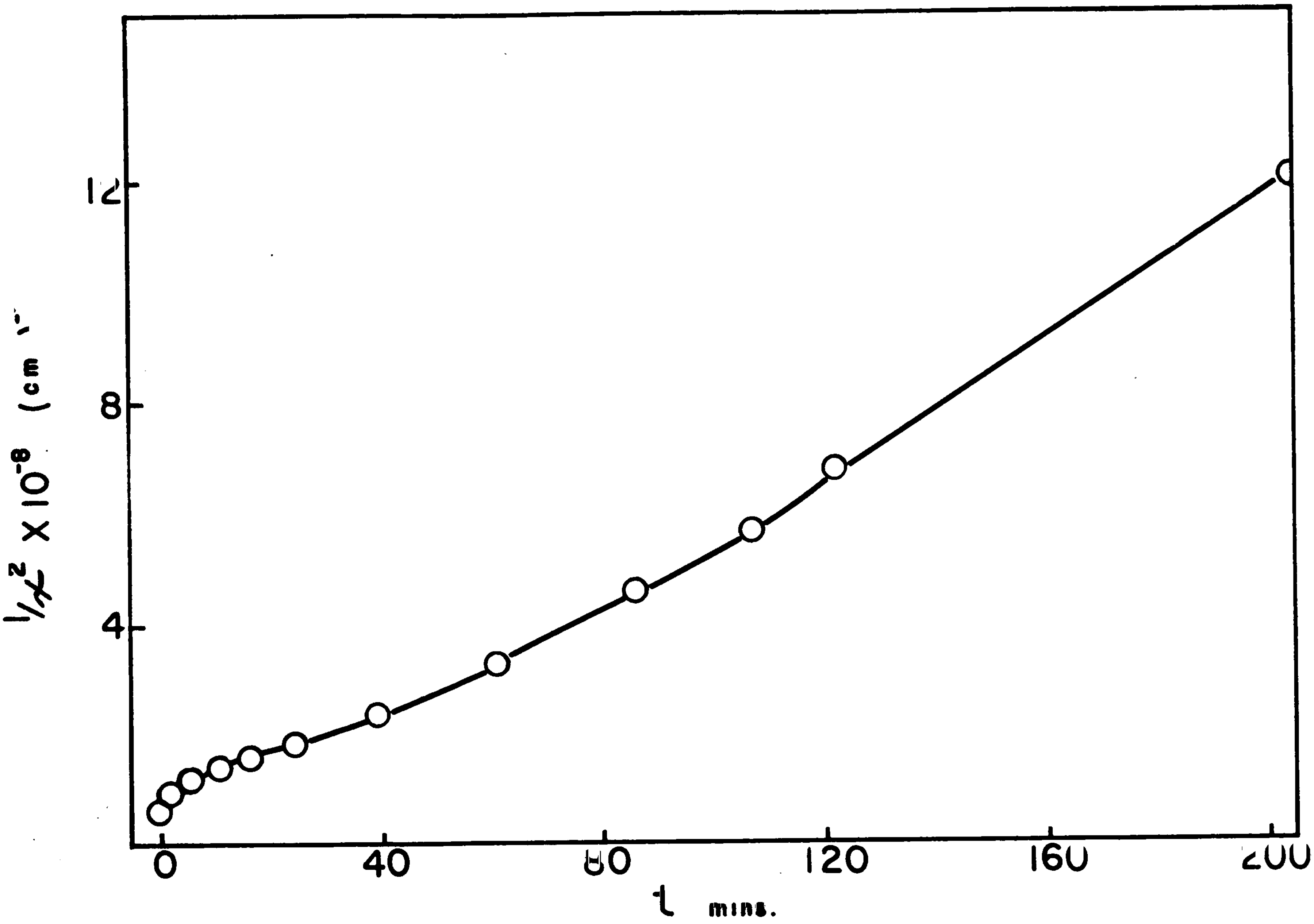
$1/\chi^2$ X 10^{-8} (cm
12
8
4
0
40
80
120
160
200
t mins.

FIGURE 16

Plots of $\frac{1}{r^2}$ vs. Time for Runs:

No. 7A: l_b = 1.32 cm.

No. 8A: l_b = 1.99 cm.

No. 9A: l_b = 2.54 cm.

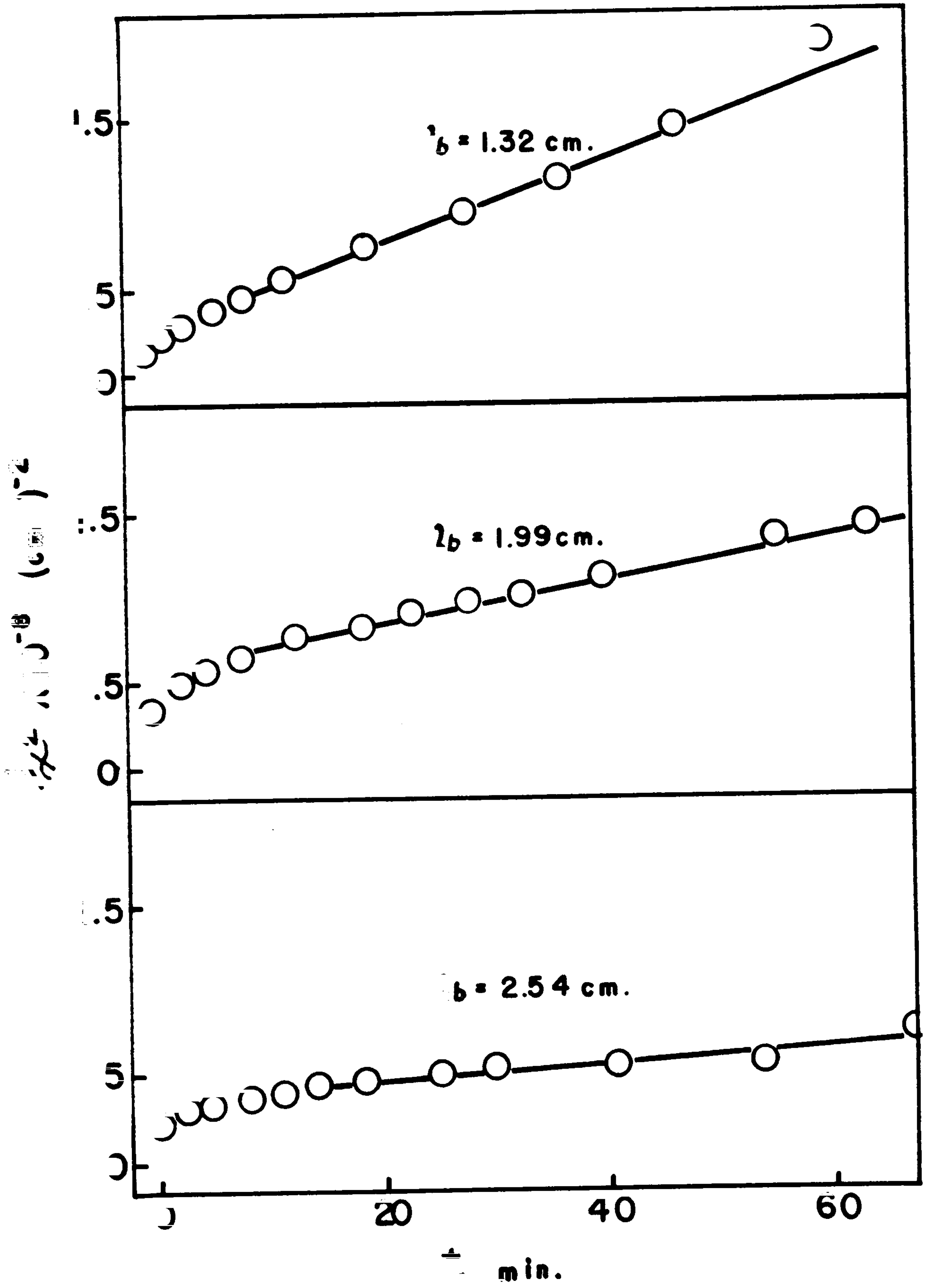
1.5
.5
0
l_b = 1.32 cm.
:.5
.5
0
l_b = 1.99 cm.
.5
5
0
l_b = 2.54 cm.
0
20
40
60
t min.
$\chi^2 \times 10^{-8}$ (cm)$^{-2}$

FIGURE 17

Plot of $\frac{1}{r^2}$ vs. Time for Runs:

No. 8A: r = 0.104 cm.

No. 10B: r = 0.152 cm.

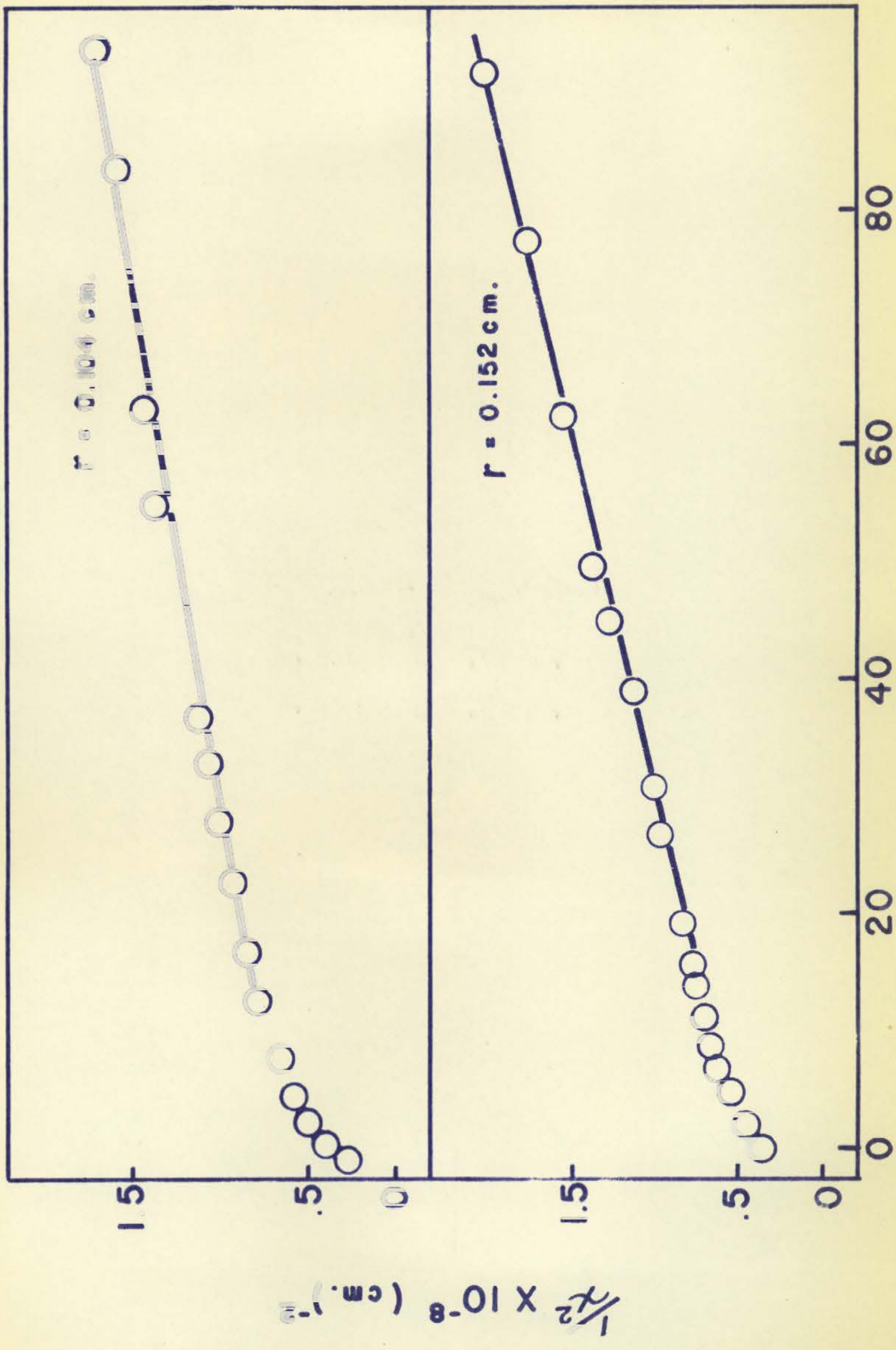
r = 0.104 cm.
r = 0.152 cm.
1.5
.5
0
1.5
.5
0
0
20
40
60
80
t min.
1/x² X 10⁻⁸ (cm.)⁻²

FIGURE 18

Plots of $\frac{1}{r^2}$ vs. Time for Runs:

No. 12A: viscosity - 1.51 c.p., interfacial tension - 72.6 dynes/cm.

No. 13A: " - 0.844 c.p., " " - 26.4 dynes/cm.

No. 8A: " - 0.844 c.p " " - 74.6 dynes/cm.

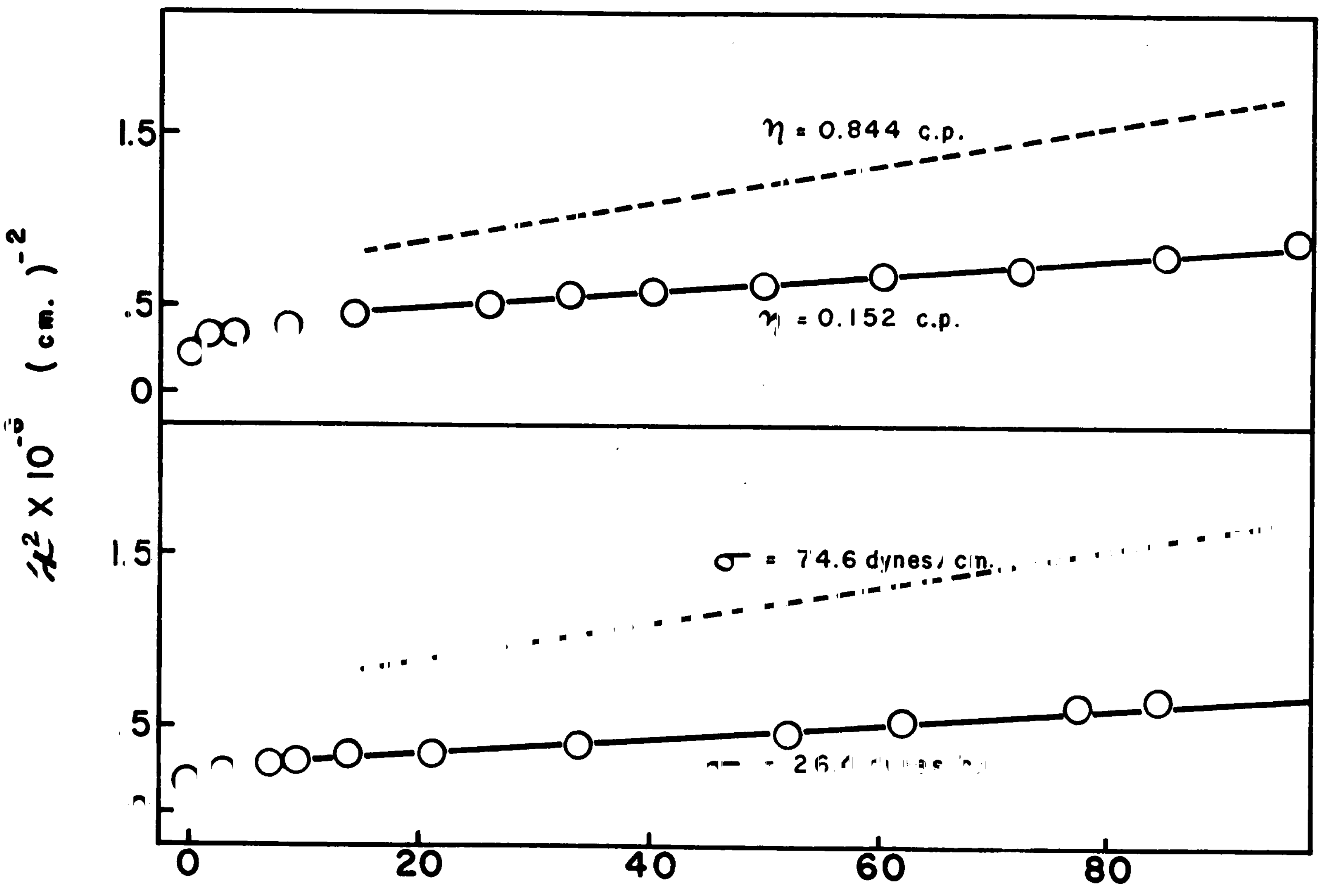
$\kappa^2 \times 10^{-6}$ (cm.)$^{-2}$
1.5
.5
0
1.5
.5
0
20
40
60
80
η = 0.844 c.p.
η = 0.152 c.p.
σ = 74.6 dynes/cm.
σ = 26.4 dynes/cm.

run in water, 8A. Run 13A was carried out in a medium of lowered surface tension. The greater the viscosity of the liquid, the slower the rate of flow from the film and similarly the smaller the surface tension. The effect of these variables on the rate of drainage from the film is in qualitative accord with Equation (25).

IV. Photographic Observations on Moving Bubbles

From measurements in the inclined flowmeter, it was calculated than an entrapped air bubble can offer the same resistance to flow as a 10 to 20 cm. length of the capillary tube. From Poiseuille's law, the equivalent driving pressure is calculated to be from 350 to 700 dynes/cm^2. The existence of such a large pressure drop across the bubble should result in a marked deviation from the assumed cylindrical shape. This statement is based on the following theoretical argument.

Considering the bubble illustrated in Plate I, if in the direction of flow there is a pressure drop (P_1-P_2) across the bubble which results from the difference between the pressures P_1 and P_2 at the forward and backward ends of the bubble then, since the pressure, P_b, inside the bubble is everywhere uniform, it follows that

$$P_b = P_1 + \frac{2\sigma}{r_1} = P_2 + \frac{2\sigma}{r_2}$$

where r_1 and r_2 are the main radii of curvature of the forward and backward ends respectively, but $P_2 > P_1$ therefore $r_2 > r_1$.

Plate III shows the results of a series of photographs on a bubble of length 1.2 cm. taken at various bubble velocities. Differences in curvature are not readily discernible. The photographs in Plate IV are

PLATE III

Photoflashes of Bubble, $l_b = 1.2$ cm., Taken at Various Bubble Velocities, U_b.

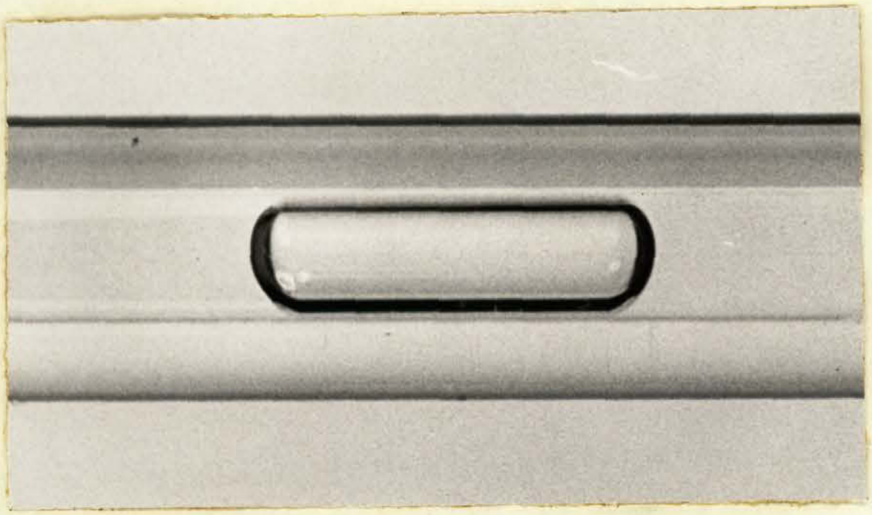

U_b = 0.148 cm/sec.

→

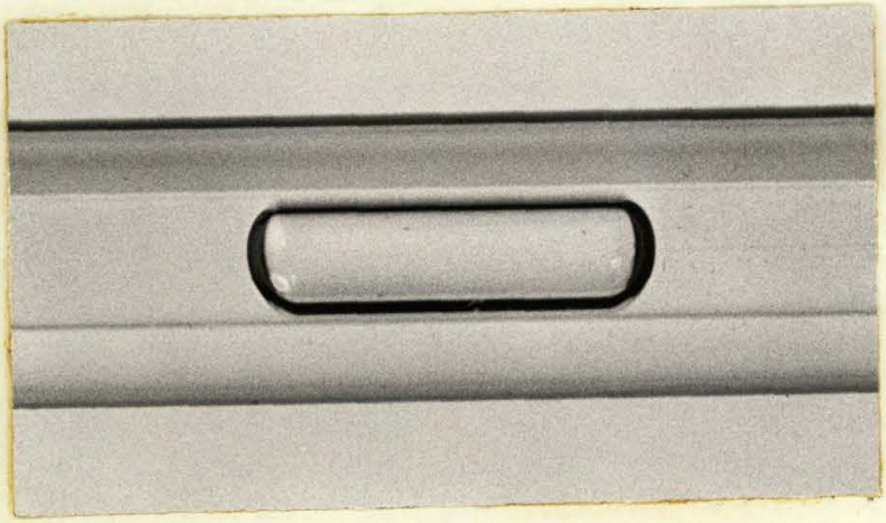

U_b = 0.31 cm/sec.

→

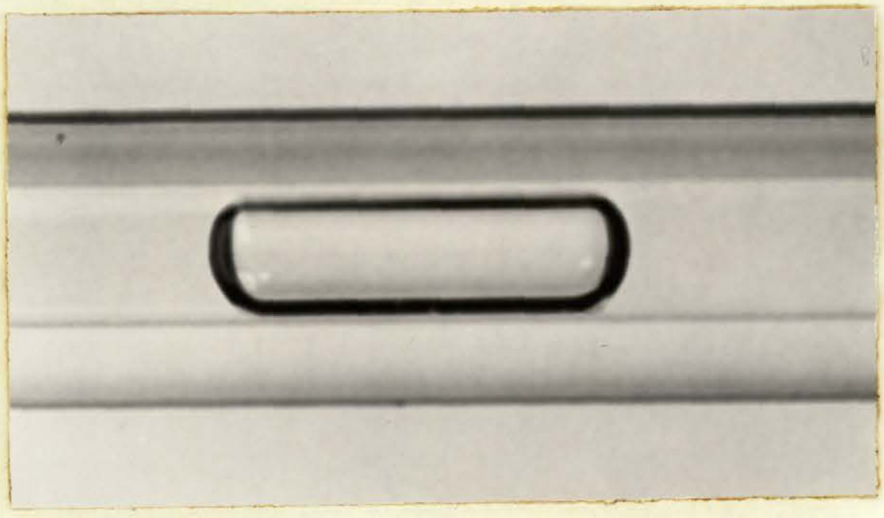

U_b = 1.32 cm/sec.

→

PLATE IV

Photoflashes of Bubble, $l_b = 0.45$ cm., Taken at Various Bubble Velocities, U_b.

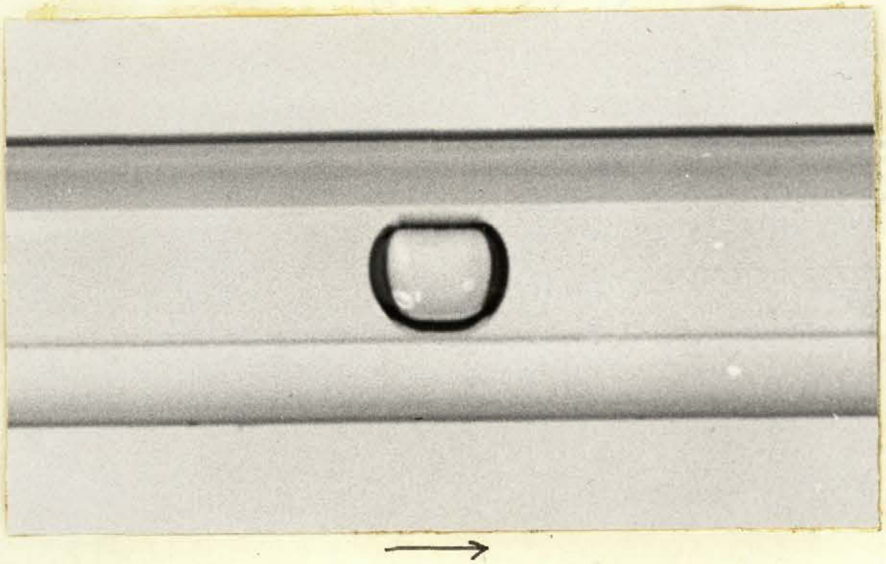

$U_b = 0.22$ cm/sec.

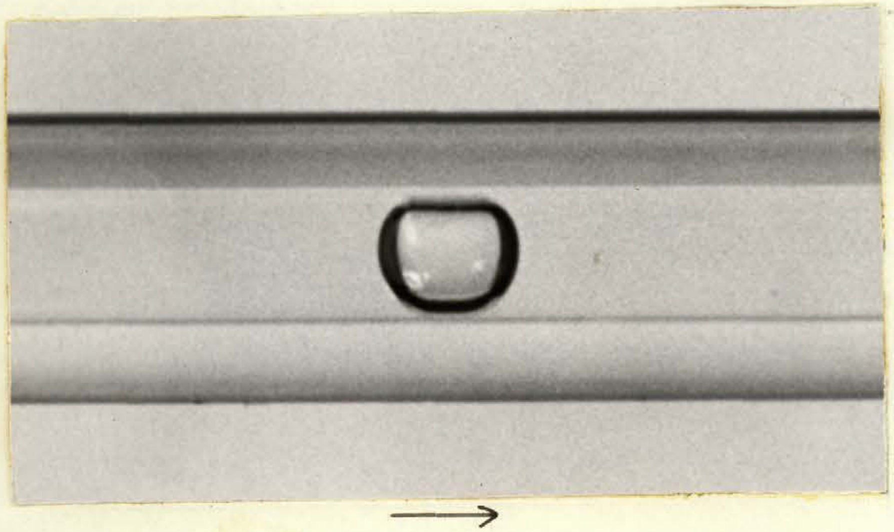

$U_b = 1.19$ cm/sec.

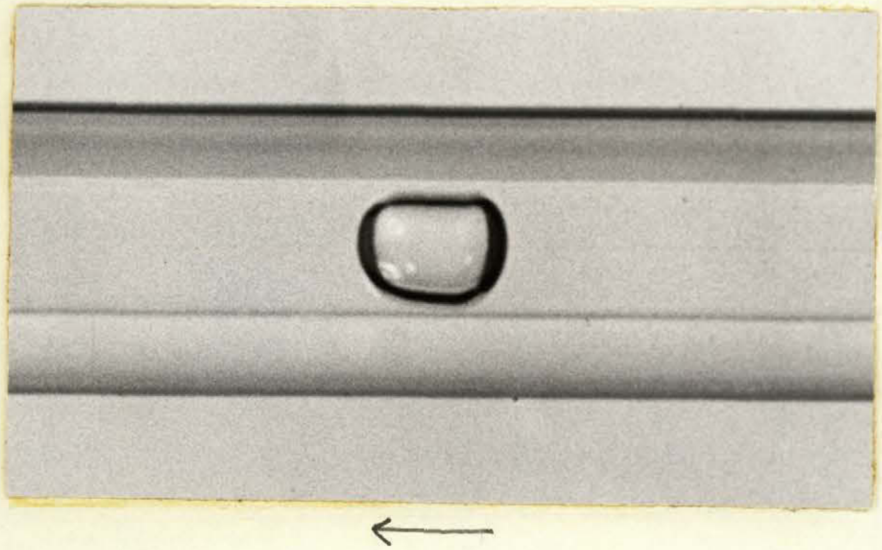

$U_b = ?$

a similar series on a .45 cm. bubble. At relatively high bubble velocities the difference in curvature of the front and rear menisci become very pronounced.

Thus the theoretical prediction was confirmed for a short air bubble but no conclusion was possible in the case of a relatively large one.

Another interesting observation which is most probably associated with the bullet-like shape of the bubble during flow is recorded in Plate V. The phenomenon, which has been termed "the ripple effect", consisted in the appearance of a distinct ripple which travelled from the front to the back end of the bubble when its direction was suddenly reversed. In the photographs the ripple appears as a small hump at the top of the bubble and as an uneveness in the film thickness at the bottom.

It has been suggested that the "ripple effect" is due to a reversal of the bullet shape of the bubble. This is a possibility although in a thin liquid annulus the sudden reversal of the direction of flow could conceivably produce other disturbances such as eddies, which would have a similar appearance.

PLATE V

"Ripple Effect"

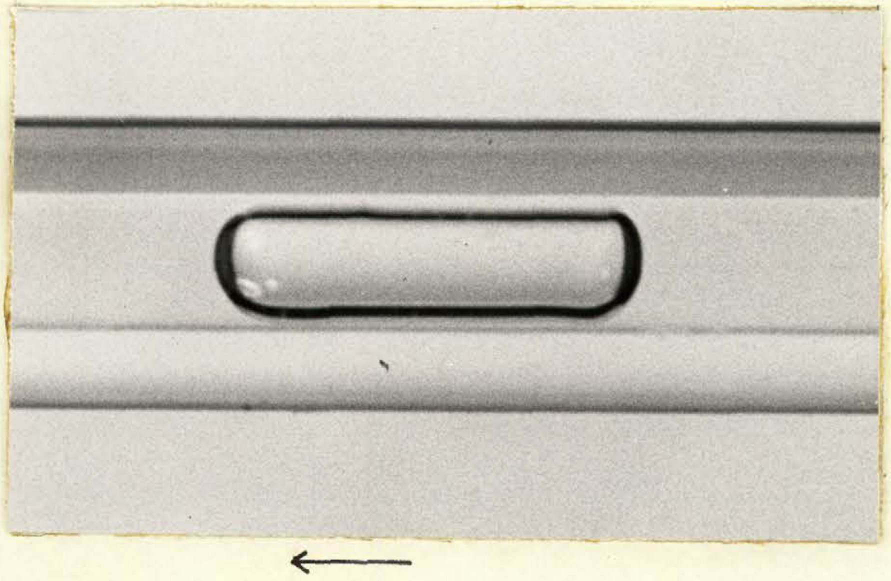

PLATE V

Photoflashes of Bubble, $\ell_b = 1.0$ cm., To Show "Ripple Effect".

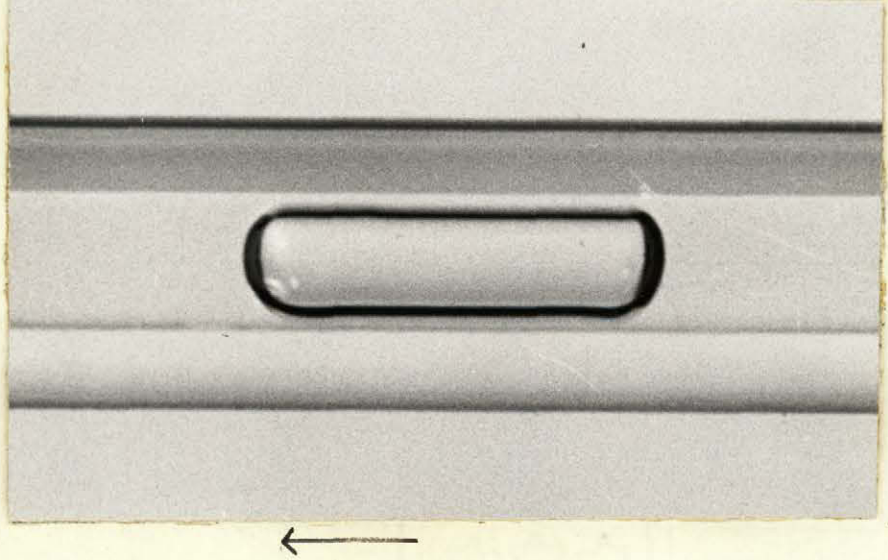

GENERAL DISCUSSION

The discussion which follows is divided into three parts. The first deals with the correlation of film thickness values calculated from flow resistance measurements with those values obtained from the conductance measurements. In the second part, the significance of the basic assumptions underlying the derivation of Equation (7) are re-examined in the light of the experimental results which have been presented. The third part is concerned with the mechanism of flow of air bubbles through capillary channels.

I. Correlation of Calculated and Measured Film Thicknesses

Since conductance measurements were confined to the velocity range below 1 cm./sec. while measurements in the inclined flowmeter were made at bubble velocities above 2 cm./sec., it is obvious that a direct comparison of the calculated and measured film thicknesses is not possible. However if the straight line corresponding to the plot of τ vs. $\sqrt{U_b}$ for run No. 44 is extrapolated upward and the flowmeter data from Table III for all bubble lengths greater than 0.76 cm. are plotted on the same graph, then Figure 19 is obtained. All the calculated values of τ fall below the extrapolated conductance curve.

Under the circumstances, the correlation is quite satisfactory. Although it is not certain that the extrapolated line corresponds to the true curve, it is unlikely that it should be very far wrong, as may be concluded from the data of Fairbrother and Stubbs (1), who worked over the range of velocities from 0.8 to 5.0 cm./sec. There were a number of factors operative in the inclined flowmeter measurements which decreased the accuracy and reproducibility of the experiments and which made perfect agreement with conductance measurements unlikely. These were:

FIGURE 19

Correlation Plot of Measured and Calculated
Values of Film Thickness, χ vs. $\sqrt{U_b}$

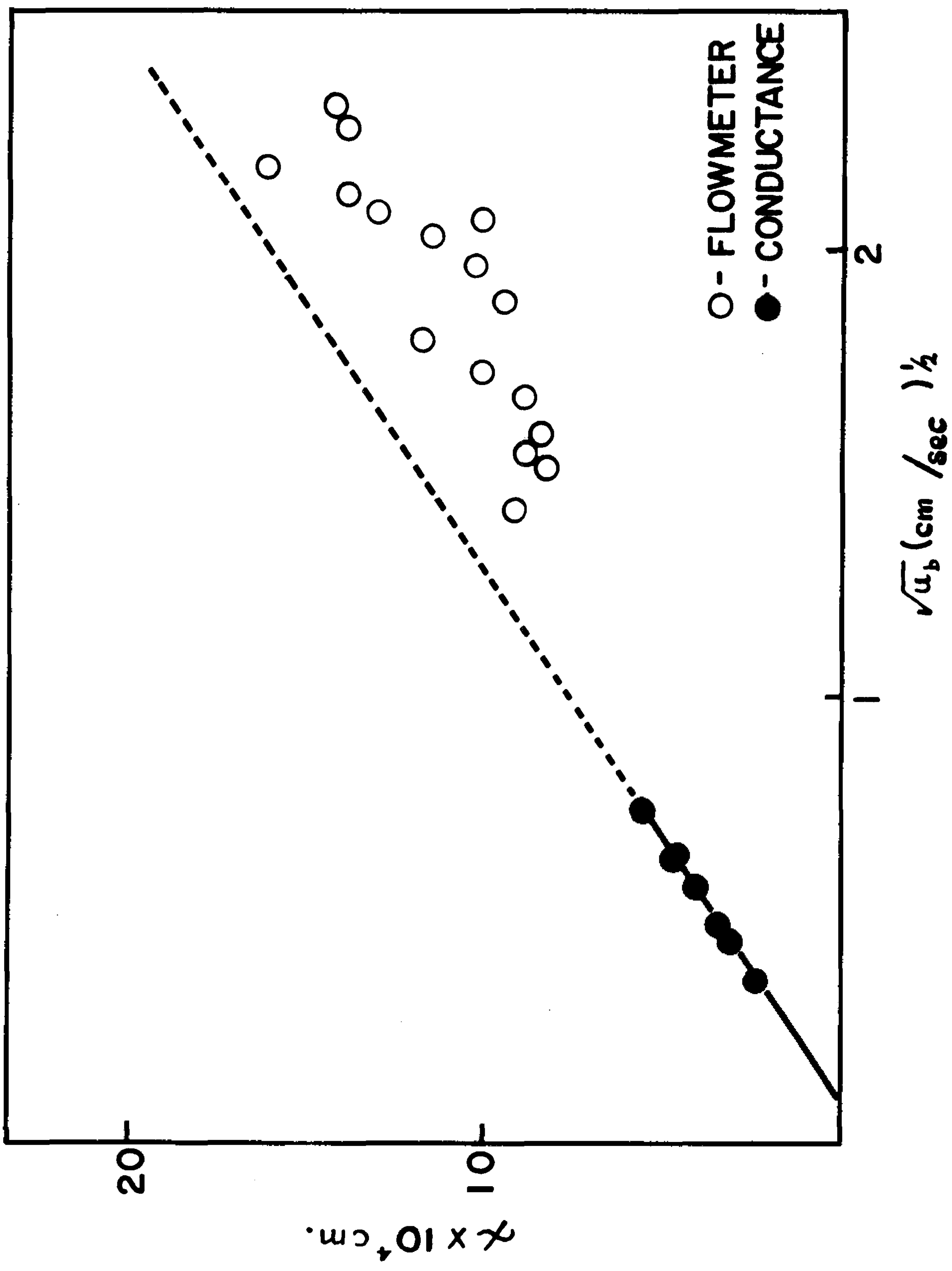
○ - FLOWMETER
● - CONDUCTANCE
$\sqrt{u_b}$ (cm/sec)$^{1/2}$
1
2
$\alpha \times 10^4$ cm.
10
20

(a) In the inclined flowmeter the bubble velocity decreased progressively during the course of a measurement. Since conductance measurements, carried out on a bubble at rest, indicate that there is a time lag in establishing the steady state (or "equilibrium") value of τ, during flow the film thickness is probably greater than the corresponding steady state value. Conductance measurements show also that rate of change of film thickness is a function of bubble length, hence the mean value of τ is also.

(b) Equation (20) from which values of τ were calculated assumes a cylindrical bubble. If the bubble takes any shape which offers greater hydrodynamic resistance than a cylinder, then the calculated value of film thickness will be lower than the true average value. It has been shown in a previous section that the shape of the flowing bubble tends to be conical or bullet-like. For the movement of a slightly inclined plane across a plane surface, from which it is separated by a thin film of fluid, the coefficient of friction increases with increasing inclination of the plane (19). Obviously, the two cases are not identical since any increase in drag causes the bubble to readjust its shape, however, for the same average τ the conical shape will offer greater resistance to flow.

(c) When a bubble travels through a vertical capillary tube, it flows eccentrically. However, if the capillary is at an angle then the axis of the bubble is no longer parallel to the axis of the tube and the analogy of the inclined plane again suggests that in this situation the bubble offers a greater resistance to flow than the corresponding cylindrical bubble at the same average film thickness.

In his investigation of the rising bubble viscometer, Barr (20) observed that a very slight deviation of the tube from the vertical considerably affected the rate of rise.

In view of the above factors the agreement between calculated and measured film thicknesses is reasonably good and the scatter of the calculated τ is not surprising. It follows that the general hypothesis, which is the basis of Equation (7), viz. that the observed decrease in permeability of a capillary tube with an entrapped air bubble is due to the tangential drag on the surface of the bubble resulting from the shearing of the thin liquid film surrounding the bubble, is sound.

Regarding the validity of the conductance method for measuring τ, one may only point to the results which are consistent and in qualitative agreement with theoretical considerations. Furthermore, the results for stationary bubbles confirm the observations of Elton (7) who showed that the liquid film between a small air bubble and a concave lens against which it is pressed undergoes rapid and then slow decrease with no sign of a fixed minimum film thickness as claimed by Derjaguin (8).

Conductance measurements show that the bubble acts as an air-filled elastic balloon which readily undergoes deformation when it is acted upon by an external force and which, on the other hand, always attempts to recover a spherical shape when the applied force is relaxed. As a result of this, liquid is squeezed out of the surrounding film and the motion of the liquid appears to depend on the ordinary laws for viscous flow between planes. Measurements indicate that the film thickness is a function of U_b, r, l_b, η and σ. The relationship between these variables accounts for the variation in permeability with bubble length and bubble velocity.

The existence of a critical bubble length beyond which, within the range of measurements, τ was independent of l_b, was unexpected. Barr (20) reported a similar observation in studying the rate of rise of air bubbles in tubes whose diameter (0.48 cm. to 2.4 cm.) was small compared to the air bubble. He found the rate of ascent, U_b, to be independent of bubble length over a wide range of lengths. In the present case it appears that the increased drag is just balanced by the increased force required to compress the larger bubble.

Interestingly enough, Barr observed no simple relation between bubble velocity, diameter of tube and the viscosity of the liquid. He attributed this to the fact that surface tension is operative in determining the shape of the bubble. This statement was confirmed by the conductance measurements which show the film thickness to increase with decreasing surface tension. These measurements also confirmed the importance of the dimensionless group $\frac{U_b \eta}{\sigma}$ which has been used by several workers (1, 20, 21) to characterize measurements on thin liquid films.

II. Significance of Assumptions Involved in the Derivation of Equation (7).

The correlation which was obtained between calculated and measured values of τ implies that the assumptions involved in the derivation of Equation (7) were sound. In view of this fact, it is of interest to examine the significance of these assumptions. These were: (a) the bubble moves as a solid plug, (b) the bubble is cylindrical and τ/r is small, and (c) there exists a constant velocity gradient, U_b/τ, across the liquid film.

The first assumption is important in relation to hydrodynamic theory. If the bubble moves as a solid plug then there must be a discontinuity of velocity gradient at its surface which is most easily explained by assuming that the surface layers possess an abnormally high viscosity which do not transmit any shear to the gas inside, i.e. within the bubble, circulation is absent.

The question of circulation within fluid drops moving through another liquid is an old one. Assuming circulation within fluid spheres, Hadamard (22) derived a correction to Stokes' law which predicted that the velocity of fall of a fluid sphere is greater than that of a rigid sphere by an amount dependent upon the ratio of the viscosity of the sedimenting drop to that of the suspending medium. For the limiting case where the ratio is zero, the predicted sedimentation rate is 1.5 times that calculated from Stokes' equation. Obviously, an air bubble in water approaches the limiting case.

Barr (23) reports that up to 1930 there was evidence both for and against Hadamard's hypothesis, although it was generally agreed that small spheres (about 0.2 cm. diameter) behave as solids. Recently Garner (24) has shown that in the free sedimentation of fluid drops at low Reynolds' number the predicted velocity gradients are absent. Manley and Mason (25) found that the period of rotation of a small air bubble in a shear field was the same as that of a rigid sphere.

The results of this investigation, of course, suggest that circulation was absent within the bubbles. Another argument against circulation is the fact that calculated film thicknesses are lower than the measured values, which suggests that the hydrodynamic resistance was greater than assumed in the derivation of Equation (7). If circulation did occur the reverse would have been found?

The absence of circulation carries with it the implication that a rigid skin surrounds the bubble. Certainly the apparent behaviour of the bubble as a flexible solid, which was also assumed in all our theoretical treatments, does not make this concept hard to believe. McBain and Henniker point out in a recent review (26) that the surface zone of most liquids, where the molecules are subject to an asymmetric force field, is many molecules deep. It is not unreasonable to assume that in this zone the liquid would exhibit an abnormally high viscosity. McBain and

Henniker do not assume long-range forces but, rather, point to the orienting influence of short-range forces on successive layers. Furthermore, they quote numerous examples to show the orienting effect of solids on liquid films, often as thick as 0.5 micron, which causes them to behave as semi-solids. The analogy between these films and the apparent increase in viscosity of the films surrounding stationary bubbles after several thousand minutes is noteworthy.

Assumptions (b) and (c) are closely related since the velocity gradient influences the shape of the bubble. As seen previously, both theory and experiment argue against the assumption of a cylindrical bubble. In all likelihood, however, for bubbles which are from 3 to 6 times the radius of the capillary, this assumption is good to a first approximation.

The actual shape of a stationary bubble obviously must be ellipsoidal if a pressure maximum exists at the centre of the film which causes liquid to flow towards each end. This results in two equal and opposite parabolic distributions of velocities, one in each half of the film. When the bubble is in motion the shape of the bubble tends to become conical due to the pressure drop across it, and the forward motion of the bubble superimposes a linear distribution of velocities onto the parabolic distribution. The resultant bubble shape is a compromise between a cone and an ellipsoid. The difficulty in predicting the actual shape and in taking it into account in hydrodynamic calculations is obvious. However, since the parabolic distributions are in opposite directions (though they are not necessarily equal for a moving bubble) the assumed linear distribution of velocities probably represents an acceptable average.

In the calculations which led to their empirical relation (Equation (1)), Fairbrother and Stubbs assumed that the liquid velocity was uniform across the film. Thus from the velocity of the bubble they calculated

$V_a = U_b \pi r^2$, where V_a is the apparent velocity of flow. From the measured volume of liquid which flowed, they obtained V_t, the true velocity of flow. Then from the equation

$$\frac{V_a - V_t}{V_a} = \frac{U_b \pi r^2 - U_b \pi (r - \lambda)^2}{U_b \pi r^2}$$

they calculated λ. If a constant velocity gradient exists across the film, then one half the volume of the film is dragged along with the bubble so that the preceding equation should read

$$\frac{V_a - V_t}{V_a} = \frac{U_b \pi r^2 - U_b \pi (r - \lambda)^2 + \pi r \lambda U_b}{U_b \pi r^2}$$

from which Equation (1) is modified to

$$\lambda = r\sqrt{\frac{U_b \eta}{\sigma}} \qquad (27)$$

This equation now predicts film thicknesses twice as great as those predicted by Equation (1). Interestingly enough, the conductance data give slopes of the λ vs. $\sqrt{U_b}$ plots which are intermediate between the slopes predicted by Equations (1) and (27). This suggests that either the empirical equation does not apply under these conditions, or the velocity gradient is actually not constant. Both alternatives are probably involved.

III. The Flow of Air Bubbles Through Capillary Spaces

The results of this investigation show that the resistance to capillary flow offered by an entrapped air bubble can be explained without recourse to the Jamin effect. In the present case, it was shown conclusively that no angle of contact existed, hence the Jamin hypothesis did not apply. In most cases of flow through porous materials it would be difficult to establish whether the observed resistance to flow is due to the Jamin effect or to viscous drag as in the present experiments. The actual system involved is of paramount importance since, for a liquid-solid system, when the liquid is non-wetting, it is unlikely that a liquid film would exist.

When dealing with flow in non-uniform channels the film-surrounded bubble will offer additional resistance due to the work involved in deforming the bubble. Gardesen (10) claims that for the flow of oil and gas through sand, the Jamin effect is zero or very small, the bulk of the resistance being offered by gas bubbles being forced through narrow openings.

Beazley, Johnson and Maass (11) attribute the resistance encountered in forcing gas through wet wood entirely to the Jamin effect. In view of the present results this explanation does not appear to be completely justified on the basis of their experimental evidence. Until some method for distinguishing the two types of resistance is found, the exact nature of the resistance to flow in porous systems cannot be determined. In some cases the conductance method may afford a means of distinguishing the Jamin effect and the film resistance effect.

Beyond the critical bubble length, and for a given capillary radius, the dimensionless quantity $\underline{U_b}$ appears to determine the thickness of the film, hence the resistance to flow if the bubble is cylindrical. It is obvious, however, that any theoretical relation expressing $\underline{\gamma}$ as a function of measurable quantities must take into account U_b, η, σ, l_b, r and some factor which is dependent on the actual shape of the bubble. In an attempt to derive such an expression, the analogy between the mechanism of film lubrication and the flow of a cylindrical air bubble surrounded by a thin film was noted. Using the differential equation which expresses the pressure within a lubricating film as a function of the distance between the two solid planes, the upper one being in motion, the following relation was derived (cf. Appendix D):

$$\chi = \sqrt{\frac{M \, \ell_b U_b \eta}{\left(\pi + \frac{\sigma}{a}\right)}} \tag{28}$$

where π is the pressure outside the film and M is a function of the ratio χ_i/χ_o, χ_i being the film thickness at the front of the bubble and χ_o, that at the rear. For reasonable values of χ_i/χ_o, Equation (28) predicts values of $\underline{\chi}$ which are of the right order of magnitude.

Although it is of no practical use, this equation, which offers a solution for a limiting case, does indicate the type of approach which is required in treating the problem theoretically.

APPENDIX A

Calculation of the Mean Effective Pressure in the Inclined Flowmeter.

Referring to Figure 2 and using the technique outlined by Barr (18), the mean effective pressure during flow of the meniscus over the distance $(X_o - X)$ was calculated as follows.

If h is the head at any instant t, then from Figure 2

$$h = X \sin\theta + \frac{A_1}{A_2} X \tag{A-1}$$

and the pressure, P, is

$$P = X\rho g \left(\sin\theta + \frac{A_1}{A_2}\right) \tag{A-2}$$

Assuming Poiseuille's law, the rate of discharge at any time t is

$$-A_1 \frac{dX}{dt} = kP \tag{A-3}$$

(where k contains some mean effective value for L) substituting for P and integrating

$$\int_X^{X_o} \frac{dX}{X} = \frac{k\rho g}{A_1} \left(\sin\theta + \frac{A_1}{A_2}\right) \int_o^t dt \tag{A-4}$$

$$\ln \frac{X_o}{X} = \frac{kt\rho g}{A_1} \left(\sin\theta + \frac{A_1}{A_2}\right)$$

$$kt = \ln \frac{X_o}{X} A_1 \frac{1}{\left(\sin\theta + \frac{A_1}{A_2}\right)\rho g} \tag{A-5}$$

If P_{mean} is the mean effective pressure, then

$$\frac{A_1 (X_o - X)}{t} = kP_{mean} \tag{A-6}$$

Substituting in (A-6) for kt

$$P_{mean} = \frac{(X_o - X)\,(\sin\theta + \frac{A_1}{A_2})\rho g}{\ln \frac{X_o}{X}} \tag{A-7}$$

It is to be noted that in the above derivation it was assumed that Poiseuille's law applies. The present investigation has shown that this assumption is incorrect in the case of a capillary tube with an entrapped air bubble. However, since there was no relation connecting the pressure and the volume rate of flow at any time t when an air bubble was present, P_{mean} as given by Equation (A-7) was used to calculate ϕ_c. Rough observations of the rate of change of U_b with X over the range $(X_o - X)$ showed that equations similar to (A-3) and (A-6) could be applied without too great an error. This is probably due to two facts: (a) the bubble resistance factor varies inversely as U_b and (b) the bullet-like shape of the bubble with its consequently greater hydrodynamic resistance is more pronounced at higher U_b (cf. Plate IV), while at lower bubble velocities, when the film is thinner, this fact is relatively less important.

APPENDIX B

Derivation of Equation (20) for the Equivalent Capillary Length.

Referring again to Figure 2

$$P = \rho g X \left[\sin\theta + \frac{A_1}{A_2} \right] \qquad \text{(B-1)}.$$

Furthermore if l_b' is the equivalent capillary length of a bubble of length l_b, i.e. the length of capillary tubing which offers the same resistance to flow as the bubble, then by Poiseuille's law

$$P = \frac{8\eta}{\pi r^4} \left[(a + X - l_b) + l_b' \right] \pi r^2 \left(\frac{-dX}{dt} \right) \qquad \text{(B-2)}$$

where $(a + X - l_b)$ represents the length of liquid-filled capillary, while l_b' is the equivalent length of capillary corresponding to the bubble. Rearranging Equation (B-2)

$$\left[(a - l_b + l_b') + X \right] \frac{dX}{X} = \frac{\rho g r^2}{8\eta} \left[\sin\theta + \frac{A_1}{A_2} \right] dt \qquad \text{(B-3)}$$

Assuming l_b' is constant over $(X_o - X)$, then on integration, Equation (B-3) becomes

$$(a - l_b + l_b') \ln \frac{X_o}{X} + (X_o - X) = \frac{\rho g r^2}{8\eta} \left[\sin\theta + \frac{A_1}{A_2} \right] t_b \qquad \text{(B-4)}$$

When no bubble is present $l_b = l_b'$ and Equation (B-4) reduces to

$$a \ln \frac{X_o}{X} + (X_o - X) = \frac{\rho g r^2}{8\eta} \left[\sin\theta + \frac{A_1}{A_2} \right] t_o \qquad \text{(B-5)}$$

which is equivalent to Equation (17).

Subtracting Equation (B-5) from (B-4)

$$(l_b' - l_b) \ln \frac{X_o}{X} = \frac{\rho g r^2}{8 \eta} \left[\sin\theta + \frac{A_1}{A_2} \right] (t_b - t_o) \qquad \text{(B-6)}$$

whence

$$l_b' - l_b = \frac{B \left[\sin\theta + A_1/A_2 \right]}{\eta} (t_b - t_o) \qquad \text{(B-7)}$$

where

$$B = \frac{\rho g r^2}{8 \ln \frac{X_o}{X}} \qquad \text{(B-8)}$$

The assumption that l_b' is constant over the distance $(X_o - X)$ is not quite correct since the variation in pressure necessarily brings about a decrease in U_b. However, as mentioned in Appendix A, the more pronounced conical shape of the bubble at higher velocities seemed to compensate for the lower hydraulic resistance of the thick film and vice versa at low velocities. The result being that over the range of measurements l_b' could be assumed constant without too great an error. This assumption, along with the assumption that the mean effective pressure with and without a bubble is the same (Appendix A), was responsible partly for the scatter of the points in Figure 19 since the relativeerror varied with l_b, θ, U_b etc.

APPENDIX C

Derivation of Equation of Motion for the Liquid Film Surrounding a Stationary Bubble.

Let l_b be the length of a bubble enclosed in a capillary tube of radius a where l_b is sufficiently large so that the bubble may be approximated by a cylinder of length l_b and radius r (Figure C-1). Let x be the distance measured from the centre of the bubble parallel to the capillary wall.

FIGURE C-1

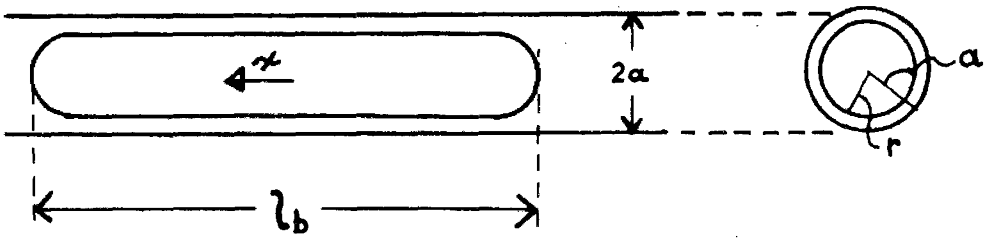

For simplification the coaxial cylinders formed by the bubble surface and the inner capillary wall are imagined to be split open lengthwise to give two parallel planes separated by a distance $h = a - r$ (Figure C-2).

If now the upper plane formed by the surface of the bubble descends with a velocity V at any instant t towards the plane surface of the inner capillary wall to which it remains parallel, and separated from it by a fluid of viscosity η. At instant t let h be the uniform thickness of the fluid film. This process occurs as a result of surface tension, whereby the bubble tends to assume a spherical shape, a pressure is developed within the film and liquid is squeezed out. The mean velocity of the fluid at x is

$$\frac{Vx}{h} \qquad \text{(C-1)}$$

FIGURE C–2

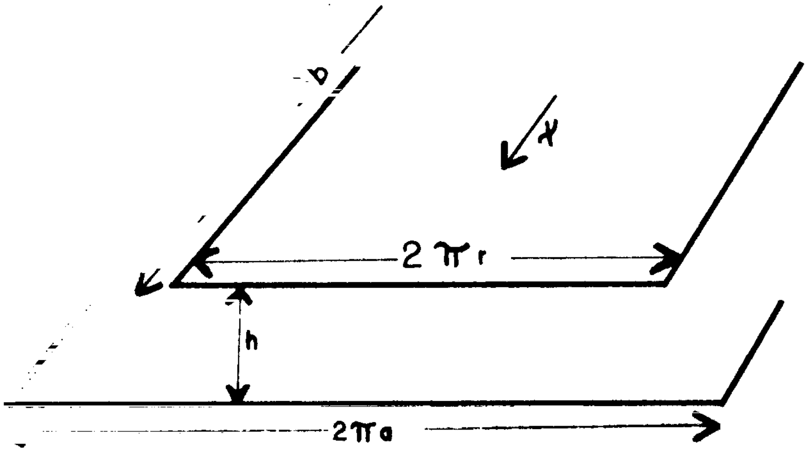

The pressure gradient is (19)

$$\frac{dp}{dx} = \frac{-12\eta V x}{h^3} \qquad \text{(C-2)}$$

Integrating

$$p = \frac{6\eta V}{h^3}\left[\frac{l_b^2}{4} - x^2\right] \qquad \text{(C-3)}$$

and

$$P_{max.} = \frac{6\eta V}{h^3}\frac{l_b^2}{4} = \frac{3}{2}\frac{\eta V l_b^2}{h^3} \qquad \text{(C-4)}$$

Since the pressure curve is parabolic, the mean pressure is 2/3 of $P_{max.}$ And the total load W on the bubble surface is

$$W = \frac{\eta V l_b^3 \, 2\pi r}{h^3} \qquad \text{(C-5)}$$

Since $$V = \frac{-dh}{dt} \qquad \text{(C-6)}$$

then substituting for V, Equation (C-5) becomes

$$\frac{dh}{dt} = \frac{-W\,h^3}{\eta \ell_b^3 2\pi r} \qquad \text{(C-7)}$$

Considering Figure C-1, if P_1 is the pressure outside the film, P_2 is the average pressure within the film and P_b is the pressure inside the bubble then assuming the bubble is a perfect cylinder with hemispherical ends

$$P_b = P_1 + \frac{2\sigma}{r} \qquad \text{(C-8)}$$

and

$$P_b = P_2 + \frac{\sigma}{r} \qquad \text{(C-9)}$$

so that

$$P_2 = P_1 + \frac{\sigma}{r} \qquad \text{(C-10)}$$

From Equation (C-10) it follows that

$$W = \left[P_1 + \frac{\sigma}{r}\right] 2\pi r \ell_b \qquad \text{(C-11)}$$

substitution for W in Equation (C-7) yields

$$\frac{dh}{dt} = \frac{-h^3}{\eta \ell_b^2}\left[P_1 + \frac{\sigma}{r}\right] \qquad \text{(C-12)}$$

$$t = k\left[\frac{1}{h^2} - \frac{1}{h_o^2}\right] \qquad \text{(C-13)}$$

where h_o is the film thickness when $t = 0$ and assuming h is small so that a can be substituted for r

$$k = \frac{\eta \ell_b^2}{\left(P_1 + \frac{\sigma}{a}\right)} \qquad \text{(C-14)}$$

From the construction of the cell, P_1 was always constant.

The assumption that h is uniform along the length of the bubble obviously is incorrect since there is a pressure variation from the centre of the film to the edge which causes the bubble to take an ellipsoidal shape. Equation (C-13) is of qualitative value, however, in predicting how ℓ_b, η, σ and r affect the rate of change of film thickness.

PPENDIX D

erivation of Equation (28) From Film Lubrication Theory

. Pressure Equation for an Inclined Plane Unlimited in one Direction

et the plane Z = 0, which is unlimited in the direction of X nd Y (Figure D-1), be the lower of two planes. The upper plane, unlimited n the direction of Y. extends only from $x = x_o$ to $x = x_i$ and intersects he plane Z = 0 on the line $x = 0$.

IGURE D-1

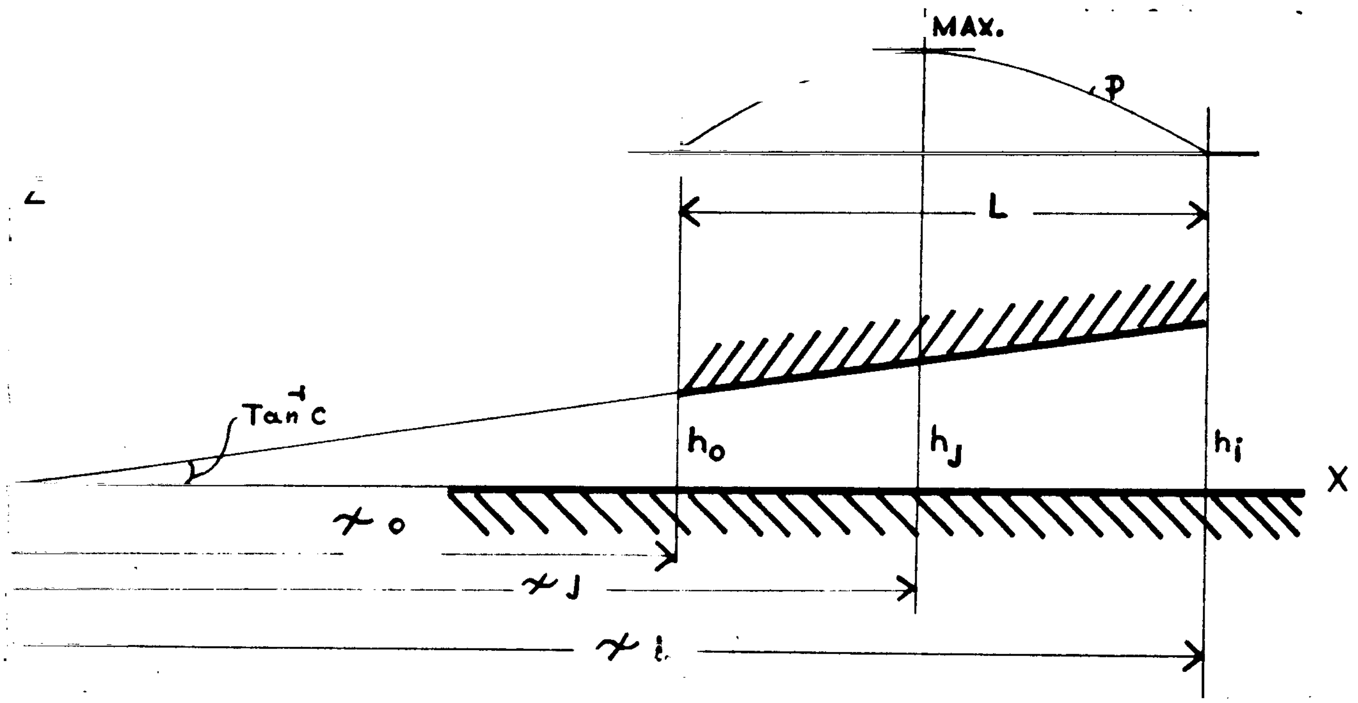

ssumptions:

1) The distance between the planes is everywhere small and is given y

$$= c x$$

here c is the tangent of the small angle between the planes.

2) The upper plane moves over the lower with velocity U in the

direction of *X*.

(3) The fluid velocity in the direction of *Y* is zero.

(4) The system is immersed in fluid so that the pressure both in front of and behind the moving plane is π and is constant.

(5) None of the conditions varies in the *Y* direction so that $\frac{\partial h}{\partial y}$ and $\frac{\partial p}{\partial y}$ are zero.

The general differential equation determining the value of p everywhere in the film between the two planes therefore becomes

$$\frac{\partial}{\partial \chi}\left(h^3\frac{\partial p}{\partial \chi}\right) + 6\eta U\frac{\partial h}{\partial \chi} = 0 \qquad \text{(D-1)},$$

and on integration

$$h^3\frac{\partial p}{\partial \chi} + 6\eta U\,(h-hj) = 0 \qquad \text{(D-2)}$$

where *hj* is the value of *h* when $\frac{\partial p}{\partial \chi} = 0$
i.e. at a point χj where *p* has a maximum or minimum value. On rearrangement, Equation (D-2) becomes

$$\frac{\partial p}{\partial \chi} = -6\eta U\left(\frac{1}{h^2} - \frac{hj}{h^3}\right) \qquad \text{(D-3)}$$

$$= \frac{-6\eta U}{c^2}\left(\frac{1}{\chi^2} - \frac{\chi j}{\chi^3}\right) \qquad \text{(D-4)}$$

Since $\frac{\partial p}{\partial \chi}$ is positive when $h < hj$ and negative when $h > hj$ it follows that *p* has a maximum value at $\chi = \chi j$ between $\chi = \chi_i$ and $\chi = \chi_o$.

Integrating Equation (D-4)

$$p = \frac{6\eta U}{c^2}\left(\frac{1}{\chi} - \frac{\chi j}{2\chi^2} - C\right) \qquad \text{(D-5)},$$

but since $p = \pi$ both when $\chi = \chi_i$ and when $\chi = \chi_o$

$$\Pi = \frac{6\eta U}{c^2}\left(\frac{1}{h_o} - \frac{h_j}{2h_o^2} - C\right) = \frac{6\eta U}{c^2}\left(\frac{1}{h_i} - \frac{h_j}{2\,{}_i^2} - C\right) \qquad \text{(D-6)}$$

from which

$$h_j = \frac{2h_i h_o}{h_o + h_i} \qquad \text{(D-7)}$$

Thus, the point of maximum pressure is nearer to h_o than to h_i, and

$$\frac{6\eta UC}{c^2} = \Pi - \frac{6\eta U}{c^2(h_o + h_i)} \qquad \text{(D-8)}$$

By substitution for h_j and C, Equation (D-5) becomes

$$p = \Pi + \frac{6\eta U}{c^2(h_o + h_i)}\left\{\frac{h_o + h_i}{h} - \frac{h_o h_i}{h^2} - 1\right\} \qquad \text{(D-9)}$$

Equation (D-9) determines the pressure at all points between the two planes.

The total load, W, on the upper plane per unit of width in the direction Y is

$$W = \int_{h_o}^{h_i} (p - \Pi)\, dh$$

$$= \frac{6\eta U}{c^2}\left\{\ln\frac{h_i}{h_o} + \frac{2h_o - h_i}{h_o + h_i}\right\} \qquad \text{(D-10)}$$

B. Application to Moving Bubble

Let us consider now the application of the above derivation to the motion of an air bubble in a capillary tube of radius a when the bubble moves with steady velocity U_b. Since there is a pressure drop across the flowing bubble, then its shape must be bullet-like. However, the flow of

FIGURE D-2

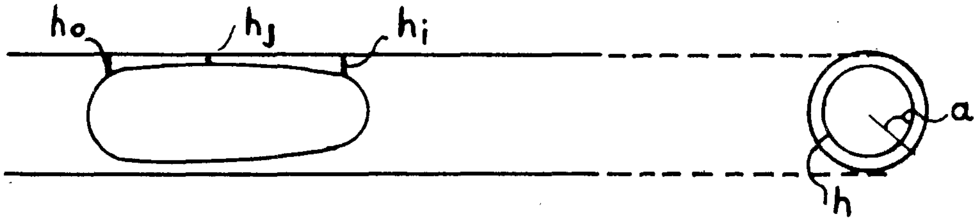

a loaded inclined plane over a thin liquid film tends to produce a point of maximum pressure in the film, the position of which is given by Equation (D-7) The shape of the bubble will therefore be a compromise between an ellipse and a bullet as shown in Figure D-2.

If h is small then the bubble may be considered as a cylinder of radius a. This assumption is made to simplify certain calculation wherein it involves a negligible error, however, as regards the hydrodynamic resistance of the bubble, it is important to take into account even a slight inclination of the bubble surface.

Applied to a moving bubble, it is obvious that assumption (1) above is not strictly valid since the angle of attack is actually negative past the point of maximum pressure.

Assumptions (2), (3) and (5) are quite valid in this case.

It can be shown that, in the conductance cell used in this investigation, assumption (4) is true to a first approximation since the pressure drop across the bubble was small compared to the pressure at any point inside the capillary.

If now the lower plane, Z = 0, in Figure D-1 is replaced by the surface of a cylinder whose axis is parallel to the X coordinate (this opened cylindrical surface corresponds to the inner surface of the capillary) and the upper plane extending from $x = x_o$ to $x = x_i$ is replaced by a surface which possesses a slight curvature away from the lower plane (this is the opened surface of the bubble) such that on any plane $X = k$, the distance $\underline{h}$ between the lower surface and the upper one is constant (N.B. the effect of buoyancy is ignored), and h_i/h_o is always a little greater than 1.

Equation (D-10), expressing the load on the film per unit width in the $\underline{Y}$ direction, when applied to the bubble surface becomes

$$W = \frac{6\eta U_b}{c^2}\left\{\ln\frac{h_i}{h_o} + 2\frac{h_o - h_i}{h_o + h_i}\right\} \qquad \text{(D-11)};$$

putting $r = \frac{hi}{ho}$, then Equation (D-11) becomes

$$W = \frac{M\eta U_b \ell_b{}^2}{h_o{}^2} \qquad \text{(D-12)}$$

where $$M = \frac{6}{(r-1)^2}\left\{\frac{2(r-1)}{r+1} - \ln r\right\} \qquad \text{(D-13)}$$

Since Equation (D-12) is the load per unit width on the surface of the film, it must be multiplied by the width of the bubble, i.e. of the cylinder which approximates it, viz. 2 a, to get the total load on the surface. Furthermore, if the pressure in front of the moving bubble is P_1, and behind it P_2, r_1 and r_2 are the corresponding radii of curvature of the front end and back end, P is the average pressure within the film and P_b is the pressure within the bubble, then

$$P_b = P + \frac{\sigma}{a}$$

$$= P_1 + \frac{2\sigma}{r_1}$$

$$= P_2 + \frac{2\sigma}{r_2}$$

In the conductance cell $P_1 \simeq P_2 = \Pi$ throughout the length of capillary tube, and $r_1 \simeq r_2 \simeq a$, whence

$$P = \Pi + \frac{\sigma}{a} \tag{D-14}$$

Then by Equation (D-12)

$$W\,2\pi a = \frac{M\eta U_b l_b^2}{h_o^2}\,2\pi a = 2\pi a l_b\left(\Pi + \frac{\sigma}{a}\right) \tag{D-15}$$

and

$$h_o^2 = \frac{M\eta U_b l_b}{\left(\Pi + \frac{\sigma}{a}\right)} \tag{D-16}$$

SUGGESTIONS FOR FUTURE WORK

The results of this preliminary investigation indicate that a detailed study, both theoretical and experimental, of the factors which determine the film thickness surrounding a moving air bubble should lead to a greater understanding of the "bubble effect". A proposed apparatus for such a study should incorporate facilities to allow measurement of: the film thickness, the pressure causing flow, the pressure drop across the capillary and the rate of flow over a wide range of bubble velocities, bubble lengths and capillary diameters.

SUMMARY

The decrease in permeability of a capillary tube containing an entrapped air bubble whose shape is approximately cylindrical has been shown to result from the hydrodynamic resistance to flow of the moving bubble due to the presence of a thin liquid film surrounding it.

The presence of a liquid film was shown by conductance measurements across a capillary tube containing an entrapped air bubble. The conductance method was applied to determine the average thickness of the liquid film and its variation with bubble velocity, bubble length, capillary radius and viscosity and surface tension of the liquid medium. It was shown that the variation was in qualitative agreement with theoretical predictions based on the assumptions that the bubble moved as a solid plug and that flow within the liquid film was viscous.

From the experimental results, a new mechanism is proposed to explain the resistance to flow through porous media of liquids containing entrapped air bubbles.

BIBLIOGRAPHY

1. Fairbrother, F., and Stubbs, A.; J. Chem. Soc. p. 527 (1935)
2. Schiff, H.; McGill University - Private Communication
3. Gunning, H.E., and Gordon, A.R.; J. Chem. Phys. 10, 126 (1942)
4. Jones, G. and Bradshaw, B.C.; J.A.C.S. 55: 1780 (1933)
5. Jones, G., and Prendergast, M.J.; J.A.C.S. 59, 731 (1937)
6. Bikerman, J.; "Surface Chemistry", Academic Press N.Y. (1947)
7. Elton, G.A.; Proc. Roy. Soc. 194-A: 259 (1948)
8. Derjaguin, B.; Discussion of the Faraday Society: "The Electrical Double Layer" p. 203 (1939-40)
9. Gavelin, G.; Pulp Paper Mag. Can. 55: 191 (1954)
10. Gardesen, I.I.; Oil and Gas J. 28: 115 (1930)
11. Beazley, W.B., Johnston, H.W. and Maass, O.; Canada, Forest Service - Bulletin 95 (1939)
12. Poynting, J.H., and Thomson, J.J.; A Textbook of Physics
13. Smith, W.O. and Crane, M.D.; J.A.C.S. 52: 1345 (1930)
14. Vaillant, M.P.; Compt. rend. 156 p. 307
15. Biefer, G.J. and Mason, S.G.; J. Colloid Sc. 9:20 (1954)
16. Jamin, M.J.; Compt. rend. 50: 172 (1860) cited by reference (13)
17. Michell, A.G.M.; "Mechanical Properties of Fluid" p. 123, Blackie and Son Ltd., London (1923)
18. Barr, Guy; "A Monograph of Viscometry" p. 74, Oxford Press, London (1931)
19. Purday, H.F.P.; "Streamline Flow", Constable and Co. London (1949)
20. Reference (18) p. 261
21. Phil. Mag., 44: 1002 (1922)
22. Hadamard: Compt. rend. 152: 1735 (1911) cited by Barr, reference (18) p. 189
23. Reference (18) p. 191
24. Garner, F.H.; Trans. Inst. Chem. Engrs. (London) 28, 88 (1950)

25. Manley, R.St. J., Mason, S.G.; McGill University - Private Communication

26. McBain, J.W. and Henneker, J.C.; "Colloid Chemistry" vol. VII, ed. by J. Alexander, Reinhold Pub. Corp. N.Y. (1950)

CLAIMS TO ORIGINAL RESEARCH AND CONTRIBUTION TO KNOWLEDGE

1. The effect of freeze-drying on the physical properties of paper has been evaluated and new evidence was obtained concerning the mechanism of bonding in paper.

2. The effect of freeze-drying and of solvent-exchange drying on the sorptive properties of softwood cellulose fibres was evaluated over a range of relative humidities.

3. Evidence from mercury penetration experiments has been presented to show that freeze-drying increases intrafibre and interfibre pore sizes.

4. From the investigation it was concluded that drying by sublimation modified the physical properties of the fibres.

5. The presence of an entrapped air bubble has been shown to decrease the permeability of a capillary tube. The decrease in permeability has been shown to result from the hydrodynamic resistance of the moving bubble due to the presence of a thin liquid film surrounding it.

6. A method has been developed for the measurement of the average thickness of the liquid film surrounding an air bubble entrapped in a capillary tube. The method has been applied to study the effect of viscosity and surface tension of the liquid medium, bubble velocity, bubble length and capillary radius on the thickness of the liquid film surrounding moving and stationary air bubbles.

7. A new mechanism has been proposed to explain the resistance to flow of porous materials due to the presence of air bubbles in the capillary spaces.